Role of ammonia in mitochondrial function, morphology and metabolism: implications for the pathogenesis of hepatic encephalopathy

Inaugural-Dissertation

zur Erlangung des Doktorgrades
der Mathematisch-Naturwissenschaftlichen Fakultät
der Heinrich-Heine-Universität Düsseldorf

vorgelegt von

Leonie Drews

aus Hamburg

Düsseldorf, Juli 2019

aus dem Institut für Biochemie und Molekularbiologie I
der Heinrich-Heine-Universität Düsseldorf

Gedruckt mit der Genehmigung der
Mathematisch-Naturwissenschaftlichen Fakultät der
Heinrich-Heine-Universität Düsseldorf

Berichterstatter:

1. Prof. Dr. Andreas Reichert

2. Prof. Dr. Nikolaj Klöcker

Tag der mündlichen Prüfung: 09.10.2019

„Phantasie ist wichtiger als Wissen, denn Wissen ist begrenzt“

Albert Einstein

Table of contents

1. Introduction

1.1. The origin of mitochondria

Mitochondria are ubiquitous organelles, found in nearly all eukaryotic cells. According to the endosymbiotic theory, they are originated from α-proteobacteria, which were engulfed by eukaryotic ancestor cells about 2 billion years ago and developed in symbiosis to become the mitochondria we know today (Lane and Martin, 2010; Sagan, 1967). During evolution most of the genes encoded by mitochondrial DNA (mtDNA) were translocated to the chromosomes of the cellular nucleus. Animal mtDNA is a small, circular, extrachromosomal genome with a size typically ranging between 15-20 kDa. In humans, it is encoding for 37 genes. Twenty-two encode for transfer-RNAs, 13 encode for protein subunits of respiratory chain complexes and two for ribosomal RNAs. Together with RNAs and proteins imported from the cytoplasm, encoded by the nucleus, mitochondria are able to maintain their own DNA replication, transcription and translation of proteins (reviewed in Boore, 1999). In the 1970s, researchers were trying to find competing theories on the origin of mitochondria; however, in the 1980s these theories, *e.g.* on endogenous development of mitochondria, could be rejected. With 16S rRNA sequencing it was possible to clearly show the origin of mitochondria from a prokaryotic group, later known as α-proteobacteria (reviewed in Zimorski et al., 2014).

1.2. Mitochondrial organization

Mitochondria are double-membrane organelles. Between the outer and the inner mitochondrial membrane is the intermembrane space, inside the inner membrane the mitochondrial matrix is located. Infoldings of the inner membrane, supported by the mitochondrial contact site and cristae organizing system (MICOS) complex, form the cristae membrane. Tubular openings connect the inner mitochondrial membrane with the cristae membrane, which are termed cristae junctions (Pfanner et al., 2014). Embedded in the inner mitochondrial membrane of the cristae are the mitochondrial respiratory complexes I to IV, as well as complex V, the F_1F_O-adenosine triphosphate (ATP)-synthase. Each mitochondrion contains multiple mtDNA molecules. The distribution of mtDNA among daughter mitochondria occurs randomly upon cell division. Usually, all molecules of mtDNA are identical, which is known as homoplasmy. Nevertheless, deleterious mutations can occur in some, but not all mtDNA molecules, causing heteroplasmy in affected tissues (DiMauro and Davidzon, 2005).

1.3. Mitochondrial functions

One of the main functions of mitochondria is the production of ATP via oxidative phosphorylation (OXPHOS). In the first step of OXPHOS electrons, derived from NADH and $FADH_2$, are transferred onto O_2. NADH-dehydrogenase (complex I) transfers two electrons from NADH to the co-factor flavin mononucleotide (FMN), which can be further protonated to $FMNH_2$. The reaction produces one NAD^+. The electrons are then transferred to ubiquinone (also known as coenzyme Q_{10}) in the mitochondrial membrane. Four protons are transported from the matrix to the cristae space. Another independent pathway in the respiratory chain is mediated via succinate-dehydrogenase (complex II). With the help of the co-substrate $FADH_2$, two electrons are transferred to ubiquinone. In contrast to the first reaction no protons are transported into the intermembrane space here. Ubiquinone passes the electrons on to the cytochrome-*c*-reductase (complex III), which transfers them to cytochrome *c*. In this process two protons are translocated to the intermembrane space. Cytochrome-*c*-oxidase (complex IV) carries electrons from cytochrome *c* onto molecular oxygen, thereby generating H_2O and transferring four protons over the inner mitochondrial membrane (Fig. 1) (Müller-Esterl, Biochemie, 1st edition 2004; Stryer, Biochemie, 8th edition 2018). The respiratory chain complexes I to IV create an electrochemical gradient across the inner membrane. The transport of electrons across the electron transport chain (complex I to IV) to oxygen is coupled to the transport of protons across the inner membrane from the matrix to the inner membrane space. The proton gradient is then used to power the F_1F_O-ATP-synthase (complex V) in order to synthesize ATP. Protons move back into the matrix through the F_1F_O-ATP-synthase, in that way inducing a rotation of the F_O-subunit γ. An estimated number of about 3 protons are needed to synthesize one ATP and each complete cycle synthesizes three ATP from ADP + P_i. Through this process mitochondria produce the highest proportion of ATP from all energy pathways in the animal cell (Friedman and Nunnari, 2014; Stryer, Biochemie, 8st edition 2018; Müller-Esterl, Biochemie, 1st edition 2004). The five complexes of the respiratory chain are organized in supercomplexes (SCs) of defined stoichiometry. Complexes I, III and IV form SC I+III_2+IV, which is capable to transfer electrons from NADH to O_2 with the help of the mobile electron carriers ubiquinone and cytochrome *c*. Therefore, it is termed the respirasome. Other SC formed less frequently are SC I+III_2, SC III_2+IV and dimers from CIV and CV. Importantly, the ratio of SCs is different regarding species and tissue distribution and can as well be altered in response to metabolic demands of the respective cell. The functions of the SCs remain subject to discussion; however, it has been shown that besides the fact that the respirasome is capable of respiring solely, SCs can affect membrane stability and reduce the amount of reactive oxygen species (ROS) produced during electron transport (reviewed in Letts and Sazanov, 2017).

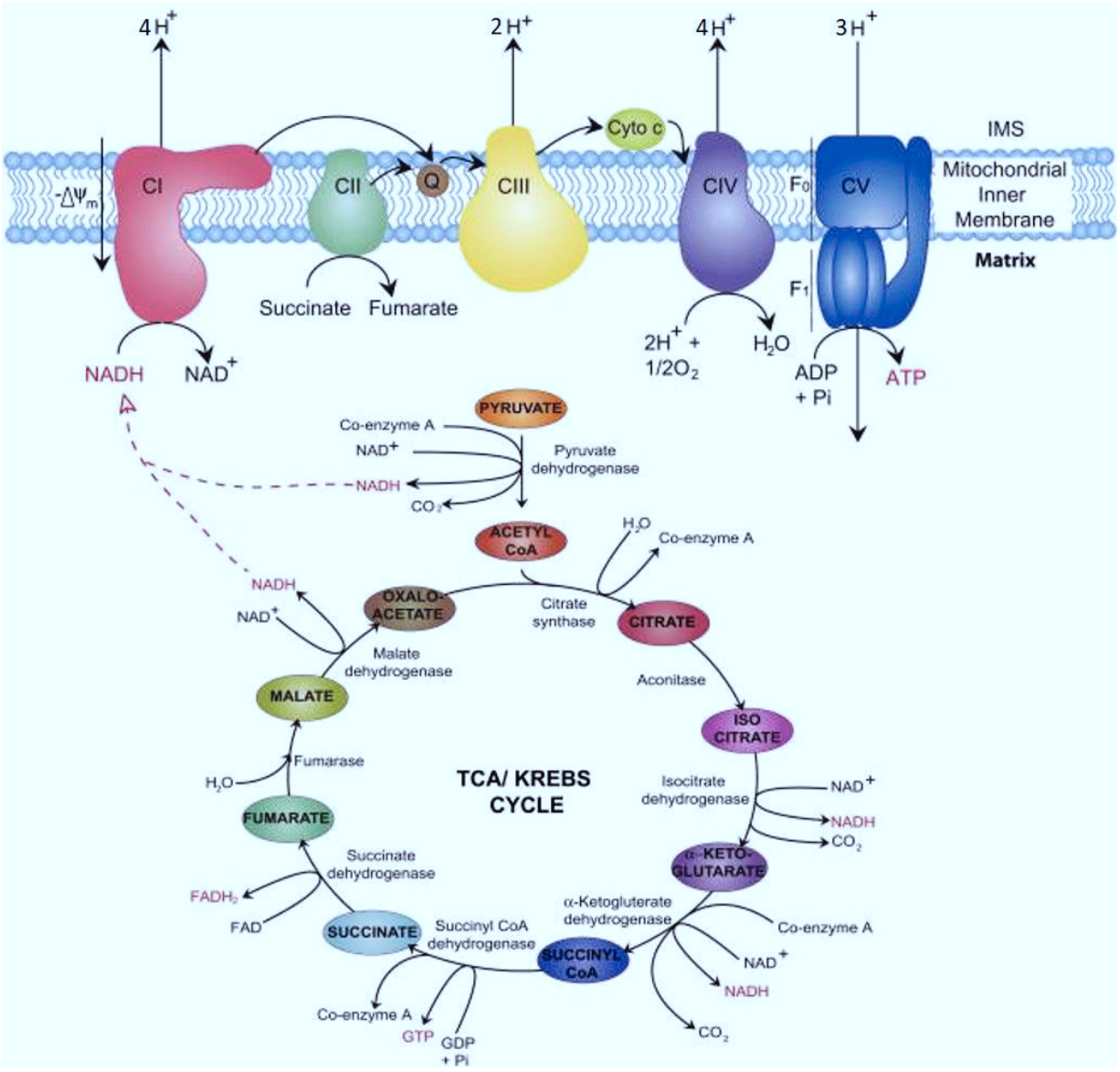

Figure 1: Mitochondrial energy metabolism. Acetyl-CoA, derived from pyruvate from glycolysis, fatty acid oxidation or other catabolic processes mediates the start of the TCA-cycle. The TCA-cycle consists of nine subsequent reactions with the same starting and end product, oxaloacetate. The cycle produces reducing equivalents NADH and $FADH_2$ needed for oxidative phosphorylation. The four complexes of the electron transport chain create a proton gradient across the inner mitochondrial membrane, which fuels the synthesis of ATP via the F_1F_O-ATP-synthase (Image modified from Osellame et al., 2012).

The interlinkage between glycolysis in the cytosol and energy metabolism in mitochondria, namely tricarboxylic acid (TCA)-cycle and oxidative phosphorylation, is mediated via pyruvate. Pyruvate results from glycolysis and is converted to acetyl-coenzyme A (acetyl-CoA) by oxidative decarboxylation under aerobic conditions. The TCA-cycle, located in the mitochondrial matrix, is a closed circle of nine subsequent

reactions with oxaloacetate as starting and end product. In the starting reaction the citrate synthase combines oxaloacetate with acetyl-CoA to form citrate. The coenzyme A is hydrolytically cleaved off. Citrate is then isomerized to isocitrate by aconitase via the intermediate *cis*-aconitate. In the next step isocitrate dehydrogenase forms α-ketoglutarate from isocitrate, which leads to the production of NADH and CO_2. This reaction is the key reaction determining the direction of the cycle. Subsequently another dehydrogenase, namely α-ketoglutarate dehydrogenase, catalyzes the formation of succinyl-CoA, again producing NADH and CO_2. Then succinate is formed by the succinyl-CoA dehydrogenase. Succinate is used to form fumarate via the enzyme succinate-dehydrogenase, by this producing $FADH_2$. Fumarase converts fumarate to malate and malate is converted to oxaloacetate by malate dehydrogenase, whereby again NADH is produced. Oxaloacetate is the final product as well as the starting product of the TCA-cycle (Fig. 1). The oxidoreductases of the TCA-cycle produce the reducing equivalents NADH and $FADH_2$ needed for OXPHOS. Generally, all the pathways are strongly intertwined. The enzyme succinate dehydrogenase is part of the TCA-cycle as well as of the respiratory chain. Additionally, products from degradation of fatty acids and amino acids mainly enter the TCA-cycle via acetyl-CoA and *vice versa* the TCA-cycle provides precursors for the biosynthesis of amino acids, fatty acids as well as nucleotides (Müller-Esterl, Biochemie, 1st edition 2004).

The electrochemical gradient created by the respiratory chain is also utilized for another important function of mitochondria, the maintenance of calcium (Ca^{2+}) homeostasis. Mitochondria are capable of accumulating Ca^{2+} through the mitochondrial calcium uniporter (mCU) as well as releasing the ion through Na^+/ Ca^{2+} antiporters. Calcium homeostasis is crucial as many biological functions depend on calcium, *e.g.* an uptake of too many Ca^{2+}- ions by mitochondria leads to apoptosis (Contreras et al., 2010).

Mitochondria are also responsible for the degradation of fatty acids, by β-oxidation. Short-chain fatty acids ($<C_{10}$) can diffuse into the mitochondrial matrix. Due to the lack of a transporter in the inner mitochondrial membrane, long-chain fatty acids (C_{10}-C_{20}) have to be converted to a transportable form. Long-chain fatty acids enter the mitochondria as acylcarnitine. In the matrix the transport molecule carnitine is released and acyl-CoA is degraded in four subsequent reactions, gradually removing one C_2-entity after the other. This results in the production of acetyl-CoA, which is then fueled into the TCA cycle (Müller-Esterl, Biochemie, 1st edition 2004).

Apoptosis is mediated via two main pathways: the extrinsic or death receptor pathway and the intrinsic pathway, which is facilitated by mitochondria. All pathways end in the same terminal pathway initiating caspase 3 activation and hence DNA fragmentation, degradation of proteins, formation of apoptotic bodies, expression of ligands for phagocytic cells and finally phagocytic uptake and digestion of cellular content (Elmore, 2007). The intrinsic pathway is induced by a signal from the tumor suppressor protein

p53 to express the *bax*-gene. The encoded protein Bax, together with other members of the Bcl-2 family located in the outer mitochondrial membrane mediates the release of cytochrome *c* from the cristae space into the cytosol. Here, it binds to Apaf-1 and initiates the terminal caspase activation cascade (Osellame et al., 2012; Müller-Esterl, Biochemie, 1st edition 2004).

As mitochondria cannot be formed *de novo* by an organism, mitochondrial biogenesis is defined as the division and growth of already existing organelles and can refer to changes in organelle number, as well as size and mass (Jornayvaz and Shulman, 2010). The major regulator of mitochondrial biogenesis is peroxisome proliferative activated receptor-γ coactivator 1α (PGC-1 α) (Puigserver et al., 1998), a co-transcriptional regulation factor inducing biogenesis via a cascade of transcription factors downstream. Besides cell division, also external factors such as exercise or low temperatures can trigger mitochondrial biogenesis (reviewed in Jornayvaz and Shulman, 2010). Furthermore, it was recently found that iron deprivation can also decrease mitochondrial biogenesis on transcriptional level (Rensvold et al., 2016). Iron, as one of the most abundant elements found in nature (Frey and Reed, 2012), is of utmost importance for proper mitochondrial functions. For example, iron deficiency was found to negatively influence the activity of respiratory chain complexes already in 1986 (Dallman, 1986). Iron-sulfur clusters are part of the complexes I, II and III in the respiratory chain and are important for proper electron transport (Müller-Esterl, Biochemie, 1st edition 2004). The synthesis of heme, a porphyrin ring including a ferrous iron needed for many biological functions, *e.g.* as a prosthetic group of hemoglobin, starts in the mitochondria. The biosynthesis includes eight enzymatic steps, partly taking place in the mitochondria and in the cytosol (Ogun and Valentine, 2019).

Furthermore, mitochondria are employed in many other functions, *e.g.* signaling through mitochondrial ROS.

1.4. Mitochondrial role in diseases

The classical type of a mitochondrial disease arises from a mutation in mtDNA or nuclear genes encoding for mitochondrial proteins, especially of the respiratory chain (DiMauro and Davidzon, 2005; DiMauro and Schon, 2003). To date, about 275 loci are known to cause disease (Saneto, 2017). They are among the most common inherited neuromuscular diseases and in total have a prevalence of approximately 1 in 5000 births. These diseases often manifest in the brain or in skeletal muscles, as these tissues are typically in need of plenteous energy and have a low capacity to regenerate as they are post-mitotic tissues (Scarpelli et al., 2017). All mtDNA diseases lead to defects in respiration; nevertheless, the clinical phenotype of these diseases is manifold (Fig. 2). Still, some characteristics are frequently found in mitochondrial

diseases. Many patients present with a mix of neurological and myopathic symptoms, for instance myoclonic seizures, ataxia and muscle weakness. Muscle biopsies often show ragged-red fibers, originating from massive sarcolemmal proliferation of mitochondria. Another common symptom is lactic acidosis, resulting from the inability of muscles to perform proper respiration. Hence, pyruvate from glycolysis is converted to lactate and enters the blood stream. Examples of mitochondrial diseases include MERRF syndrome (myoclonic epilepsy with ragged-red fibers), featuring many of the classical symptoms mentioned above or MELAS syndrome (mitochondrial encephalomyopathy, lactic acidosis and stroke-like episodes), presenting with stroke-like episodes and infarctions in the brain (Chan, 2006).

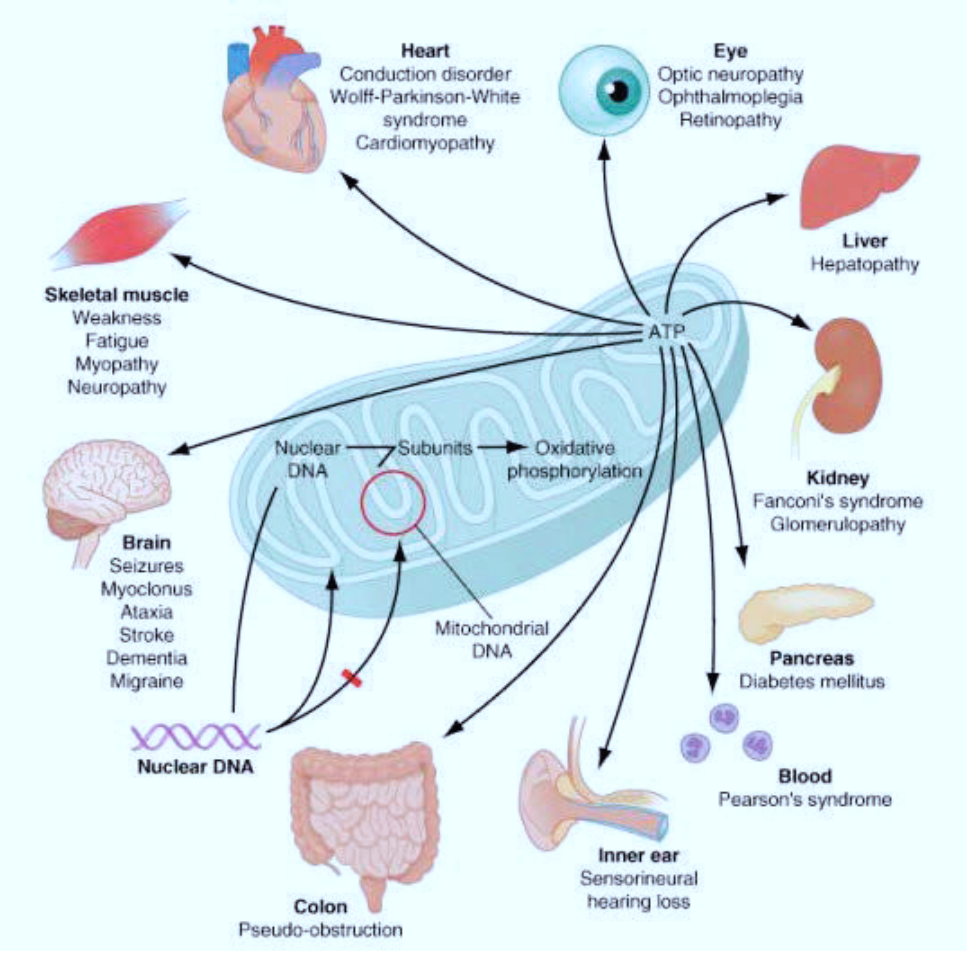

Figure 2: Typical manifestations of mitochondrial diseases. Mitochondrial diseases can present with manifold symptoms. Common are manifestations in brain, muscles and heart, as these tissues are post-mitotic and especially energy dependent and hence more vulnerable to mitochondrial dysfunctions. Other tissues can also be effected, such as the eyes (optic atrophy 1), the liver or kidneys (Image from Kasper et al., 2008).

Diseases caused by mtDNA mutations have different properties than diseases caused by genomic mutations, due to the different characteristics of mitochondrial biology. As they are transmitted only

maternally, the pattern of hereditability differs from other mutations and mutations cannot be compensated by a healthy father. Also, the severity of disease often increases with age, as mutations in mtDNA accumulate over time. mtDNA is distributed randomly among daughter mitochondria, which can lead to a unequal distribution of pathogenic DNA in different tissues by chance. This variation can lead to the accumulation of pathogenic mtDNA in specific tissues and beyond a certain threshold, cells lose their function. Tissues with a high energetic demand, such as the brain, skeletal muscle or heart are affected faster, as they strongly depend on respiration (Chan, 2006; DiMauro and Davidzon, 2005; DiMauro and Schon, 2003; Yoneda et al., 1994). Mutations in nuclear genes responsible for mitochondrial dynamics (explained in section 1.5.) can also cause a set of detrimental diseases, for instance, mutations in *MFN2* (mitofusin 2) can cause Charcot-Marie-Tooth subtype 2A. Diseases from this group are characterized by problems in long motor and sensory nerves, *e.g*. those enervating hands and feet (Züchner et al., 2004). *OPA1* (optic atrophy 1) mutations are the cause of autosomal dominant optic atrophy, a disease resulting in the loss of vision by degeneration of retinal ganglion cells (Alexander et al., 2000; Delettre et al., 2002). Apart from diseases directly associated with mutations in mtDNA or nuclear genes encoding for fusion and fission factors, a role of mitochondria in many other diseases has been discussed. Mitochondrial dysfunction might play a role in the pathogenesis of type 2 diabetes mellitus (T2DM). The most important feature of T2DM is insulin resistance, a state where the insulin receptor-activated cascade to activate glucose transporters is impaired. As defective mitochondria in the muscle can lead to a reduction in fatty-acid oxidation and thereby inhibit glucose transport it is possible that mitochondria have a role in this common disease (Gerbitz et al., 1995; Lowell and Shulman, 2005). Of note, there is evidence for an association between mitochondrial dysfunction and cancer. As mentioned above, many types of mitochondrial dysfunctions increase with age. Therefore, it was proposed that mitochondrial dysfunction with age could play a role in the carcinogenesis of age-related cancer (Singh, 2006). Additionally, many differences have been found between the structure and function of mitochondria in healthy cells and cancer cells. Differences were found with regard to metabolic activity, the molecular composition of the mitochondrial inner membrane (Garcea et al., 1980) and mutations of mtDNA were found in a variety of cancers (reviewed in Modica-Napolitano and Singh, 2004 and Singh, 2006). Neurodegenerative diseases are on the rise in western civilization and little is known about the mechanisms behind these disorders. Alzheimer's disease (AD) and Parkinson's disease (PD) are among the most common degenerative syndromes these days. Studies suggest a role of mitochondria also in the pathogenesis of these two disorders. It is suggested that misfolded proteins are translocated to the mitochondrial membrane where they could promote the release of cytochrome *c* thereby promoting apoptosis (Hashimoto et al., 2003).

For AD, evidence for mitochondrial contribution was already discovered as early as 1970, when electron microscopy studies revealed changes in the mitochondrial oxidative activity in neurons as well as a contribution of mitochondria to plaque formation (Johnson and Blum, 1970). Later it was found that the activity of mitochondrial enzymes pyruvate dehydrogenase and α-ketoglutarate dehydrogenase are decreased in the Alzheimer brain (Gibson et al., 1988; Sorbi et al., 1983). In addition, decreased oxygen consumption in the brain of AD patients was shown by positron emission tomography (PET) (Frackowiak et al., 1981), as well as a reduction in cytochrome oxidase activity (Parker et al., 1990). A more recent study by Kukreja *et al.* links the increase of mtDNA mutations with age to the accumulation of pathogenic amyloid plaques and atrophy in mice brains (Kukreja et al., 2014). However, despite a lot of research, it is still not clear whether a mitochondrial contribution to AD is a primary or secondary event or whether it is causative or not (Swerdlow, 2018). Evidence for an involvement of mitochondrial dysfunction in the pathogenesis of PD is manifold. Complex I deficiency has been found in the *substantia nigra* of *post-mortem* brain samples as well as a change in immunoreactivity against α-ketoglutarate in the brain, only to name a few (Orth and Schapira, 2002).

1.5. Mitochondrial dynamics and quality control

Mitochondria are highly dynamic organelles, which are connected to form a network in the entire cell and are constantly remodeling via fission and fusion events (Fig. 4). By this the network can distribute and mix solutes, metabolites and proteins (Chan, 2006), but also the electrochemical gradient (Twig et al., 2006). This mechanism suggests that the network is able to complement damaged mitochondria, thereby possibly recovering their function to maintain a healthy network within the cell (Chan, 2006). Fusion recruits functional mitochondria into the network, while fission can destine damaged mitochondria to be removed via autophagy or mitophagy (Elmore et al., 2001; Priault et al., 2005). In order to maintain a healthy mitochondrial network mitochondrial fission and fusion need to be balanced. Loss of fusion causes hyperfragmentation, the formation of numerous small and round mitochondria, which leads to the loss of mtDNA and severe defects in oxidative phosphorylation (Chen et al., 2005; Hermann et al., 1998). In turn, loss of fission leads to hyperfusion resulting in a highly interconnected tubular network with similar detrimental effects as loss of fusion (Hanekamp et al., 2002; Parone et al., 2008). Mitochondrial fusion requires the coordinated fusion of the inner and outer mitochondrial membranes (Fig. 3). This is mediated by two evolutionary distinct integral membrane proteins, MFN1 and MFN2, together with OPA1 in mammals (Meeusen et al., 2004). MFN1 and 2 are GTPases localized to the outer mitochondrial membrane and mediate fusion of this membrane. It is thought that the cytosolic parts of the proteins form complexes

with MFN1/2 from opposing membranes thereby tethering the membranes. The inner membrane is fused with the help of the dynamin-like GTPase OPA1. OPA1 is thought to tether inner mitochondrial membranes prior to fusion similar to MFN1/2 (reviewed in Friedman and Nunnari, 2014 and Hoppins et al., 2007). In order to fuse, mitochondria have to be in close proximity. Likely, this is achieved by cytoskeletal-dependent mitochondrial movement and positioning (Hoppins et al., 2007). How exactly fusion works on a mechanistic level still remains largely unknown. In mammals, mitochondrial fission is catalyzed by dynamin-related protein (DRP) 1, a GTPase with the ability to self-assemble. DRP1 assembles into helical structures and winds around the outer mitochondrial membrane at constriction sites (Ingerman et al., 2005; Labrousse et al., 1999). Interactions between the different GTPase domains on DRP1s catalyzes the hydrolysis of GTP, which in turn is believed to result in a conformational change of the helical structures coordinating the segregation of outer and inner mitochondrial membrane (Ford et al., 2011; Fröhlich et al., 2013). DRP1 localizes to discrete spots on the mitochondria, but only a subset of these spots mark future sites of fission. The recruitment mechanism of DRP1 to the mitochondria is still unclear, as most of the protein resides in the cytosol (Chan, 2006). Another fission protein is FIS1 (mitochondrial fission 1), whose distinct role in mammalian segregation of mitochondria is not yet clear. Knock-out of FIS1, an 18-kDa protein anchored to the outer membrane, in mammalian cells does not disrupt the localization of DRP1 (Lee et al., 2004). However, in yeast it is clear that Dnm1 (yeast homolog of DRP1) localization to mitochondria relies on the outer mitochondrial protein Fis1 and other adaptor proteins (Mozdy et al., 2000). FIS1 is discussed as a DRP1 receptor, but this is not yet known. Another possible DRP1 adaptor could be mitochondrial fission factor (MFF). Otera and colleagues analyzed the DRP1 recruitment in mammalian cells and found that MFF knock-down led to the release of DRP1 spots from the outer mitochondrial membrane together with a more tubular network. Further, overexpression of MFF markedly increased recruitment of DRP1 as well as mitochondrial fission. Additionally, they showed that fission can proceed in the absence of FIS1, supporting an important role of MFF as an adaptor for DRP1 (Otera et al., 2010). Furthermore, contact sites of the endoplasmic reticulum (ER) and mitochondria are discussed as designated sites of fission. It was found that mitochondrial division occurs at ER-mitochondrial contact sites and thereby mediates constriction even before recruitment of DRP1 (Friedman et al., 2011). This association could be due to ER proteins involved in fission or rather be mediated by mechanical forces (Friedman et al., 2011; Helle et al., 2017). Fission is essential for autophagy as it can produce metabolically different daughter mitochondria with reduced membrane potential. These are less likely to fuse back with the dynamic network and can easily be targeted by autophagy (Twig et al., 2008).

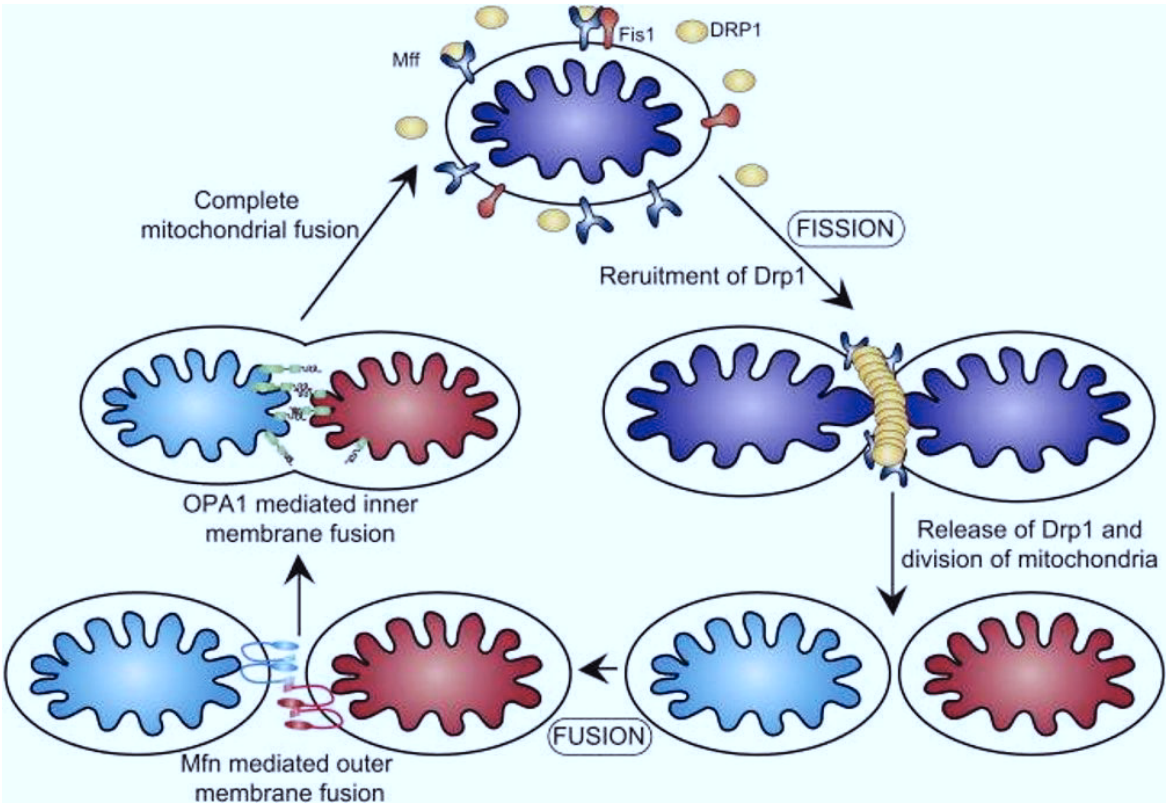

Figure 3: Mitochondrial fission and fusion. Fusion of the mitochondria outer membrane is mediated by MFN1/2, while fusion of the inner membrane is done by OPA1 (left). DRP1 facilitates mitochondrial fission, supported by adaptor protein MFF with a possible contribution of FIS1 (right) (Image modified from Osellame et al., 2012).

Autophagy is a highly conserved process, the name derives from Greek and literally means self-eating. Autophagy is needed to remove superfluous or damaged cell material or even full organelles in order to recycle *e.g*. the amino acids. Selective autophagy, in contrast to bulk autophagy, involves the removal of a specific cellular compartment or organelle. This requires a cargo-specific receptor protein to mark the cargo for degradation. The disposal is then mediated by a general machinery forming the double-membrane autophagosome around the cargo. The autophagosome fuses with the lysosome to form the autolysosome where lysosomal enzymes degrade the contents to reusable units, for example amino acids. The latter steps are general and identical for bulk autophagy and specific autophagy. The selective degradation of mitochondria is termed mitophagy. This is a crucial step of mitochondrial quality control to remove dysfunctional mitochondria. A key function of the fusion-fission dynamics is to prevent damaged mitochondria to fuse back to the network, which are then disposed by mitophagy (Figge et al., 2013; Schäfer and Reichert, 2009; Twig et al., 2008). Naturally, accurate organelle turnover requires removal and biogenesis (Fig. 4). Mitochondrial biogenesis is crucial for maintaining healthy mitochondria

and can be triggered, *e.g.* by different stimuli such as exercise or cold exposure and is mediated via the transcriptional coactivator PGC-1α (Seo et al., 2010).

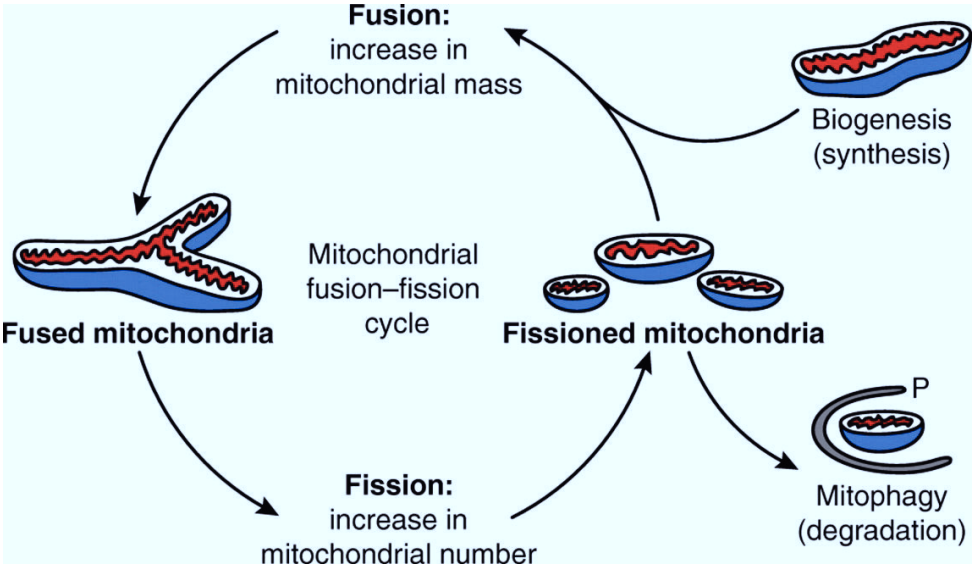

Figure 4: Mitochondrial fission and fusion dynamics. Mitochondria undergo constant fusion and fission cycles. If mitochondria are damaged they lose the ability to fuse back to the network and can be degraded by mitophagy. To maintain a healthy network mitochondrial biogenesis provides new mitochondria when needed (Image from Seo et al., 2010).

Mitochondria can be removed by the receptor-mediated pathway, where a membrane-bound receptor is activated by phosphorylation and then interacts with a protein on the autophagosomal membrane (*e.g.* microtubule-associated protein 1B light chain 3 (LC3)) and is degraded after fusion with the lysosome. Another pathway is the ubiquitin-mediated pathway, where proteins on the outer mitochondrial membrane become ubiquitinated, then recruit adapter proteins, such as p62, which in turn recruit autophagosome membrane-bound proteins (Fig. 5). The autophagosome fuses with the lysosome and mitochondria are degraded (reviewed in Zimmermann and Reichert, 2018). The maintenance of mitochondrial quality control employing fusion, fission, mitophagy and mitochondrial biogenesis are crucial to maintain a healthy organelle and cellular environment.

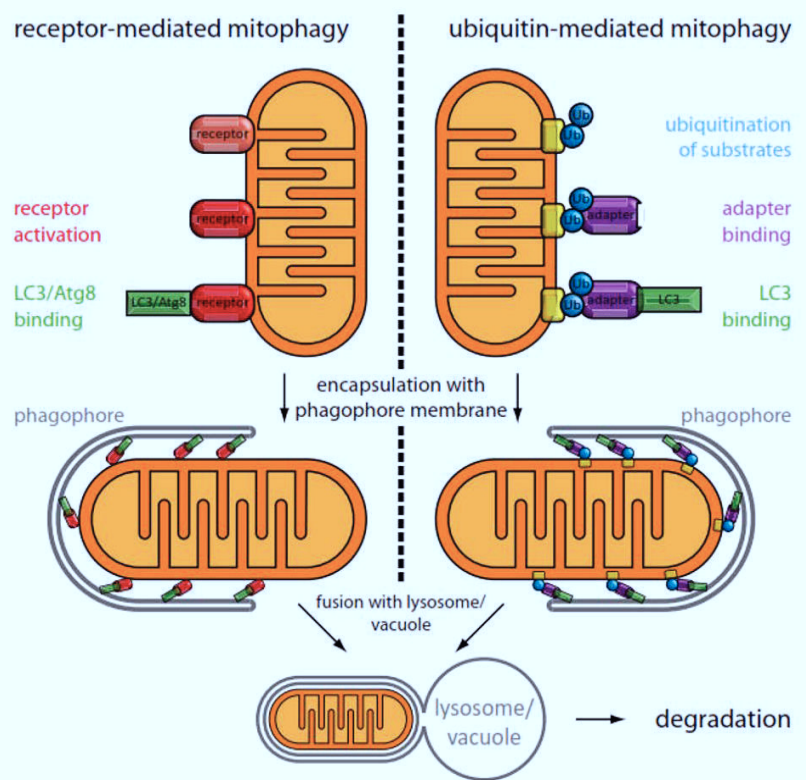

Figure 5: Pathways of mitophagy. Removal of mitochondria can be mediated by the receptor-mediated or the ubiquitin-mediated pathway. In the receptor-mediated mitophagy (left) a receptor on the outer mitochondrial membrane is activated and then binds a protein on the phagophore membrane, *e.g.* LC3. In the ubiquitin-mediated mitophagy (right) a substrate on the outer mitochondrial membrane is ubiquitinated. An adapter binds to the ubiquitin, which then in turn binds to LC3 on the phagophore membrane. In both pathways the mitochondrion is encapsulated by the phagophore membrane after LC3-binding, this fuses with the lysosome and mitochondria are degraded (Image from Zimmermann and Reichert, 2018).

1.6. Glutamate dehydrogenase

Glutamate dehydrogenase (GDH) catalyzes the reversible oxidative deamination of glutamate to α-ketoglutarate and ammonia using the co-factor NAD^+ (Smith, 1979). Mammalian GDH is a protein with the size of about 56 kDa (Mastorodemos et al., 2009) and consists of 558 amino acids (UniProt P49448, UniProt P00367). Humans have two isoforms of GDH, encoded by two distinct genes: *GLUD1* and *GLUD2*. Intron-containing *GLUD1* is widely expressed, and sometimes referred to as a housekeeping gene (Mavrothalassitis et al., 1988). On the other hand, *GLUD2* is an X-linked intronless gene, which is expressed mainly in neural and testicular tissues (Shashidharan et al., 1994). Of note, all mammals carry the *GLUD1* gene; however, *GLUD2* can only be found in humans and great apes. The evolution of *GLUD2* is thought to result from retroposition of the *GLUD1* gene in an ape ancestor less than 23 million years ago (Burki and

Kaessmann, 2004; Shashidharan et al., 1994). The two isoforms have different properties. For instance, GDH1 is heat resistant, while GDH2 is heat labile (Plaitakis et al., 2000; Shashidharan et al., 1997). GDH1 and GDH2 are highly homologous with about 97% amino acid sequence similarity when omitting the targeting sequence (Mastorodemos et al., 2009). GDH2 is localized to mitochondria, while GDH1 can be found in the cytosol as well as in mitochondria (Rosso et al., 2008). Human glutamate dehydrogenase 1 (hGDH1) shows high levels in liver, brain and kidney, while hGDH2 is found mainly in Sertoli cells of human testis, kidney and the brain. In the human brain, hGDH2 is expressed in astrocytes (Zaganas et al., 2012). *In vivo*, under physiological conditions GDH almost exclusively catalyzes the reaction towards the direction of the oxidative deamination of glutamate, producing α-ketoglutarate and free ammonia. This is most likely due to the high concentrations of glutamate and rather low concentrations of ammonium ions in the mitochondria (Adeva et al., 2012). Nevertheless, from the chemical side the reaction is reversible (Fig. 6). Glutamate dehydrogenase in mammals is an enzyme of key importance. Not only does it catalyze the conversion of glutamate to α-ketoglutarate, thereby being an important reaction of anaplerosis. Additionally, it interconnects amino acid and carbohydrate metabolism and is involved in energy production, ammonia management and neurotransmitter recycling.

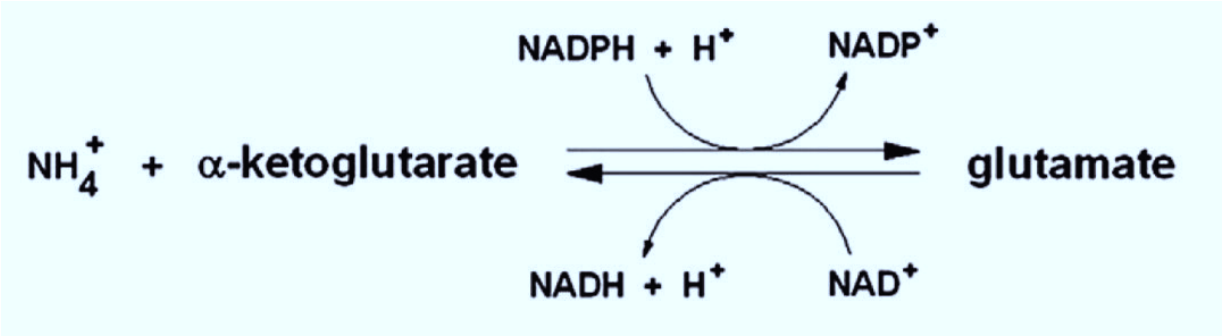

Figure 6: Reaction catalyzed by glutamate dehydrogenase. The enzyme glutamate dehydrogenase (GDH) catalyzes the NAD^+-dependent oxidative deamination of glutamate into α-ketoglutarate and *vice versa*. The formation of glutamate produces H_2O, while together with α-ketoglutarate H^+ and NH_4^+ is formed. As α-ketoglutarate is part of the TCA-cycle the GDH reaction is an important anaplerotic reaction (Image from: Adeva et al., 2012).

1.7. Energy and ammonia metabolism in the human brain

Besides oxidative phosphorylation, glycolysis is another way for the cell to generate ATP and is located outside of mitochondria in the cytosol. Glycolysis breaks down glucose and can occur in the absence (anaerobic) or presence of oxygen (aerobic). The end product of the anaerobic glycolysis is lactate, while

pyruvate is the end product of the aerobic pathway. The net output of glycolysis are two ATP and two NADH molecules. Under aerobic conditions the energy pathway proceeds to the TCA-cycle and OXPHOS thereby generating considerably more ATP from one molecule of glucose than from glycolysis alone. Pyruvate links glycolysis and the other energy-producing pathways downstream. Pyruvate, produced by glycolysis, is converted into acetyl-CoA, which enters the TCA-cycle (Fig. 1). (Akram, 2013; Müller-Esterl, Biochemie, 1st edition 2004).

The brain is a heterogenous tissue consisting of neurons and non-neuronal cells, the glial cells. Glial cells have three subtypes, namely oligodendrocytes, microglia and astrocytes. Little is yet known about the metabolism of oligodendrocytes and microglia. The metabolism of neurons and astrocytes have distinct features. Both take up glucose and utilize it through glycolysis, followed by the TCA-cycle and oxidative phosphorylation. However, net production of TCA-cycle intermediates occurs only in astrocytes, as this requires carboxylation of pyruvate to form oxaloacetate, a reaction catalyzed by pyruvate carboxylase, which is not present in neurons. One of the TCA-cycle intermediates is α-ketoglutarate, which can be utilized to form the neurotransmitters glutamate or γ-aminobutyric acid (GABA) in neurons. As there is no net production of these important intermediates the astrocytes provide neurons with important molecules, serving as the housekeeping cells of neurons (reviewed in Hertz and Kala, 2007). Glutamine is mostly produced by astrocytes via the glutamine synthetase (GS), whose expression in the brain was predominantly found in astrocytes (Yamamoto et al., 1987). GS catalyzes the synthesis of glutamine from glutamate and free NH_4^+ in an ATP-dependent reaction. Glutamine is then transferred from astrocytes to neurons, where it is hydrolyzed by phosphate-activated glutaminase (PAG) and used for the production of the neurotransmitters glutamate and GABA, hereby releasing ammonium ions. Additionally, glutamate released as a neurotransmitter is recycled by astrocytes and again used to produce glutamine by the GS. This process is also called the glutamate-glutamine cycle and is tremendously important for the proper function of excitatory neurotransmission by neurons (Fig. 7) (Adeva et al., 2012; Stobart and Anderson, 2013).

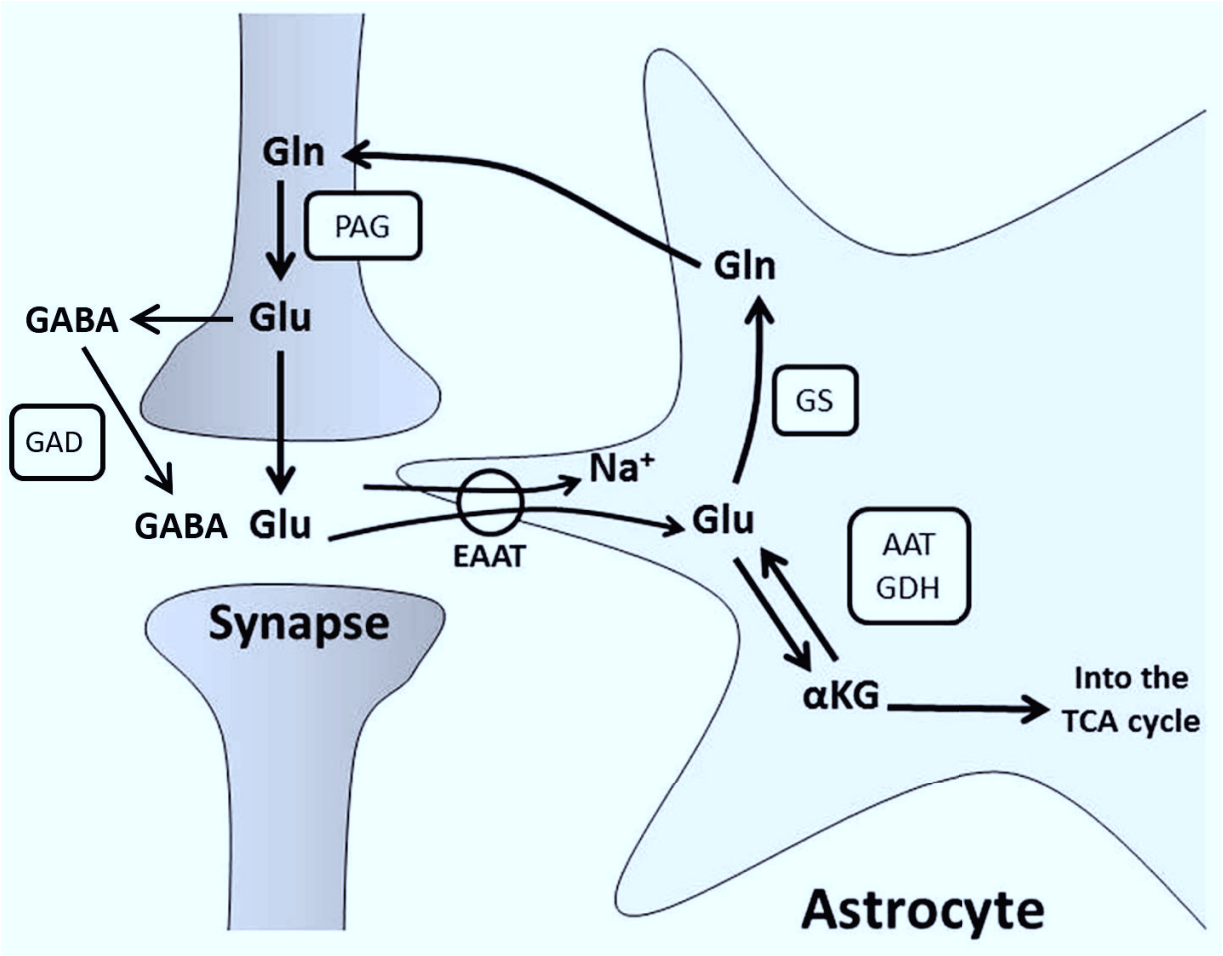

Figure 7: Glutamate-glutamine cycle. Astrocytes provide neurons with glutamine (Gln), which is converted to glutamate (Glu) by phosphate-activated glutaminase (PAG) in the neurons. Glutamate is a neurotransmitter and is taken up from the synaptic cleft by astrocytes via the excitatory amino acid transporter (EAAT), to be recycled back to glutamine by glutamine synthetase (GS). Alternatively, glutamate can be reversibly converted to α-ketoglutarate by glutamate dehydrogenase (GDH) or aspartate aminotransferase (AAT), which is an important metabolite for the TCA-cycle. For GABAergic neurotransmission glutamate is converted to γ-aminobutyric acid (GABA) by glutamate decarboyxlase (GAD). GABA recycling is not depicted (Image modified from Stobart and Anderson, 2013).

Another process in the brain confined to astrocytes is glycogenolysis and glycogen degradation. Glycogen serves as a high-molecular carbohydrate storage, which can be rapidly converted into pyruvate or lactate and metabolized in the TCA-cycle in situations of high energy demands. Similarly, acetate oxidation to form acetyl-CoA for the TCA-cycle can only be performed in astrocytes, but not in neurons (Adeva et al., 2012; reviewed in Hertz and Kala, 2007). Hence, neurons depend on astrocytes for many reactions and pathways of utmost importance. Additionally, ammonia has an important role in many of these important reactions. Generally, ammonia dissolves in water to form ammonium ions (NH_4^+), which are incorporated into amino

acids and other nitrogen-containing molecules. In aqueous solutions, ammonia is a base (NH_3). The pK_a of the reaction $NH_3 + H^+ \rightarrow NH_4^+$ (and *vice versa*) is 9.3. Therefore, at physiological pH (ca. 7.4) mostly the protonated form NH_4^+ is present. The physiological concentration of ammonium in human plasma is 0.2-0.3 mM (Suárez et al., 2002) and ammonium ions are continually produced and consumed during cell metabolism. Some important reactions were already described above, including the GS and GDH reactions. These two enzymes are among the enzymes primarily involved in the metabolism of free ammonium ions. The reaction catalyzed by the mitochondrial glutaminase (Gln --> Glu + NH_4^+) also releases a free ion. Similarly, asparaginase produces free ammonium and aspartate from asparagine. Aminotransferases, cytosolic and mitochondrial enzymes, transfer amino groups between amino acids and their corresponding keto acids; however, without the generation or consumption of free ammonium ions (reviewed in Adeva et al., 2012). Usually, free ammonia is detoxified and removed from the body via the urea-cycle, mainly in the liver, and subsequent excretion via urine through the kidneys. However, the urea-cycle is not present in brain cells and hence, ammonium cannot be detoxified this way from the brain (Stryer, Biochemie, 8th edition 2018).

1.8. Hepatic encephalopathy

Hepatic encephalopathy (HE) is a common neuropsychiatric complication in patients with severe liver damage. About 50-70% of patients with liver cirrhosis develop HE or minimal HE (Al Sibae and McGuire, 2009; Patidar and Bajaj, 2015). As HE is symptomatically not very different from encephalopathies with other causes, the presence of a severe liver dysfunction is necessary for the diagnosis. Liver failure can result from alcohol or drug abuse, hepatitis infection or liver cancer, but HE can also be a consequence of a portosystemic shunt, which leads to the distribution of blood derived from the intestine into the body circulation without prior removal of toxins through the liver (Cash et al., 2010). HE has long been considered a fully reversible condition after liver transplantation; however, in 2010 a persistence in cognitive impairment in patients with preceding episodes of overt HE was reported (Bajaj et al., 2010). Others have shown a reversibility of learning impairment after liver transplantation (Acharya et al., 2017). Therefore, the full reversibility of HE after liver transplantation still remains controversially discussed. In any way, liver transplantations remain the only curative option and offer a huge improvement on the quality of life of HE patients.

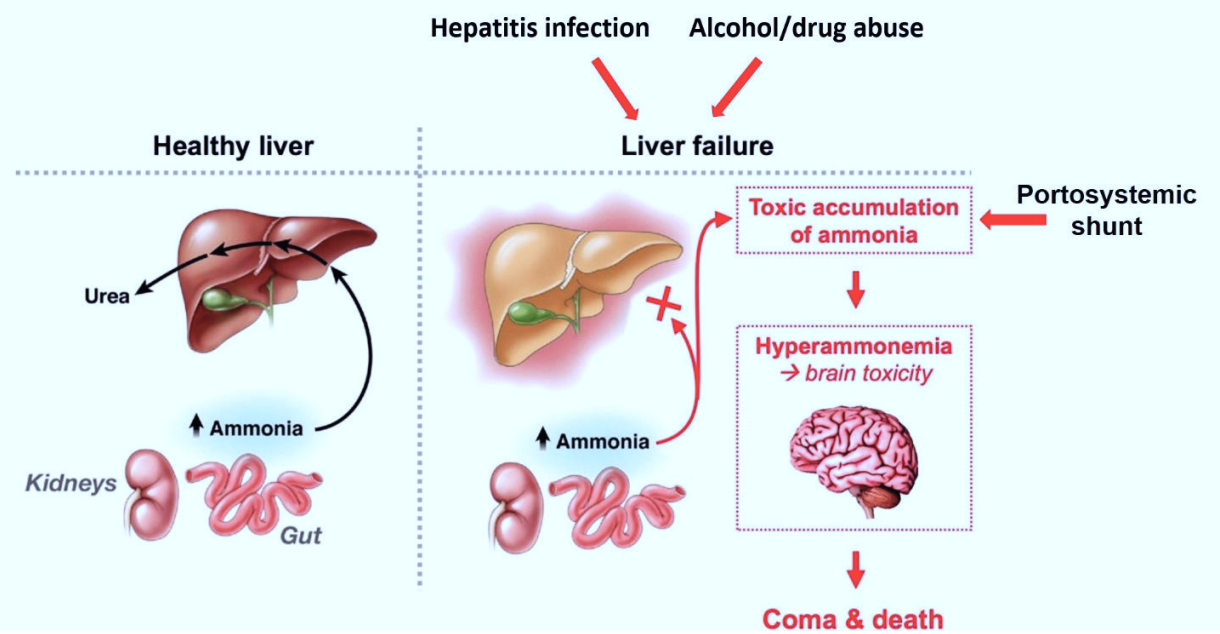

Figure 8: Pathogenesis of hepatic encephalopathy. In healthy people, ammonia derived from the gut and other minor sources is converted to urea in the liver and excreted via the kidneys. In the case of liver failure, due to hepatitis infection, alcohol/drug abuse or after portosystemic shunting ammonia cannot be properly detoxified by the liver and thus accumulates in the blood stream. From there it can enter the brain, in detail astrocytes, through the blood-brain-barrier and lead to hepatic encephalopathy. Symptoms can be severe, leading to hepatic coma and death (Image modified from Jalan and Lee, 2009).

Severe symptoms can be found in about 30% of patients after portosystemic shunt surgery and approximately 30% of patients with end-stage liver disease have severe encephalopathy approaching hepatic coma (Al Sibae and McGuire, 2009). Symptoms can be mild to severe, ranging from personality changes, impaired intellect, disturbed sleeping and depressed level of consciousness to hepatic coma and death (Cash et al., 2010). HE with cirrhosis has a very poor prognostic and, without liver transplantation, the one-year survival rate is only 42% after the first episode of HE. Liver transplantation still is the only curative approach of the disease (Bustamante et al., 1999). Patients with liver failure suffer from neurological dysfunctions; however, despite decades of research the mechanisms causing these dysfunctions are still largely unknown (Cash et al., 2010).

Classifications of HE

The degree of mental disturbances in patients with HE is classified by the West-Haven criteria. If patients are in coma the Glasgow Coma Scale is a more reliable test. Another possibility is the use of the portal-systemic encephalopathy score to describe the clinical severity of HE. This evaluates the following parameters: mental status, presence and intensity of asterixis (also known as “flapping tremor”), time

needed to complete tests for intellectual function, venous ammonia levels and abnormalities in the electroencephalogram. In clinical practice still the West-Haven criteria are most commonly used. They are based on the level of consciousness, personality and intellect, neurological signs and electroencephalogram (Cash et al., 2010) and categories are minimal and grade I to IV (Ferenci, 2017). Two classification systems are used to assess HE. One is based on the underlying hepatic abnormality and the types of HE are termed A (for **A**cute liver failure), B (for portosystemic **B**ypass) or C (for **C**irrhosis) (Ferenci et al., 2002). The second is based on duration and characteristics of neurological dysfunction and is divided into episodic HE, persistent HE and minimal HE. Episodic HE occurs over a short time span and differs in severity, often initiated by precipitating factors. Persistent HE is a chronic progression and minimal HE presents with only subtle cognitive impairments. The first two types are often called overt HE opposed to minimal HE, which can also be called covert HE (Cash et al., 2010; Ferenci et al., 2002; Patidar and Bajaj, 2015).

Pathogenesis of HE

There are many hypotheses on the pathogenesis of HE, which are not necessarily mutually exclusive. One of the most widely accepted hypothesis suspects ammonia to be the primarily responsible neurotoxin. The gastrointestinal tract produces most of the body's ammonia by bacterial digestion of nitrogenous sources and from break-down of glutamine by the enterocytes. In the healthy person, ammonia is transported to the liver via the portal vein. There, ammonia is detoxified via the urea cycle and can be excreted through the kidneys (Patidar and Bajaj, 2015). If liver dysfunction is too severe, the organ is not capable of detoxifying ammonia properly and hence, the toxin accumulates in the blood stream (Fig. 8, 9). Another source of ammonia in patients is muscle wasting, which is a common complication in patients (Fig. 9). Muscles are a second important site for ammonia-removal next to the liver (Ferenci, 2017) and play a minor, yet significant, part in ammonia removal via glutamate in the skeletal muscles (Patidar and Bajaj, 2015). Ammonia levels in the blood rise and the toxin can pass the blood-brain-barrier (Ott and Larsen, 2004) and enter the astrocytes. Astrocytes, which account for about 30% of the cortical brain mass, are the brain cells that primarily metabolize ammonia and hence, changes in this cell type are considered the most important factors in brain dysfunctions (Häussinger et al., 2000).

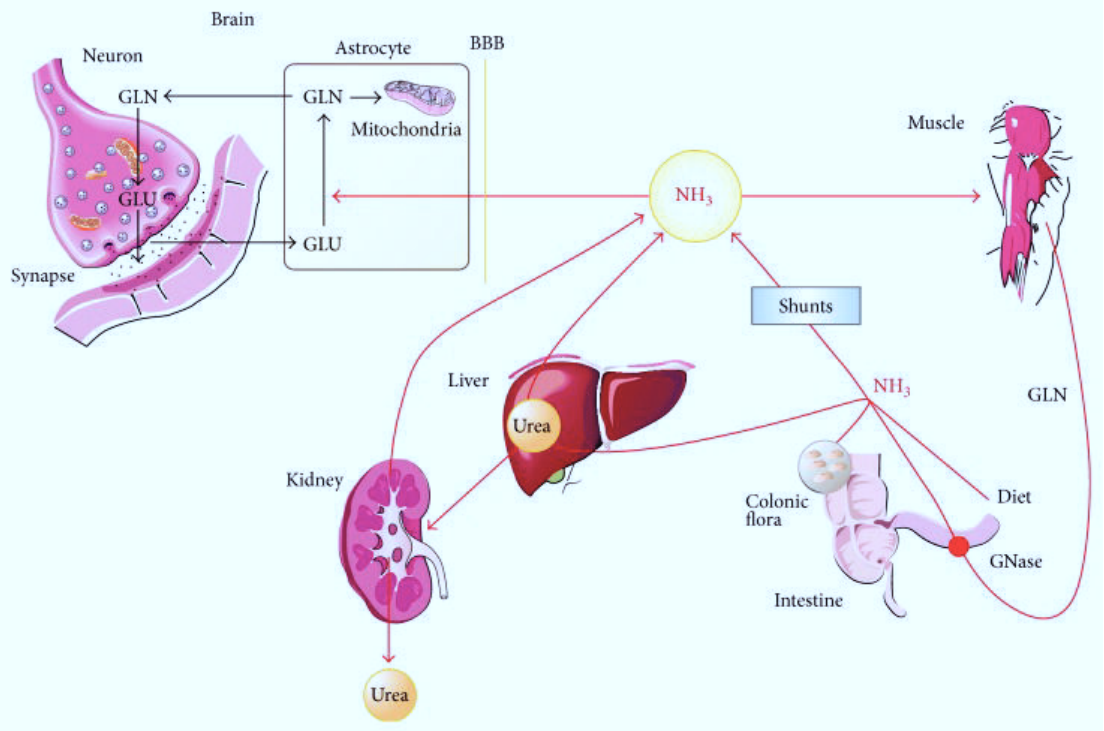

Figure 9: Fate of ammonia. Ammonia (NH_3) is derived from the intestine and, in smaller amounts, from the skeletal muscles. In healthy people, it is transformed to urea in the urea cycle in the liver and excreted via the kidneys. In portosystemic shunting ammonia does not reach the liver for detoxification. Ammonia can enter the astrocytes in the brain through the blood-brain-barrier (BBB). Ammonia is incorporated into glutamine (GLN). Glutamine is transported to the neurons where it is converted to glutamate (GLU) as a neurotransmitter and is recycled by the astrocytes (Image from Cordoba, 2014).

Astrocytes serve as “housekeepers” for neurons, providing them with nutrients (Norenberg, 1987). They are mostly affected by hyperammonemia, most likely, because ammonia is primarily metabolized by glutamine synthetase in astrocytes (Martinez-Hernandez et al., 1977). In patients suffering from HE, 90% have elevated serum ammonia concentrations and the health state of patients is improving when lowering the concentration of ammonium in the serum. However, for unknown reasons, sometimes the concentration of ammonia in the blood only poorly correlate with severity of disease. Possibly, this results from an increased uptake in the brain independent of serum concentrations. Studies also show a strong correlation between glutamine (possibly derived from ammonia) in the cerebrospinal fluid (CSF) and the degree of HE (Cash et al., 2010; Watanabe et al., 1984). In addition to the ammonia derived from the gut, several precipitating factor can cause an increase in ammonia concentrations and lead to an aggravation of HE or initiate an episode of HE. Precipitating factors can be gastrointestinal bleeding, kidney injury,

constipation, electrolyte imbalances, certain medications (*e.g.* benzodiazepines), infection or diet (Cash et al., 2010; Patidar and Bajaj, 2015).

Treatment options

General treatment focusses on the reduction of precipitating factors and plasma levels of ammonia. Managing precipitating factors is especially important as almost 90% of patients can be treated by prevention of these factors (Strauss et al., 1992). Episodes of overt HE can be treated with drugs described in the following paragraph; however, most of them were not subject to randomized controlled studies, but are merely used based on clinical observations (Ferenci, 2017). Non-absorbable disaccharides, such as lactulose, are applied orally or with an enema in order to control bowel movements. Additionally, the substance is thought to promote growth of *Lactobacillus bifidus*, whose metabolism produces less ammonia in the colon than other bacteria, due to decreased urease activity. Lactulose is not digested and reaches the intestine, where it is metabolized by the gut flora to lactate and acetate, causing a decrease of fecal pH and thereby increasing fecal nitrogen excretion. Hence, less ammonia reaches the blood stream (Cordoba, 2014; Ferenci, 2017). The antibiotic Neomycin can be used as it inhibits the enzyme glutaminase (Hawkins et al., 1994). However, it can be toxic after long-term use (Cordoba, 2014). Rifaximin, a broad-spectrum antibiotic is widely used in HE treatment, because antibiotics are known to reduce the intestinal flora, thereby automatically reducing the amount of produced ammonia by bacteria. The administration of oral branched-chain amino acids (BCAAs) is an additional treatment option; however, the mechanism of action of this treatment is not known. The improved clinical outcome might be due to a positive nutritional effect of BCAA supplementation. Drugs serving as metabolic ammonia scavengers are frequently used. These have been used for patients with inborn urea-cycle defects for many years and include ornithine phenylacetate and glyceryl phenylbutyrate (Cordoba, 2014; Ferenci, 2017). L-ornithine-L-aspartate (LOLA) is involved in the muscular and hepatic metabolism of ammonia and can be given enteral or parenteral to enhance the metabolic conversion and thereby detoxification of ammonia in both tissues (Al Sibae and McGuire, 2009). For many years the dietary recommendation for HE patients was to restrict protein intake to avoid ammonia from amino acid catabolism. Nowadays, this approach is not followed anymore as there was no evidence for any benefits to clinical outcomes. On the contrary, malnutrition will lead to an even weaker health state of patients. The recommendations now are small snacks distributed over the day including a late-night snack to avoid periods of fasting (Cordoba, 2014; Ferenci, 2017). Importantly, none of these treatments are a curative approach and only serve to decrease symptoms and end acute episodes of HE or to prevent new episodes in recurrent HE.

Effects of hyperammonemia and precipitating factors

Several consequences of hyperammonemia have already been described. When ammonia crosses the blood-brain-barrier it enters the astrocytes. Ammonia detoxification in these cells by glutamine synthetase leads to the accumulation of glutamine, which causes astrocyte swelling (Cash et al., 2010). One explanation for this could be the increase in intracellular osmolarity from the formation of glutamine. That glutamine concentrations are indeed increasing in the brain of HE patients has been determined in autopsy brain tissues (Ferenci, 2017). This could also be the reason for the development of brain edema. In a rat model it was shown that brain swelling secondary to ammonia infusion can be prevented by inhibitors of glutamine synthesis. Other factors such as hyponatremia can enhance the effects of ammonia on brain swelling even more (Cordoba, 2014; Córdoba et al., 1998). Brain edemas are dangerous as they can progress to intracranial hypertension and lead to subsequent death (Cordoba, 2014). Inflammation counts as one of the precipitating factors of HE and is also an important pathological aspect. Patients with cirrhosis suffer from liver inflammation, which can lead to changes in the intestinal microbiota. This is exacerbated further by infections or gastrointestinal bleeding. Obesity is also known to change the composition of the gut microbiota. The pro-inflammatory milieu together with a change in microbiota releases even more pro-inflammatory cytokines. This, together with high levels of ammonia, can contribute to the development of cerebral edema (Patidar and Bajaj, 2015). It has been suggested that ammonia can bind to the GABA receptor complex on astrocytes, which can lead to the production of neurosteroids, which are known GABA agonists (Palomero-Gallagher and Zilles, 2013). Derivatives of neurosteroids are benzodiazepines and benzodiazepine-like substances. GABA is the main inhibitory neurotransmitter in the human brain and functions through the GABA receptor complex. Therefore, elevation in neurosteroids can inhibit neurotransmission (Ahboucha and Butterworth, 2004; Cash et al., 2010). If possible the administration of exogenous benzodiazepines should be stopped in HE (Cash et al., 2010); however, it has been proposed that endogenous benzodiazepines-like compounds with a GABA agonist effect exist (Butterworth, 2016). Two neurosteroid precursors, allopregnanolone and pregnanolone were found in the brains of hepatic coma patients increased to pathophysiologically relevant concentrations (Butterworth, 2016). Data to support the role of GABA agonists in the pathogenesis of HE have shown a transient improvement of the mental state of some patients after treatment with flumazenil, which is a benzodiazepine receptor antagonist (Barbaro et al., 1998). Nevertheless, it is not known exactly why natural benzodiazepine-like substances increase in HE patients. Only in a rat HE model it has been shown so far that precursors for natural benzodiazepines were produced by the intestinal microbiota (Yurdaydin et al., 1995). Also, an increase of GABA has been shown in the CSF of HE patients (Al Sibae and McGuire, 2009).

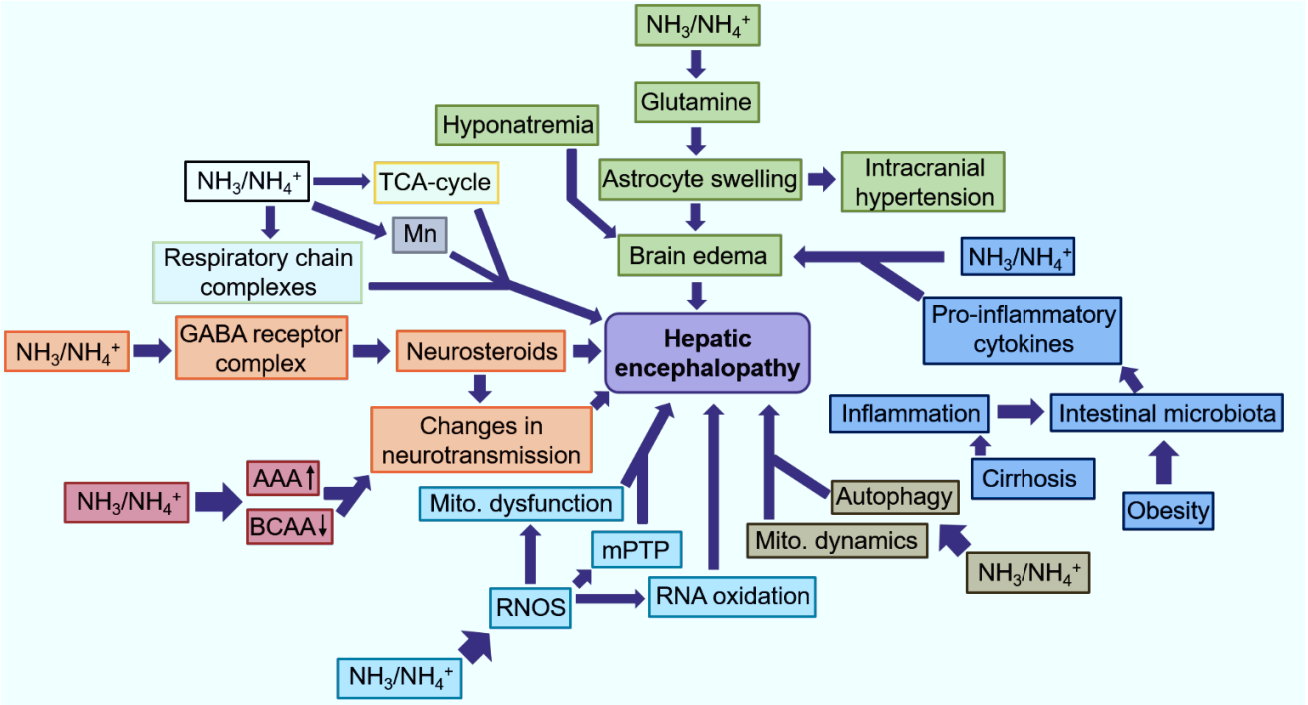

Figure 10: Possible consequences of hyperammonemia. Many mechanisms are discussed on how high ammonia leads to hepatic encephalopathy. This scheme gives an overview of all major pathways discussed in the text. GABA: γ-aminobutyric acid, Mn: Manganese, AAA: aromatic amino acids, BCAA: branched chain amino acids, RNOS: reactive oxygen/nitrogen species, mPTP: mitochondrial permeability transition pore, mito.: mitochondrial.

Other neurotransmitters such as serotonin, acetylcholine and glutamate are also discussed to contribute to the pathogenesis of HE. As an example, glutamate neurotransmission was disturbed in a rat model of HE (Michalak et al., 1996). The neurotransmission of the brain is regulated by amino acids and their precursors, a disturbance of the concentrations and balances can be detrimental. It was found that in patients with severe liver dysfunction the plasma concentrations of the aromatic amino acids (AAA) tryptophan, tyrosine and phenylalanine were increased, while BCAAs were decreased, compared to healthy controls. This can result in the production of false neurotransmitters, namely octopamide and phenylethanolamide. An imbalance in BCAAs and AAAs has also been speculated to competitively inhibit the normal neurotransmitters dopamine and norepinephrine (Capocaccia et al., 1979; Ferenci and Wewalka, 1978; Morgan et al., 1978). Serotonin is a neurotransmitter with a broad function and has also been suggested to contribute to HE. The metabolism of serotonin has been found to be selectively sensitive to the degree of portosystemic shunting and hyperammonemia in the rat brain. Serotonin and its precursors were significantly increased in the brains of rats with a portal vein stenosis, mimicking HE (Lozeva et al., 2004). Difficulties in movement (*e.g.* spasms, restlessness, tremor) could result from dopaminergic dysfunctions. Interestingly, the observed accumulation of manganese in the basal ganglia of

patients could be a compensatory mechanism of the brain as manganese can normalize low levels of dopamine in basal ganglia (Montes et al., 2001; Rose et al., 1999). Nonetheless, manganese in higher concentrations can also be toxic. As symptoms of HE are similar to those after manganese intoxication it is not clear whether the accumulation of manganese in basal ganglia is beneficial or detrimental and whether symptoms of HE possibly result from increased manganese levels (Cash et al., 2010; Cordoba, 2014). Another mechanism has emphasized a possible role of oxidative and nitrosative stress. An increase of free radicals can lead to mitochondrial dysfunction, energy failure as well as an opening of the mitochondrial transition pore (Häussinger and Schliess, 2008; Norenberg et al., 2004). Another link between ROS and reactive nitrogen species (RNS) and ammonia toxicity is RNA oxidation. It was found in mice and rats that cerebral RNA oxidation in astrocytes and neurons is another consequence of hyperammonemia. RNA oxidation can effect gene expression and local protein synthesis, opening up a whole new possible mechanism in the pathogenesis of HE (Görg et al., 2008). In cultured rat astrocytes and *post-mortem* brain tissues of patients, biomarkers for senescence were increased and proliferation in cultured cells was reduced. In detail, proliferation induced by epidermal growth factor and brain-derived neurotrophic factor was inhibited, pointing towards an association of ammonia toxicity and premature astrocyte senescence (Görg et al., 2015). In a rat model it was shown that after bile duct ligation the enzyme activity of the respiratory chain complexes was decreased in many brain regions, which suggests a role of mitochondria in ammonia-induced toxicity (Dhanda et al., 2017). Another observation with regards to a mitochondrial contribution to HE is a change in mitochondrial dynamics and autophagy in the *substantia nigra* of mice with acute liver failure. Fission of mitochondria as well as mitophagy were induced in the *substantia nigra* of HE mice (Bai et al., 2018). Furthermore, a study in rats with induced acute liver failure showed an inhibition of the respiratory chain complexes I, III and IV in the cerebellum and cerebral cortex of the animals (Boer et al., 2009). Additionally, a role of the TCA-cycle has been discussed. Some TCA-cycle enzymes, *e.g.* pyruvate dehydrogenase and isocitrate dehydrogenase were discussed to be inhibited by ammonia (Katunuma et al., 1966; Zwingmann et al., 2003). Research regarding changes in the TCA-cycle and pathogenesis of HE show many discrepancies. Different results were found regarding the levels of different TCA-cycle intermediates (α-ketoglutarate, citrate, oxaloacetate) as well as enzyme activity, *e.g.* activity of α-ketoglutarate dehydrogenase (α-KGDH). Possible reasons for the discrepancies could be different HE models or the varying duration of ammonia exposure (reviewed in Rama Rao and Norenberg, 2012).

There is evidence that many pathological mechanisms exist or even co-exist (summarized in Fig. 10). Nevertheless, there is no doubt that an increase in ammonia concentration is the most important characteristic of hepatic encephalopathy (Cash et al., 2010). Additionally, it is clear that HE is at least partly

a secondary effect of altered communication between astrocytes and neurons leading to a disturbance in consciousness (Cordoba, 2014).

1.9. Objectives and aims

Despite decades of research little is known about the early events in the pathogenesis of hepatic encephalopathy and the molecular mechanisms behind it. It is clear that the increase in ammonia concentration plays an important role in disease development; however, how exactly an increase in ammonia mediates neurological dysfunctions remains fundamentally unknown. Recent research points towards a role of mitochondria in HE pathogenesis. An increase in mitochondrial fission and mitophagy was found in the *substantia nigra* of a mouse model of HE (Bai et al., 2018). In a rat model induction of HE led to a decrease in activity of the respiratory chain enzymes (Dhanda et al., 2017), as well as in the brain of a rat model of acute liver failure (Boer et al., 2009). Additionally, some studies point towards a role of the TCA-cycle and energy metabolism in HE pathogenesis. For example, an inhibition of the enzymes pyruvate dehydrogenase and isocitrate dehydrogenase by ammonia was found (Katunuma et al., 1966; Zwingmann et al., 2003). However, contradicting results were found on this issue and a contribution of the TCA-cycle is still controversially discussed.

Dysfunctional mitochondria also play a role in many other diseases, such as autosomal optic atrophy 1 or Parkinson's disease (Delettre et al., 2002; Orth and Schapira, 2002). Contributions of mitochondria have been found in the pathogenesis of diabetes (Gerbitz et al., 1995; Lowell and Shulman, 2005) and cancer (Modica-Napolitano and Singh, 2004; Singh, 2006), but especially in neurodegenerative diseases. These examples are only few to emphasize the importance of mitochondria in human health.

As mentioned above, there is increasing evidence of a contribution of mitochondria in the pathogenesis of HE. HE is a common neurological dysfunction in liver failure leading to death. To date there is no cure besides liver transplantation and even after transplantation it is not yet clear if full neurological function is restored. Hence, the aim of this research was as follows:

General aim: Determine the role of mitochondria in the pathogenesis of hepatic encephalopathy.

In detail the following questions were addressed:

1. What is the role of mitochondrial fission and fusion dynamics?
2. Is there a change in mitochondrial bioenergetics induced by ammonia in astrocytes?
3. Does hyperammonemia result in metabolomic changes?
4. What are the molecular mechanisms in the pathogenesis of HE?
5. What can be done to determine possible treatment options against HE?
6. Are there so far unknown factors contributing to the pathogenesis of HE?

2. Material and methods

2.1. Chemicals, kits and media

Table 1: Chemicals, kits and media used in this study

Name	**Company**
^{15}Ammonium chloride ($^{15}NH_4Cl$)	Sigma-Aldrich, Taufkirchen, Germany
Acetonitrile	VWR, Radnor PA, USA
Agar	Sigma-Aldrich, Taufkirchen, Germany
Albumin, fraction V (BSA)	Carl Roth GmbH & Co. KG, Karlsruhe, Germany
AllPrep RNA/Protein Extraction Kit	Qiagen, Hilden, Germany
Ammonium chloride (NH_4Cl)	VWR, Radnor PA, USA
Ammonium peroxodisulfate (APS)	Carl Roth GmbH & Co. KG, Karlsruhe, Germany
Ampicillin	Sigma-Aldrich, Taufkirchen, Germany
Antimycin A	Sigma-Aldrich, Taufkirchen, Germany
Bradford solution	Sigma-Aldrich, Taufkirchen, Germany
Bromophenol blue	Merck Millipore, Burlington MA, USA
Carbonylcyanid-m-chlorophenyl hydrazone (CCCP)	Sigma-Aldrich, Taufkirchen, Germany
Chloroform	VWR, Radnor PA, USA
Complete protease inhibitor	Roche Diagnostics, Basel, Switzerland
D-Galactose	Sigma-Aldrich, Taufkirchen, Germany
D-Glucose	Sigma-Aldrich, Taufkirchen, Germany
DH5-alpha Competent *E. coli*	New England Biolabs GmbH, Frankfurt am Main, Germany
Dimethyl sulfoxide (DMSO)	Sigma-Aldrich, Taufkirchen, Germany
Di-potassium hydrogen phosphate (KH_2PO_4)	Merck Millipore, Burlington MA, USA
Dulbecco's modified eagle medium A14430	Thermo Fisher Scientific, Carlsbad CA, USA
Dulbecco's modified eagle medium D5030	Sigma-Aldrich, Taufkirchen, Germany
Dulbecco's modified eagle medium D5546	Sigma-Aldrich, Taufkirchen, Germany
Dulbecco's phosphate buffered saline (PBS)	Sigma-Aldrich, Taufkirchen, Germany
Ethylenediaminetetraacetic acid (EDTA)	Merck Millipore, Burlington MA, USA
Effectene Transfection Kit	Qiagen, Hilden, Germany

Ethanol absolute	VWR, Radnor PA, USA
Fat-free milk powder	Carl Roth GmbH & Co. KG, Karlsruhe, Germany
Fetal calf serum (FCS)	PAN-Biotech, Aidenbach, Germany
GlutaMax	Thermo Fisher Scientific, Carlsbad CA, USA
Glycerol	Carl Roth GmbH & Co. KG, Karlsruhe, Germany
Glycine	Carl Roth GmbH & Co. KG, Karlsruhe, Germany
Glycolysis Stress Test Kit	Agilent Technologies, Santa Clara CA, USA
Hoechst 33342 solution	Thermo Fisher Scientific, Carlsbad CA, USA
Hydrogen peroxide (H_2O_2)	VWR, Radnor PA, USA
Isopropanol	VWR, Radnor PA, USA
Kanamycin sulfate	Carl Roth GmbH & Co. KG, Karlsruhe, Germany
L-Aspartic acid	Merck Millipore, Burlington MA, USA
L-Glutamic acid monosodium salt hydrate	Sigma-Aldrich, Taufkirchen, Germany
L-Glutamine	Merck Millipore, Burlington MA, USA
L-Histidine monohydrochloride	Sigma-Aldrich, Taufkirchen, Germany
Lipofectamine RNAiMAX	Thermo Fisher Scientific, Carlsbad CA, USA
L-Isoleucine	Sigma-Aldrich, Taufkirchen, Germany
L-Leucine	Sigma-Aldrich, Taufkirchen, Germany
L-Proline	Sigma-Aldrich, Taufkirchen, Germany
L-Valine	Sigma-Aldrich, Taufkirchen, Germany
Methanol	VWR, Radnor PA, USA
Methylammonium chloride (CH_3NH_3Cl)	Merck Millipore, Burlington MA, USA
Mito Stress Test Kit	Agilent Technologies, Santa Clara CA, USA
N-acetyl-L-cysteine	Sigma-Aldrich, Taufkirchen, Germany
Normal goat serum	Sigma-Aldrich, Taufkirchen, Germany
Norvaline	Sigma-Aldrich, Taufkirchen, Germany
Oligomycin A	Sigma-Aldrich, Taufkirchen, Germany
PageRuler Prestained Protein Ladder	Thermo Fisher Scientific, Carlsbad CA, USA
Paraformaldehyde	Sigma-Aldrich, Taufkirchen, Germany
Penicillin/Streptomycin	Merck Millipore, Burlington MA, USA
Plasmid Midi Kit	Qiagen, Hilden, Germany

Polyethylenimine transfection reagent	Sigma-Aldrich, Taufkirchen, Germany
Ponceau S solution	Sigma-Aldrich, Taufkirchen, Germany
Potassium chloride (KCl)	Merck Millipore, Burlington MA, USA
Puromycin	InvivoGen, San Diego CA, USA
QuantiNova Reverse Transcription Kit	Qiagen, Hilden, Germany
QuantiNova SYBR Green PCR Kit	Qiagen, Hilden, Germany
Restore Western Blot Stripping buffer	Thermo Fisher Scientific, Carlsbad CA, USA
Ribitol	Sigma-Aldrich, Taufkirchen, Germany
Rotenone	Sigma-Aldrich, Taufkirchen, Germany
Rotiphorese Gel 40 (37,5:1)	Carl Roth GmbH & Co. KG, Karlsruhe, Germany
SDS	Carl Roth GmbH & Co. KG, Karlsruhe, Germany
Signal Fire ECL Reagent	Cell Signaling Technology, Danvers MA, USA
SOC outgrowth medium	New England Biolabs GmbH, Frankfurt am Main, Germany
Sodium chloride (NaCl)	Carl Roth GmbH & Co. KG, Karlsruhe, Germany
Sodium deoxycholate	Sigma-Aldrich, Taufkirchen, Germany
Sodium pyruvate	Thermo Fisher Scientific, Carlsbad CA, USA
Tetramethylethylenediamine (TEMED)	Carl Roth GmbH & Co. KG, Karlsruhe, Germany
Thiazolyl blue tetrazolium bromide (MTT)	Sigma-Aldrich, Taufkirchen, Germany
Trifluoroacetic acid (TFA)	VWR, Radnor PA, USA
Tris(hydroxymethyl)aminomethane (TRIS)	Carl Roth GmbH & Co. KG, Karlsruhe, Germany
Tri-sodium citrate dihydrate	Merck Millipore, Burlington MA, USA
Triton X-100	Sigma-Aldrich, Taufkirchen, Germany
Trypsin solution 1x	Sigma-Aldrich, Taufkirchen, Germany
Tryptone	MP Biomedicals Germany, Eschwege, Germany
Tween 20	Merck Millipore, Burlington MA, USA
UV-activated nanoparticles	Provided by Shirihai Group, UCLA
Yeast extract	Sigma-Aldrich, Taufkirchen, Germany
α-ketoglutaric acid	Sigma-Aldrich, Taufkirchen, Germany
β-mercaptoethanol	Sigma-Aldrich, Taufkirchen, Germany

2.2. Consumables

Table 2: Consumables

Name	**Company**
0.45 µm filter	Sartorius AG, Göttingen, Germany
15 ml tubes	Greiner Bio-One GmbH, Essen, Germany
50 ml tubes	Greiner Bio-One GmbH, Essen, Germany
96-well plate	Greiner Bio-One GmbH, Essen, Germany
Amersham nitrocellulose blotting membrane	VWR, Radnor PA, USA
Cell culture dishes (3, 6, 10 cm)	Greiner Bio-One GmbH, Essen, Germany
Cellstar cell culture flasks 175 cm^2	Greiner Bio-One GmbH, Essen, Germany
Cryotubes and lids	Greiner Bio-One GmbH, Essen, Germany
Cuvettes	Sarstedt, Nümbrecht, Germany
Empty gel cassettes combs mini (10 or 15 wells)	Thermo Fisher Scientific, Carlsbad CA, USA
Empty gel cassettes mini 1.5 mm	Thermo Fisher Scientific, Carlsbad CA, USA
Extra thick blot paper	Bio-Rad Laboratories, Hercules CA, USA
Microcentrifuge tubes (1.5 and 2 ml)	Sarstedt, Nümbrecht, Germany
Microscopy dish 3 cm glass bottom	MatTek Corporation, Ashland MA, USA
PCR soft tubes 0.2 ml	Biozym Scientific GmbH, Hessisch Oldendorf, Germany
Seahorse plates and cartridges (FluxPaks)	Agilent Technologies, Santa Clara CA, USA
Strip tubes and caps 0.1 ml (for qPCR)	Qiagen, Hilden, Germany
White sterile inoculation loop 1 µl	Sigma-Aldrich, Taufkirchen, Germany

2.3. Equipment and Software

Table 3: Equipment and software

Name	**Company**
1290 UHPLC 6530 QTOF	Agilent Technologies, Santa Clara, CA, USA
7200 GC-QTOF	Agilent Technologies, Santa Clara, CA, USA
Agilent Mass Hunter Workstation B07	Agilent Technologies, Santa Clara, CA, USA
Allegra X-15R Centrifuge	Beckman Coulter, Brea CA, USA
Aqualine AL 25 Water Bath	Lauda, Lauda-Königshofen, Germany

Avanti JXN-26 Centrifuge	Beckman Coulter, Brea CA, USA
AxioVision Software	Zeiss, Oberkochen, Germany
BioSpectrometer incl. µCuvette	Eppendorf, Hamburg, Germany
Centrifuge 5415R	Eppendorf, Hamburg, Germany
Christ RVC2_18 CD Plus (rotary evaporator)	Martin Christ Gefriertrocknungsanlagen GmbH, Osterode am Harz, Germany
DatLab 5 (Oroboros software)	Oroboros Instruments Corp, Innsbruck, Austria
Empower Chromatography Data Software	Waters Corporation, Milford MA, USA
BD FACS Canto II Flow Cytometer	BD Biosciences, Franklin Lakes NJ, USA
Fusion SL Gel Documentation System	PEQLAB, now VWR Life Science Competence Center, Erlangen, Germany
FusionCapt Advance Software	PEQLAB, now VWR Life Science Competence Center, Erlangen, Germany
GraphPad Prism 7.04	GraphPad Software, La Jolla CA, USA
Hamilton syringe 1 and 10 µl	Hamilton Company, Reno NV, USA
HERAcell Vios 250i Incubator	Thermo Fisher Scientific, Carlsbad CA, USA
IKA Schüttler Roller 10 basic	IKA-Werke GmbH & Co. KG, Staufen, Germany
neoBlock-HeizerDuo	neoLab Migge GmbH, Heidelberg, Germany
neoLab UV-lamp 2-5062	neoLab Migge GmbH, Heidelberg, Germany
Neubauer chamber	Brand GmbH & Co. AG, Wertheim, Germany
Oxygraph-2k	Oroboros Instruments Corp, Innsbruck, Austria
PerkinElmer Spinning Disk Confocal microscope	PerkinElmer, Waltham MA, USA
pH-meter	Hanna Instruments, Vöhringen, Germany
Power Supply Consort EV231	Consort bvba, Turnhout, Belgium
Professional TRIO Thermocycler	Analytik Jena, Jena, Germany
Rotor Gene 6000 HRM5Plex	Corbett Research (now Qiagen, Hilden, Germany)
Rotor-Gene Q Series Software	Qiagen, Hilden, Germany
Seahorse XFe96 Extracellular Flux Analyzer	Agilent Technologies, Santa Clara CA, USA
Tecan infinite M200 PRO	Tecan, Männedorf, Switzerland
Trans-Blot SD Semi-Dry Transfer cell	Bio-Rad Laboratories, Hercules CA, USA
Volocity Software	PerkinElmer, Waltham MA, USA

Vortex Mixer	neoLab Migge GmbH, Heidelberg, Germany
Waters Acquity UPLC Bio H-class	Waters Corporation, Milford MA, USA
XCell SureLock Mini-Cell	Thermo Fisher Scientific, Carlsbad CA, USA
Zeiss Axiovert Observer D1	Zeiss, Oberkochen, Germany

2.4. Cell culture methods

2.4.1. Cell lines

Human astrocytoma cells (MOG-G-CCM) were derived from ECACC (European Collection of Authenticated Cell Cultures, Public Health England, Salisbury, UK) and are established from an anaplastic astrocytoma of human adult brain. Cells were grown in DMEM 5546 growth medium (1 g/l Glucose, 10% FCS, 2 mM GlutaMax, 2 mM Sodium Pyruvate and Penicillin/Streptomycin) at 37 °C and 5% humidified CO_2. HeLa WT cells were grown under the same conditions as described above. Primary rat astrocytes were prepared from cerebral hemispheres of newborn Wistar rats and grown under the same conditions. These cells were kindly provided by Dr. Görg and Prof. Dr. Häussinger, Heinrich Heine University. A SIRT4 overexpressing HeLa cell line and respective control cell line were established as described below (2.5.11.) and grown under the conditions described here.

2.4.2. Preparation of cells from stocks

Cryotubes (from -80 °C or liquid nitrogen) with approximately 1×10^6 cells in freezing medium (recipe 2.4.4.) were thawed in a 37 °C water bath until about 90% of cells were thawed. The cells were transferred to a 15 ml tube and 4 ml prewarmed growth medium was added slowly and drop wise. Then, cells were centrifuged with 500 *g* for three minutes at room temperature (RT) and supernatant was discarded to remove the DMSO. The pellet was re-suspended in fresh prewarmed growth medium and cells were transferred to T175 cell culture flask at high density and grown at 37 °C and 5% humidified CO_2. Cells were used from passage 2 onwards.

2.4.3. General maintenance

Cells were grown in respective growth medium (2.4.1.) at 37 °C at 5% humidified CO_2 in T175 cell culture flasks. For passaging medium was removed and cells were washed with prewarmed PBS. To detach cells 2 ml Trypsin was added for 3-5 min and incubated at 37 °C. Cells were re-suspended in 8 ml medium and transferred to a new flask at deserved dilution.

2.4.4. Preparation of cell stocks

Cells were grown to 80-90% confluence in a T175 cell culture flask, washed and trypsinized as described before (2.4.3.). Harvested cells were centrifuged at 500 *g* for five minutes at RT and re-suspended in 4 ml ice-cold freezing medium: 16 ml DMEM (growth medium)
2 ml FCS
2 ml DMSO

The suspension was then distributed to cryotubes at one ml each with about 1×10^6 cells, placed on ice immediately and slowly frozen at -80 °C and subsequently stored at -80 °C or in liquid nitrogen.

2.4.5. Cell counting

After harvesting (2.4.3.) 10 µl of medium-cell-suspension was inserted into a Neubauer counting chamber and cells were counted under the microscope. The mean cell number of all four chambers times 10^4 determined the number of cells per milliliter.

2.4.6. Cell seeding for assays

Cells were harvested as described above (2.4.3.). After counting the number of cells with a Neubauer chamber (2.4.5.), the cells were seeded in dishes or plates in the respective cell number and left in the incubator at 37 °C overnight for attachment before further treatment. For example, 100,000 cells were seeded in a 3 cm dish; 5000 into one well of the 96-well Seahorse plate.

2.5. Molecular biology and protein biochemistry methods

2.5.1. Protein extraction from cells

Medium was aspired and cells were washed twice with ice-cold PBS. RIPA buffer including Complete Protease Inhibitor (2.10.) was added according to the size of cell dish (for example 200 µl for a 6-well plate or 3 cm dish). The cells were incubated with the RIPA lysis buffer for 30 min at 4 °C while shaking at 200-300 rpm. Subsequently, cells were scraped and centrifuged in microcentrifuge tube for 30 min at 4 °C and 9,300 *g*. The supernatant containing the proteins was stored at -20 °C if not directly used for SDS-PAGE.

2.5.2. Protein concentration with Bradford

Protein concentrations of cell lysates were determined using the Bradford assay in an Eppendorf Spectrophotometer. Bradford solution was diluted 1:5 with water and the calibration curve was determined accordingly. Cuvettes were prepared with 1 ml of diluted Bradford solution and mixed thoroughly with 1 µl water for blanks or 1 µl protein sample, respectively. Samples were incubated for 5 min at RT before measurement.

2.5.3. SDS-PAGE

Separating and stacking gel solutions were prepared according to the recipes (2.10.) at the respective percentage. Separating gel preparation was poured in mini-gel cassettes (6 × 8 cm) and left to polymerize for approximately 30 min. Beforehand, a thin layer of isopropanol was added on the gel. After full polymerization the isopropanol was removed and the prepared stacking gel was poured on top, the comb was inserted and gel was left for 30 min to polymerize. Gels can be stored in a moist paper towel at 4 °C for about a month.

To run the gel protein samples were mixed with 4 × Laemmli buffer (2.10.) and heated at 95 °C for 5 min. Gels were fixed in gel chamber and chamber was filled with SDS Running buffer (2.10.). Defined protein amounts of samples (*e.g.* 20 µg) were pipetted into gel pockets. As a standard marker PageRuler Prestained Protein Ladder was used. Current was set to 90 V for approximately 45 min until samples had left the stacking gel and then increased to 150 V for 45-60 min.

2.5.4. Western blot

The Trans-Blot SD Semi-Dry electrophoretic transfer cell was used for blotting. The blotting sandwich was stacked in the following order: One extra-thick blot paper, nitrocellulose membrane, SDS-gel, one extra-thick blot paper. Blot papers were completely soaked in blotting buffer (2.10.), membrane and gel shortly incubated in buffer. All air bubbles were carefully removed from between the layers. Blotting was done at 60 mA per gel and 25 V for 2 h. Immediately after completion of the transfer, membranes were rinsed with water and protein staining with Ponceau S solution was done to validate the quality of transfer.

2.5.5. Antibody incubation and development

After Ponceau S staining the membrane was washed with TBS buffer (2.10.) until staining was removed. Blocking was done with 5% skim milk in TBS for 1 h at RT. Decoration with the primary antibody was done at the respective concentration (Table 4) in 5% skim milk in TBS overnight at 4 °C. The next day the

membrane was washed 3 × 5 min with TBS. Secondary antibody was decorated in milk solution for 1 h at RT at respective concentration (Table 4). The membrane was washed 3 × 5 min with TBS. For development the washed membrane was moistened with Signal Fire ECL Reagent to visualize the protein signal. Signal was developed with the Fusion SL Gel Documentation System. To decorate the membrane with another primary antibody, it was stripped using Stripping buffer for 20 min at RT, followed by 3 × thorough washing with TBS buffer. Subsequently, the membrane was blocked and decorated as before.

Table 4: Primary and secondary antibodies for Western blot

1st/2nd	**Target**	**Host**	**Dilution**	**Company**
Primary	anti-HSP60	rabbit	1:10,000 in 5% milk solution	Sigma-Aldrich, Taufkirchen, Germany
Primary	anti-GLUD2	mouse	1:250 in 5% milk solution	Santa Cruz Biotechnology, Dallas TX, USA
Secondary	anti-rabbit IgG	goat	1:10,000 in 5% milk solution	Dianova, Hamburg, Germany
Secondary	anti-mouse IgG	goat	1:10,000 in 5% milk solution	Abcam, Cambridge, UK

2.5.6. MTT-Assay

Cells were seeded into a 96-well plate with a density of 7,500 cells per well in 100 µl growth medium and stored in incubator overnight. The next day the cells were treated with twelve different concentrations of NH_4Cl (0.02 mM to 40.96 mM, doubling from one step to the next) as well as H_2O and 2 mM H_2O_2 as a negative and positive control. For each concentration six wells were treated. Treatment was done for the time points 24 h, 48 h and 72 h. After incubation time the treatment medium was aspired and replaced by 100 µl medium containing 10% MTT. The plate was incubated for 2 h at 37 °C. After incubation, cells were washed with PBS and 100 µl DMSO was added. The plate was immediately put into the plate reader and read at 570 nm with 650 nm as a reference wavelength.

2.5.7. RNA/Protein extraction from cells

The extraction from cells was done with the All Prep RNA/Protein extraction kit according to the manufacturer's instructions. RNA concentration and quality was measured using the µCuvette application of the Eppendorf Spectrophotometer. RNA was stored at -20 °C while protein (native) was stored at -80 °C.

2.5.8. cDNA synthesis

The reverse transcription of RNA to cDNA was done using the QuantiNova Reverse Transcription Kit.

Genomic DNA removal step:

2 µl gDNA Removal Mix

up to 5 µg Template RNA

RNase-free water (to reach 15 µl reaction volume)

Reverse transcription Master Mix:

1 µl Reverse Transcription Enzyme

4 µl Reverse Transcription Mix (incl. Mg^{2+} and dNTPs)

15 µg Template RNA (from gDNA removal step)

Reverse transcription temperature protocol:

gDNA elimination reaction:	2 min 45 °C
Pause (add Master Mix)	
Annealing step:	3 min 25 °C
Reverse-transcription step:	10 min 45 °C
Inactivation of reaction:	5 min 85 °C

2.5.9. qPCR

Quantitative PCR (qPCR) was done with the QuantiNova SYBR Green PCR Kit with 20-40 ng cDNA from section 2.5.8. Master Mix:

10 µl 2x SYBR Green PCR Master Mix

0.5 µl Forward Primer (0.7 µM)

0.5 µl Reverse Primer (0.7 µM)

8 µl RNase-free water

1 µl cDNA template (20-40 ng)

qPCR temperature conditions:

PCR initial heat activation:	2 min 95 °C
2-step cycling (40 x):	
Denaturation:	5 s 95 °C
Annealing/extension:	10 s 60 °C
Melting curve:	65-95 °C in 1 °C steps

qPCR was performed on Rotor-Gene 6000 HRM5Plex and data was analyzed with Rotor-Gene Q Series Software. Hypoxanthine-guanine phosphoribosyltransferase (HPRT1) was used as a housekeeping gene.

Table 5: qPCR primers

Gene	Sequence Forward 5' – '3	Sequence Reverse 5' – '3
DRP1	gcacaagaggatctgtgacact	ccagaattggaagggctatg
GLUD2	cggcagagttccaagacagt	gaacgctccattgtgtatgc
HPRT1	cctggcgtcgtgattagtg	tgaggaataaacacccctttcca
MFN1	cattcatttcagttatttctgatccat	cattaaagaggaaactggtgagg
MFN2	ggaggagtgggagtagctca	tcccagtgactgccacct
OPA1	atgtatgttacgggcgcttt	aatccattaccactgttcttcca

2.5.10. Retransformation

XL1 Blue *Escherichia coli* were thawed for 20 min on ice. 10 ng of plasmid template (pEGFP-Mito) was added to 100 µl bacterial cell suspension and left on ice for incubation for 20 min. Then, cells were subject to 42 °C heat shock for 45 s followed by 2 min on ice. 900 µl prewarmed (37 °C) SOC-medium was given to the bacterial cells and they were incubated on a shaker at 37 °C for 1 h. After incubation, bacterial suspension was plated on two lysogeny broth (LB) agar plates with 50 µg/ml ampicillin (2.10.) using inoculation loops. One plate was inoculated with 90%, the second with 10% of bacterial solution and incubated overnight at 37 °C after drying the plates. The next day one colony was transferred to 50 ml of LB-medium with 50 µg/ml kanamycin (2.10.) and incubated again overnight at 37 °C on a shaking incubator. The following day a plasmid preparation with the Plasmid Midi Kit was performed. Plasmid concentration and quality was measured with the µCuvette application of the Eppendorf Spectrophotometer.

2.5.11. Transfection of plasmids and siRNA

pEGFP-Mito transfection was conducted with Effectene Transfection Reagent according to the manufacturer's instructions 24 h before imaging. Knock-down of *GLUD2* was done using Lipofectamine RNAiMAX according to the manufacturer's instructions for 48 h using reverse transfection. GLUD2 and empty vector plasmid transfections, as well as simultaneous transfection of plasmids and GDH2 siRNA were performed by reverse transfection using Lipofectamine RNAiMAX for 48 h according to the manufacturer's instructions in a Seahorse cell plate. *GLUD2* plasmid by GenScript USA Inc. with

pcDNA3.1(+) vector. As empty vector a pcDNA3.1(+) vector without insert was used. Transfection with siRNA was performed with Lipofectamine RNAiMAX according to the manufacturer's instructions. siGLUD2 was transfected in a reverse manner for 48 h.

HeLa-SIRT4-eGFP cells were kindly provided by Dr. Piekorz, Heinrich Heine University. The generation of HeLa-SIRT4-eGFP cells was done as follows: The cDNAs for eGFP and the human SIRT4-eGFP fusion protein were generated by PCR using pEGFP-N1 and pcDNA3.1-SIRT4-eGFP (Lang et al., 2017) as templates, respectively, and subsequently cloned via NheI and XhoI restriction sites into puc2CL12IPwo derived from plasmids generated earlier (Roellecke et al., 2016; Wiek et al., 2015). Constructs were verified by DNA sequencing. HeLa cells were transfected as described (Roellecke et al., 2016; Wiek et al., 2015) using polyethylenimine transfection reagent with HIV1 helper plasmid (pCD/NL-BH) (Zhang et al., 2004), envelope vector (pczVSV-G) (Pietschmann et al., 1999), and the newly generated plasmids puc2CL12eGFPIPwo or puc2CL12SIRT4-eGFPIPwo (both containing an IRES-PuroR cassette). Viral supernatants were harvested 48 h after transfection, filtered through a 0.45 µm filter and used to transduce HeLa cells. Selection with 2 µg/ml Puromycin was started 96 h after transduction and eGFP positivity was tracked by FACS analysis in the FITC-A channel using non-transduced HeLa cells as negative control.

Table 6: Plasmids

Plasmid name	**Gene**	**Company/Reference**
pEGFP-Mito	mitochondrial eGFP	Clontech Laboratories, Mountain View CA, USA
pcDNA3.1-GLUD2	*GLUD2*	GenScript USA Inc., Piscataway NJ, USA
pcDNA3.1	empty vector	Invitrogen, Thermo Fisher Scientific, Carlsbad CA, USA
pEGFP-N1	eGFP	Lang et al., 2017
pcDNA3.1-SIRT4-eGFP	SIRT4	Lang et al., 2017
puc2CL12IPwo		Roellecke et al., 2016; Wiek et al., 2015
pCD/NL-BH		Zhang et al., 2004
pczVSV-G		Pietschmann et al., 1999

Table 7: siRNAs

siRNA target/name	**Sequence(s) 5' – '3**	**Company**
GLUD2	cuaaccucuucacguguaa; uuacacgugaagagguuag	Sigma-Aldrich, Taufkirchen, Germany
Silencer Negative Control No. 1 siRNA	not available	Invitrogen, Thermo Fisher Scientific, Carlsbad CA, USA

2.5.12. Immunostaining

Cells were grown to about 50% confluence in 3 cm microscopy dishes with a glass bottom. After removal of medium cells were washed twice with prewarmed PBS. Cells were fixed with 1 ml 4% PFA, prewarmed to 37 °C, for 20 min at RT. After incubation PFA was washed off twice with PBS. Then, 2 ml of 0.15% Triton X-100 (in PBS) were added for 15 min for permeabilization. Triton X-100 was removed and 1 ml 10% goat serum in PBS was added for 15 min for blocking. After removal, 100 µl Tom20 antibody was added at a dilution of 1:200 in 1% goat serum only covering the glass bottom of the dish and incubated at 4 °C overnight. On the next day, the primary antibody was removed and samples were washed 3 × 10 min with PBS. 100 µl secondary antibody was added 1:100 for 1 h at RT in 1% goat serum only covering the glass, as before. Dishes were kept in the dark following from here. After incubation the antibody was washed off with PBS 3 × 10 min in the dark. Dishes were covered with PBS and stored at 4 °C in the dark until imaging was done with PerkinElmer Spinning Disk Confocal microscope.

Table 8: Immunostaining antibodies

1st/2nd	**Target**	**Host**	**Dilution**	**Company**
Primary	Tom20	rabbit	1:200 in 1% goat serum	Santa Cruz Biotechnology, Dallas TX, USA
Secondary	anti-rabbit IgG Alexa Fluor 488 conjugated	goat	1:100 in 1% goat serum	Thermo Fisher Scientific, Carlsbad CA, USA

2.6. Measurements of mitochondrial bioenergetics

2.6.1. Oroboros Oxygraph

Cells were seeded in 6 cm dishes and treated with NH_4Cl for respective duration. Cells were harvested and 1×10^6 untreated cells were given in chamber A and the same number of treated cells in chamber B in a total volume of 2 ml growth medium, respectively. Before measurements air calibration had to be performed. Both chambers were filled with medium, closed completely and then opened for air calibration. When there was no change in oxygen consumption anymore the medium was exchanged for cell medium. Stoppers had to be fully closed to measure. After measuring basal respiration oligomycin (1 µl from 5 mM stock in 99.9% EtOH) was injected with a 10 µl Hamilton syringe. Respiration was decreasing. When the curve was stable (no longer than 5 min after first injection) CCCP was injected with a 10 µl Hamilton syringe. CCCP was injected at steps of 1 µl (1 mM stock in DMSO), awaiting a stable plateau before next injection. CCCP leads to increase in respiration and titration of CCCP continues until

respiration has reached its highest possible level and does not increase further upon injection. To block mitochondrial respiration rotenone (1 µl from 1 mM stock in 99.9% EtOH) and antimycin A (1 µl from 5 mM stock in 99.9% EtOH) were injected directly subsequent with a 1 µl Hamilton syringe.

Table 9: Chemicals for Oroboros Oxygraph

Chemical	**Function**
Oligomycin	Inhibition of F_1F_O-ATP-synthase by blocking the proton channel in F_0 subunit, inducing the leak state of respiration.
CCCP	The protonophore transports protons over the membrane thereby uncoupling mitochondrial respiration. Induces maximal respiration or ETS (electron transport system capacity).
Rotenone	Inhibitor of complex I through inhibition of NADH oxidation and thereby electron transfer. Inhibits mitochondrial respiration.
Antimycin A	Inhibits complex III by inhibiting electron transfer. Inhibits mitochondrial respiration.

Injection of rotenone and antimycin A leads to a complete block of mitochondrial respiration. Thereby, one can measure the residual oxygen consumption (ROX), which is the oxygen consumed by other means than oxidative phosphorylation, *e.g*. oxidases.

2.6.2. Seahorse XFe96 Extracellular Flux Analyzer

Cells were plated in Seahorse cell culture plate in respective growth medium in a density creating a smooth monolayer on the day of measurement. For MOG-G-CCM this was 5,000 cells seeded 24 h before measurement, for HeLa 15,000 and for primary rat astrocytes 8,000 cells. Sufficient FCCP concentration was 1 µM for MOG-G-CCM, 0.25 µM for HeLa and 2 µM for primary rat astrocyte, respectively. Treatment with NH_4Cl (or CH_3NH_3Cl) at the respective molarity for 48, 24, 6, 4 and/or 1 h, as indicated. 1 h before measurement, cells were washed with PBS and medium was replaced by assay medium (DMEM 5030 supplemented as growth medium but without FCS and antibiotics) with or without NH_4Cl or respective reagent. For wash-out assays NH_4Cl was removed from assay medium. For live treatment NH_4Cl was added to wells directly before Seahorse plate was inserted into the machine. For rescue assays, cells were treated with respective amino acid/compound at designated molarity directly before treatment with 5 mM NH_4Cl and Mito Stress Test was performed as described. For knock-downs and overexpression of genes, cells were transfected in Seahorse cell plate as described in section 2.5.11. For measurements in galactose medium, growth medium (DMEM A14430) as well as assay medium were supplemented with 1 g/l

galactose instead of glucose. After the measurement all values for each well were normalized to cell number determined by Hoechst staining on Tecan Platereader.

2.6.2.1. Mito Stress Test Kit

Sample preparations and measurement with the Mito Stress Test Kit was done as described by the manufacturer. The sample calculations of different parameters are as follows:

$$Maximal\ respiration = (maximum\ rate\ measurement\ after\ FCCP\ injection) - (non - mitochondrial\ respiration)$$

$$Spare\ respiratory\ capacity = (maximal\ respiration) - (basal\ respiration)$$

$$Spare\ respiratory\ capacity\ (\%) = \frac{maximal\ respiration}{basal\ respiration} * 100$$

This method uses FCCP instead of CCCP. The function is the same and is described in table 9.

2.6.2.2. Glycolysis Stress Test Kit

Sample preparations and measurement with the Glycolysis Stress Test Kit was done as described by the manufacturer. The sample calculations of different parameters are as follows.

'Glycolysis' and 'Glycolytic Capacity' are defined as extracellular acidification rate (ECAR) and calculated as:

$$Glycolysis = (maximum\ rate\ measurement\ before\ oligomycin\ injection) - (last\ rate\ measurement\ before\ glucose\ injection)$$

$$Glycolytic\ capacity = (maximum\ rate\ measurement\ after\ oligomycin\ injection) - (last\ rate\ measurement\ before\ glucose\ injection)$$

2.7. Chromatography

2.7.1. Metabolomics

Cells were grown in 175 cm^3 flasks and treated with 5 mM NH_4Cl for 48, 24, 6, 4, 2 or 1 h. For harvesting, cells were trypsinized, washed with ice-cold PBS twice and counted. 1 × 10^6 cells were pelleted and

resuspended in 1:2.5:1 H_2O : methanol : chloroform, precooled to -20 °C. The suspension was mixed on a rotator at 4 °C for 10 min, centrifuged at 9,300 *g* for 5 min at 4 °C and the supernatant was used for metabolite profiling as described in section 2.7.1.1. and 2.7.1.2. All measurements were done at least in biological triplicates including non-treated controls. Peak integration and analysis was done with the Agilent Mass Hunter Workstation B07. GC-MS and LC-MS measurements were performed at CEPLAS, Heinrich Heine University with the help of Dr. Dominik Brilhaus and Dr. Tabea Mettler-Altmann.

2.7.1.1. GC-MS

Polar metabolites were analyzed by gas chromatography coupled to a time-of-flight mass spectrometer (7200 GC-QTOF) according to Fiehn and Kind (Fiehn and Kind, 2007). For relative quantification, peak areas of the compounds were normalized to the peak area of the internal standard ribitol added to the extraction buffer.

2.7.1.2. LC-MS

To follow accumulation of ^{15}N label, cells were treated with $^{15}NH_4Cl$ as above. Amino acids were analyzed by liquid chromatography coupled to a TOF MS (1290 UHPLC 6530 QTOF) according as described previously (Gu et al., 2007). Amino acid peak areas were normalized to the peak area of norvaline. Relative ^{15}N label enrichment was calculated after accounting for natural isotopic distribution.

2.8. Microscopy methods

2.8.1. Fluorescence microscopy

Cells were seeded in 3 cm microscopy dishes with glass bottom and grown to 50-70% confluence. Visualization of mitochondria was achieved by pEGFP-Mito transfection (described in 2.5.11) or immunostaining with antibodies coupled to Alexa Fluor 488 (described in 2.5.12.). Treatment with NH_4Cl was done in the microscope dish at respective concentration and duration. Imaging was done with Zeiss Axiovert Observer D1 microscope with 63x/1.46 NA oil objective (Filter: Ex 450-490 nm, Em 500-550 nm) and AxioVision Software. Else the PerkinElmer Spinning Disk Confocal microscope with the 488 nm laser, 60x/1.4 NA oil objective and Volocity software was used. At least 20 images were taken per dish. Images were processed with Fiji (Schindelin et al., 2012). Live cell imaging was done using the life support system (temperature and CO_2 control) of Spinning Disk Confocal microscope or cells were fixed with PFA (2.5.12.).

2.8.2. Mitochondrial morphology

Mitochondria were visualized with pEGFP-Mito transfection (2.5.11) or immunostaining against Tom20, as described in section 2.5.12. Treatment with 5 mM NH_4Cl was done for 1, 4, 6, 24, 48 and 72 h, respectively. At least 20 images were taken per dish and analyzed with Fiji software (Schindelin et al., 2012). Mitochondrial morphology in each cell was categorized to tubular, intermediate and fragmented (Fig. 11).

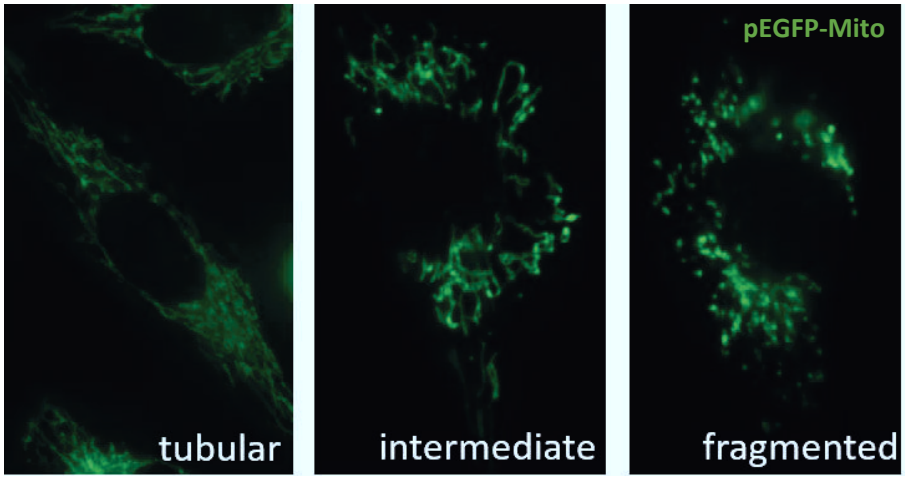

Figure 11: Categories of mitochondrial morphology. Representative images to show the different phenotypes of mitochondrial morphology in human astrocytoma cells. Cells are transfected with pEGFP-Mito to visualize mitochondria. Morphology changes from tubular (left) to intermediate (middle) to fragmented (right).

2.8.3. N-acetyl-L-cysteine treatment

100,000 MOG-G-CCM cells were seeded in 3 cm microscopy dish and transfected with pEGFP-Mito (described in 2.5.11.). Cells were pretreated in serum-free medium with 1 or 2 mM of the ROS scavenger N-acetyl-L-cysteine (NAC) 1 h prior to treatment with 5 mM NH_4Cl in full medium for 24 or 48 h. NAC was solved in serum-free medium and adjusted to pH 7.4. Ammonia treatment occurred in the presence of NAC. Imaging and determination of mitochondrial morphology was done as described before (2.8.2.).

2.8.4. Reversibility assay

Primary rat astrocytes were grown in 3 cm microscopy dishes with glass bottom to about 50-70% confluence. Cells were treated with 5 mM NH_4Cl for 72 h and mitochondrial morphology was determined. Medium was exchanged for fresh medium not containing NH_4Cl and mitochondrial morphology was determined again after removal of ammonia for 24, 48 and 72 h. Mitochondria were visualized by transfection with pEGFP-Mito as described before (2.5.11.). Images for quantification of morphology were

taken with Zeiss Axiovert Observer D1 microscope using AxioVision software (section 2.8.1). At least 20 pictures were taken per dish.

2.9. Nanoparticles

Photo-activatable nanoparticles (pa-NPs) were kindly provided by Orian Shirihai, UCLA. Pa-NPs are taken up through endocytotic pathways and accumulate in lysosomes. Upon photo-activation using UV light, pa-NPs start to swell and acidify the lysosome. Synthesis and characterization of the pa-NPs is described elsewhere (Trudeau et al., 2016). MOG-G-CCM cells were seeded in Seahorse cell culture plate and treated with 25 µg/ml pa-NPs, which were pre-incubated on cells for 4 h to enter the cells. After incubation cells were treated with 5 mM NH_4Cl for 24 h and pa-NPs were activated by UV light (5 min at 365 nm). After 24 h treatment time Seahorse cell plate was measured with Mito Stress Test Kit as described in section 2.6.2.1. Pa-NPs were handled in darkness only. Treatment groups included: -NP +NH_4Cl, +NP +NH_4Cl, -NP -NH_4Cl, +NP -NH_4Cl.

2.10. Recipes

Blotting buffer

20 mM TRIS

150 mM Glycine

20% pure ethanol

0.08% SDS

ddH_2O 1 l

pH 8.3

Freezing buffer for cells

For 20 ml

16 ml DMEM

2 ml FCS

2 ml DMSO

Laemmli buffer 4 x

250 mM 1 M TRIS-HCl pH 6.8

8% SDS

40% Glycerol

8% β-mercaptoethanol

0.02% Bromophenol blue

Lysogeny broth (LB) plates

5 g/l Yeast extract

10 g/l Tryptone

10 g/l NaCl

15 g/l Agar

ddH_2O

pH 7

Autoclaved, then addition of respective antibiotic and poured in 10 cm dishes. Dry plates stored upside down at 4 °C.

Lysogeny broth (LB) medium

5 g/l Yeast extract

10 g/l Trypton

10 g/l NaCl

ddH_2O

pH 7

autoclaved

RIPA buffer

50 mM TRIS-HCl

150 mM NaCl

1% Triton X-100

1% Sodium deoxycholate

0.1% SDS

5 mM EDTA

ddH_2O 1 l

pH 7.4

SDS Running buffer

3 g TRIS

14.4 g Glycine

1 g SDS

ddH_2O 1 l

Separating gel 10%

4.8 ml H_2O

2.5 ml Rotiphorese Gel 40

2.5 ml 1.5 M TRIS pH 8.8

100 µl 10% SDS

10 µl TEMED

100 µl 10% APS

Stacking gel 5%

3.5 ml H_2O

725 µl Rotiphorese Gel 40

650 µl 1 M TRIS pH 6.8

50 µl 10% SDS

5 µl TEMED

50 µl 10% APS

TBS 10 x

0.5 M TRIS

1.5 M NaCl

ddH_2O 1 l

pH 7.5

TBS 1 x

100 ml 10 x TBS

900 ml ddH_2O

2.11. Statistics

Statistics were done with GraphPad Prism 7.04 for windows. For multiple comparisons One-way ANOVA with Dunnett's or Tukey's *post hoc* test were performed. To compare only two groups Student's t-test was applied. Data is shown as mean ± SEM or SD as indicated.

3. Results

3.1. Ammonium chloride does not impair cellular metabolic activity at concentrations of 5 mM or below

A commonly used concentration in HE model systems is 5 mM NH_4Cl, as similar concentrations have been found in HE rat models (Swain et al., 1992). To test at which concentrations NH_4Cl is toxic to tumor cell models, I performed MTT tests using HeLa WT. Cells were treated with a concentration range between 0.02 and 40.96 mM NH_4Cl in a serial dilution. Treatment durations were 48 and 72 h. The metabolic activity-based MTT assay is a measure for cell viability, measuring the ability to reduce the MTT dye to purple formazan, which is measured by absorbance at 570 nm. Cell viability in HeLa cells was hardly affected up to 5 mM NH_4Cl at both time points (Fig. 12). Treatment with 10 mM led to a reduction of cell viability after 48 h and 72 h. This reduction in viability was further increasing with higher concentrations. After treatment with 40 mM, less than 50% of cells had intact metabolic activity. MTT tests with primary rat astrocytes for 24, 48 and 72 h of ammonia treatment were already performed in the group before and also revealed no toxic effect of 5 mM ammonia for 24 and 48 h of treatment. However, a slight reduction in viability was seen after 72 h, but this duration of treatment is rarely used here (data from PhD thesis, Kaihui Lu). Hence, the proposed concentration of 5 mM NH_4Cl is suitable to use without toxic effects and cell death in different cell types.

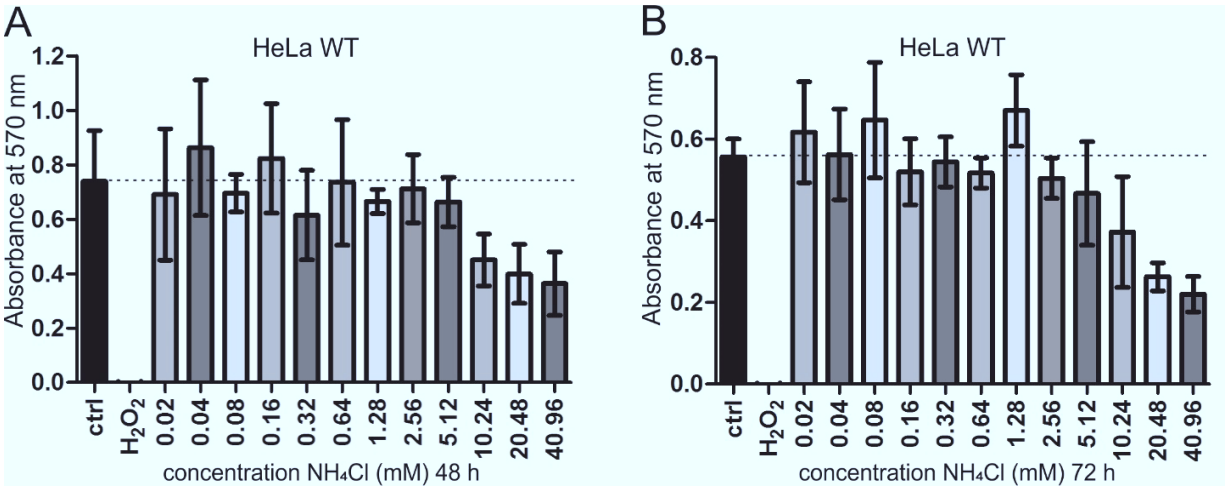

Figure 12: Ammonia does not impair cell viability at 5 mM concentration and below. MTT test was done in HeLa WT cells with NH_4Cl concentrations from 0.02 to 40.96 mM including negative control and positive control with 2 mM H_2O_2 for 48 h (A) and 72 h (B) treatment duration. Data presented as mean of 6 technical replicates ± SD (n=1).

3.2. Ammonia changes mitochondrial fusion and fission dynamics

3.2.1. Ammonium chloride induces mitochondrial fragmentation

Stress can trigger changes in mitochondrial morphology and impairment of fission and fusion dynamics have been causally linked to neuropathies in humans (Delettre et al., 2000; Züchner et al., 2004). An influence of such changes in HE after short exposure times are so far not known and are hence, of great interest. In order to test whether ammonia has an effect on mitochondrial morphology, I first used the human astrocytoma cell line MOG-G-CCM transfected with mtEGFP, a variant of GFP targeted to the mitochondrial matrix (Weber et al., 2013) to visualize mitochondria. Cells were treated with 5 mM NH_4Cl for 1 to 72 h and changes in mitochondrial morphology (tubular, intermediate, highly fragmented) were quantified using confocal fluorescence microscopy (for examples of categories see Fig. 11). The appearance of cells showing mild (intermediate) or severe (highly fragmented) mitochondrial fragmentation was evident already after 6 h of treatment when compared to controls lacking NH_4Cl or to earlier time points (Fig. 13 A, B). Conversely, the extent of mitochondria showing a tubular interconnected network-like morphology was markedly reduced by addition of ammonia. Mitochondrial fragmentation became more prominent after 24 h reaching a high steady-state level. Treatment for 48 h and 72 h with NH_4Cl did not further increase mitochondrial fragmentation. To corroborate this in primary cells I used primary rat astrocytes treated with 5 mM NH_4Cl. Likewise, mitochondrial morphology (visualized by immunostaining against Tom20) was altered by NH_4Cl (Fig. 13 A). The change towards mitochondrial fragmentation was even more rapid as it became evident already after 1 h of ammonia treatment. Additionally, the percentage of highly fragmented mitochondria at time point 48 h and later was much higher in primary rat astrocytes than in human astrocytoma cells (Fig. 13 C). Hence, mitochondrial morphology is altered very rapidly by hyperammonemia and primary rat astrocytes appear to react faster and are more sensitive to ammonia than human astrocytoma cells.

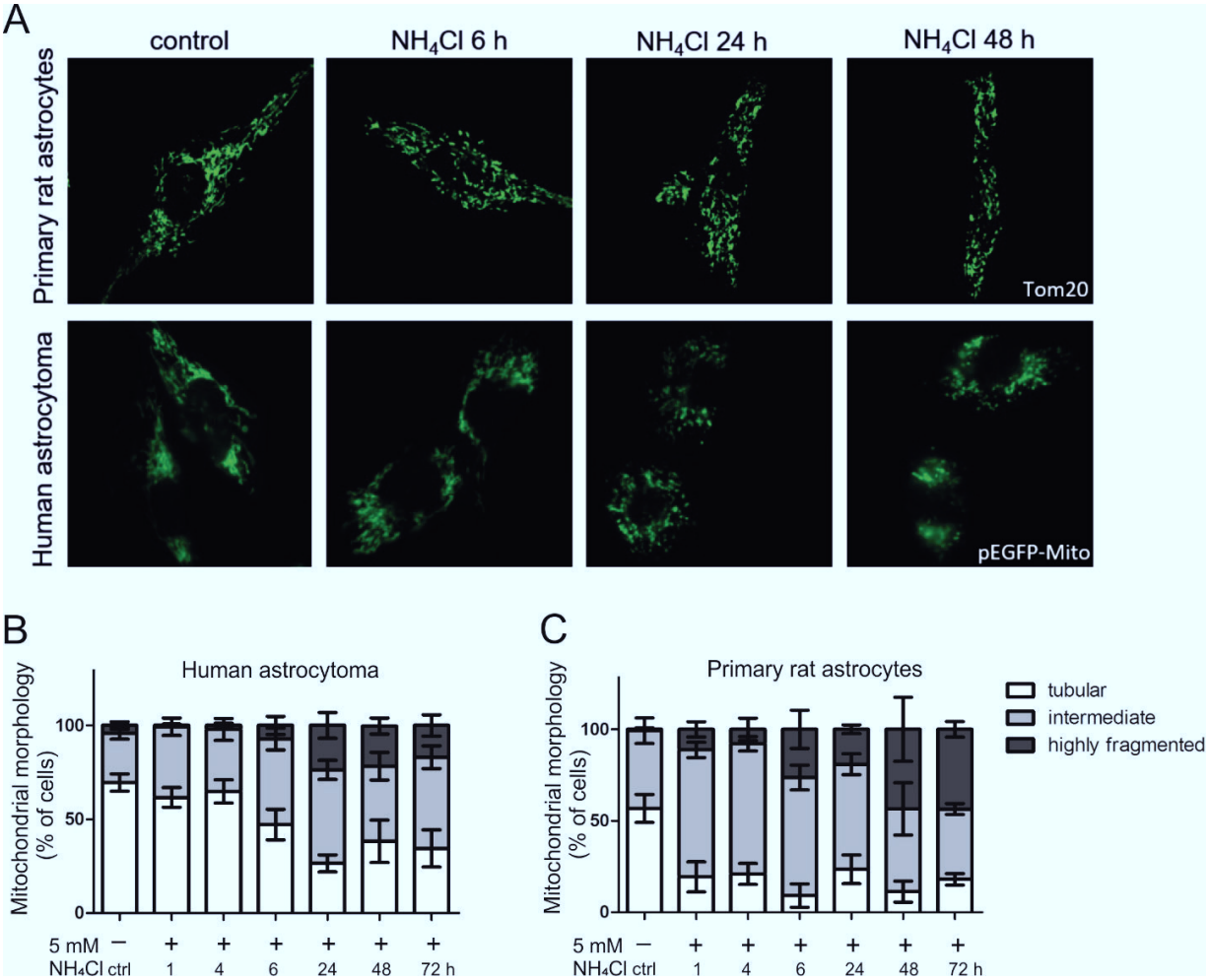

Figure 13: Mitochondrial morphology is rapidly altered by ammonia. Human astrocytoma cells were transfected with pEGFP-Mito to visualize mitochondria. In primary rat astrocytes visualization was achieved by immunostaining against Tom20. Cells were treated with 5 mM NH_4Cl for respective duration. At least 20 pictures were taken per sample showing approximately 3-5 cells each. Mitochondria were categorized to tubular, intermediate and fragmented morphological phenotype. (A) Changes in morphology of mitochondria after treatment with 5 mM NH_4Cl in primary rat astrocytes (top) and human astrocytoma cells (bottom). Time course of change in mitochondrial morphology in (B) human astrocytoma cells and (C) primary rat astrocytes. Depicted is percentage of cells with respective phenotype over time. Data presented as mean ± SD (n=3-6).

3.2.2. Scavenging of ROS decreases ammonia-induced mitochondrial fragmentation

It has been shown before by others that hyperammonemia leads to an increase in the formation of ROS (Görg et al., 2013). To investigate whether and how an increase in ROS triggers the induction of mitochondrial fragmentation, I repeated mitochondrial morphology assays shown above in the presence of NAC, a ROS scavenger. Human astrocytoma cells were transfected with pEGFP-Mito to visualize mitochondria, pretreated with 2 mM NAC for 1 h and treated with 5 mM NH_4Cl for 24 and 48 h,

respectively. A combination treatment of NAC and NH_4Cl as well as single treatments of the compounds as controls were used. Images were categorized to cells harboring tubular, slightly fragmented (intermediate) or highly fragmented mitochondria (Fig. 14). In non-treated controls and cells treated with NAC only, cells showed mostly tubular mitochondria. When treated with 5 mM NH_4Cl slight and strong fragmentation was induced, as seen before. After 24 h of treatment, NAC pretreatment reduced the number of cells with fragmented mitochondria and hence, more cells harbored tubular mitochondria. After 48 h of treatment this effect was not evident. When pretreated with NAC, ammonia treated cells had less highly fragmented mitochondria than NH_4Cl alone, but many cells with partially fragmented mitochondria were present. Thus, the difference in tubular mitochondria between cells pretreated with NAC and those not pretreated was barely evident. Scavenging of ROS with NAC reduced mitochondrial fragmentation, showing a stronger effect after 24 than after 48 h. NAC most likely only facilitates a short-term effect as it is only added once in the beginning of treatment und thus, these results to not argue against the idea that scavenging the stressor ROS could have a beneficial effect on mitochondrial morphology.

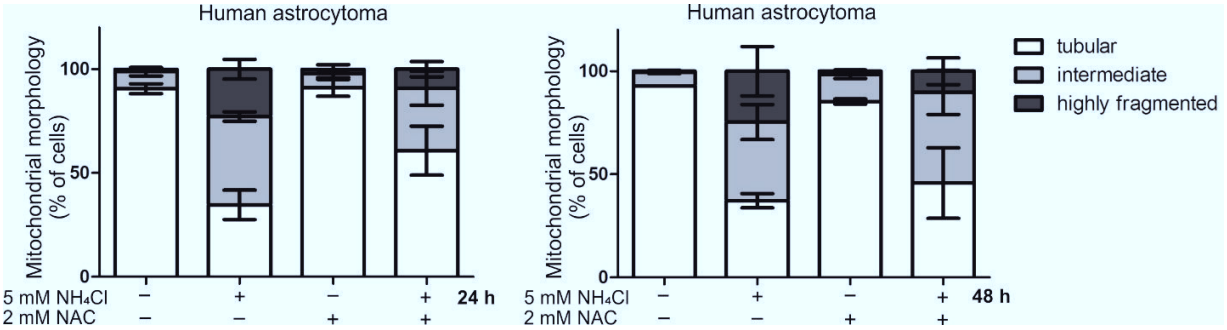

Figure 14: ROS scavenging by NAC reduces NH_4Cl-induced mitochondrial fragmentation. Human astrocytoma cells were transfected with pEGFP-Mito to visualize mitochondria. Cells were pretreated with 2 mM NAC for 1 h and treated with 5 mM NH_4Cl for 24 h (left) and 48 h (right). Controls were treated with NAC or NH_4Cl only, or left untreated. Images were taken with fluorescence microscopy. Mitochondria were categorized to tubular, intermediate and fragmented morphological phenotype. Depicted is percentage of cells with respective phenotype. Data presented as mean ± range (n=2).

The same assay was performed with primary rat astrocytes (Fig. 15). The results largely resemble the ones observed with human astrocytoma cells. NAC pretreatment reduced the ammonia-induced mitochondrial fragmentation after 24 h of NH_4Cl treatment. In this cell type the discrepancy between the treatment durations 24 and 48 h was stronger than in human astrocytoma cells. After 48 h of treatment NAC did not

reduce fragmentation, rather, the presence of cells with tubular mitochondria was even less than with NH_4Cl treatment alone. Still, the number of cells with high fragmentation remained the same.

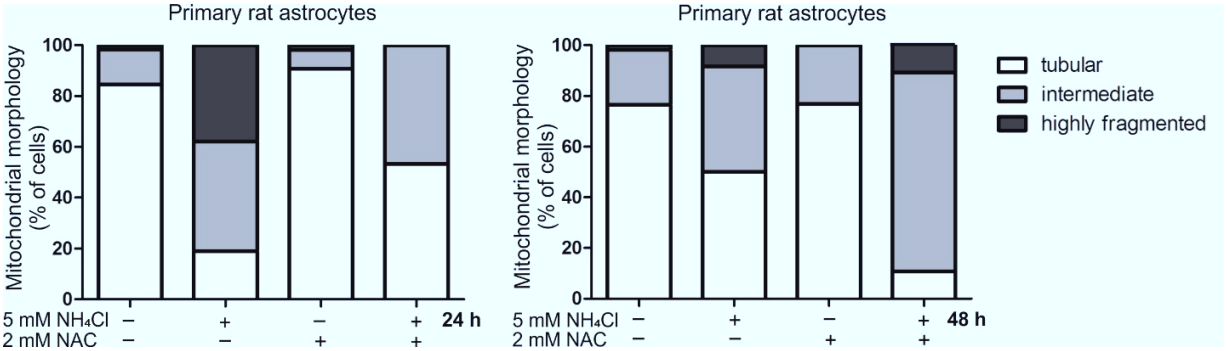

Figure 15: ROS scavenging by NAC reduces NH_4Cl-induced mitochondrial fragmentation in primary cells. Primary rat astrocytes cells were transfected with pEGFP-Mito to visualize mitochondria. Cells were pretreated with 2 mM NAC for 1 h and treated with 5 mM NH_4Cl for 24 h (left) and 48 h (right). Controls were treated with NAC or NH_4Cl only, or left untreated. Images were taken with fluorescence microscopy. Mitochondria were categorized to tubular, intermediate and fragmented morphological phenotype. Depicted is percentage of cells with respective phenotype (n=1).

3.2.3. Ammonia-induced mitochondrial fragmentation is reversible

It is controversially discussed whether HE can be considered a fully reversible disease after liver transplantation or not (Bajaj et al., 2010). Therefore, I asked whether mitochondrial fragmentation is reversible upon removal of ammonia. Primary rat astrocytes were treated with 5 mM NH_4Cl for 72 h and the morphology of mitochondria was determined, here only focusing on tubular vs. fragmented mitochondria. Mitochondria were visualized after pEGFP-Mito transfection. Medium was exchanged for fresh medium without ammonia and cells were subject to microscopy analysis after 24, 48 and 72 h of ammonia removal. Indeed, I observed in primary rat astrocytes that mitochondrial morphology, which was highly fragmented after 72 h of treatment with NH_4Cl, recovered within 24 h to a highly tubular morphology when the medium was exchanged to fresh medium lacking NH_4Cl (Fig. 16). Upon ammonia removal, the change in morphology reversed completely to the levels of healthy, untreated mitochondria. Mitochondrial fragmentation is therefore fully reversible after ammonia removal.

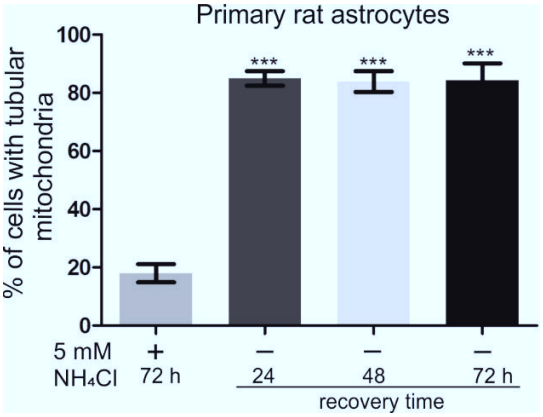

Figure 16: Ammonia-induced mitochondrial fragmentation is reversible. Primary rat astrocytes were transfected with pEGFP-Mito. Baseline analysis was done after 72 h treatment with 5 mM NH_4Cl. Other time points represent recovery time after removal of ammonia medium. Characterization of morphology to fragmented and tubular. Data represented as mean ± SD (n=3). One-way ANOVA with Dunnett's post test. ***P < 0.001.

3.3. Ammonia facilitates changes in mitochondrial bioenergetics and glycolysis

3.3.1. Ammonia decreases ability to transfer electrons in mitochondrial respiration

After the observed changes in mitochondrial morphology, I asked whether the function of mitochondria is influenced by hyperammonemia. Therefore, I tested whether ammonia modulates oxidative phosphorylation. For that, oxygen consumption of ammonia treated cells was measured using an Oroboros Oxygraph. HeLa WT cells were treated "live" (0 h) in the Oxygraph cell chamber with 5 mM NH_4Cl. No changes in basal respiration were observed; however, after inducing maximal respiration with CCCP a strong trend towards a reduction of electron transfer system capacity (ETS) in cells treated with ammonia compared to controls was observed (Fig. 17 A). The same approach was employed with human astrocytoma cells with the difference of longer treatment durations with NH_4Cl. Cells were treated 24 and 48 h, respectively. The results resemble the trend observed in live treatment of HeLa cells showing no changes in the basal respiration but a trend for reduction in ETS (Fig. 17 B, C). However, the reduction of mitochondrial respiration after longer treatment periods was not as evident. This pointed to the possibility that ammonia could negatively influence mitochondrial respiration. This prompted me to follow this up in more detail.

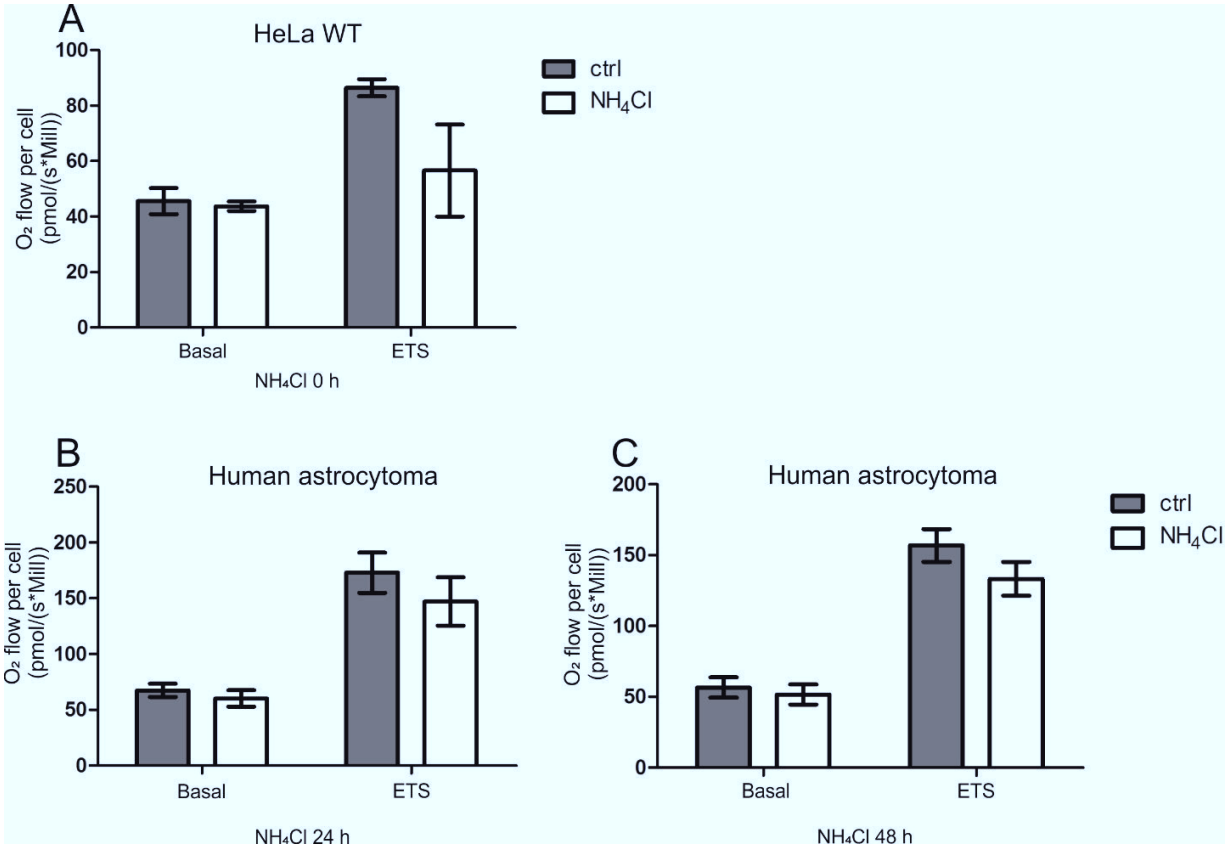

Figure 17: Ammonia reduces capacity of respiratory chain to transfer electron. Basal respiration and electron transfer system capacity (ETS) were measured in the Oroboros Oxygraph. (A) HeLa WT cells were treated live (0 h) with 5 mM NH_4Cl (n=3). (B) Human astrocytoma cells were treated 24 h with 5 mM NH_4Cl (n=6). (C) Human astrocytoma cells were treated 48 h with 5 mM NH_4Cl (n=5). Changes between treated cells and controls are not significant, only a trend is observed. Data presented as mean ± SEM.

3.3.2. Ammonia rapidly impairs mitochondrial function

To follow up the interesting results observed in the Oroboros Oxygraph showing a trend to a reduction of mitochondrial respiration after ammonia treatment, I employed another approach to measure oxidative phosphorylation. The Seahorse XFe96 Extracellular Flux Analyzer (Seahorse Analyzer) using the Mito Stress Test Kit allows to measure mitochondrial respiration with stronger precision and higher replicate number than the Oroboros Oxygraph. Oxygen Consumption Rate (OCR) is determined by subsequent injections of oligomycin, FCCP and rotenone/antimycin A (Fig. 18). Important parameters are the maximal respiration (MR) after FCCP injection and the spare respiratory capacity (SRC), calculated as described in section 2.6.2.1.

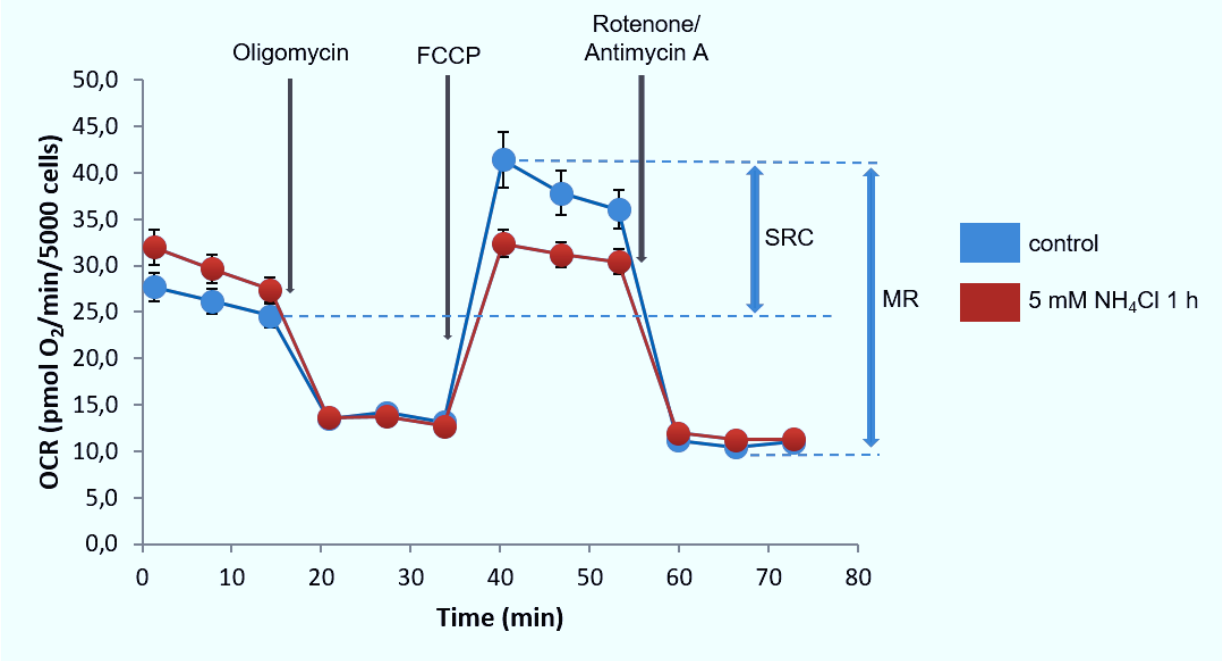

Figure 18: Workflow of Mito Stress Test Kit. Representative graph for Mito Stress Test assay comparing mitochondrial respiration of control cells with 1 h treatment with 5 mM NH_4Cl. First three measurements show basal respiration. After oligomycin injection the leak state is induced. Respiration is challenged with FCCP injections, yielding the parameters maximal respiration (MR) and spare respiratory capacity (SRC). Injection of rotenone and antimycin A blocks respiration giving the value for the residual oxygen consumption, which is subtracted from all other values.

Human astrocytoma cells and primary rat astrocytes were treated with 5 mM NH_4Cl for a defined time course and respiration (OCR) was measured with the Seahorse Analyzer. Human astrocytoma cells were measured after 1 to 48 h ammonia exposure, primary rat astrocytes for durations of 0 h (live) to 6 h, respectively. In both cell types the strongest reduction in OCR was seen at short time points or even immediately in primary rat astrocytes (Fig. 19). This demonstrates an effect of ammonia on cellular function within only minutes after exposure. Interestingly, the effect on mitochondrial respiration was recovering over time and was weaker at longer treatment durations, but for spare respiratory capacity still significant (Fig. 19 A) in human astrocytoma cells. Looking at maximal respiration the reduction in respiration was not significant anymore after 6 h of treatment, so a true recovery is evident over time (Fig. 19 B). In primary rat astrocytes a recovery was observed from live treatment (0 h) to longer treatment periods (Fig. 19 C, D). These data are consistent with results obtained in the Oroboros Oxygraph, were the reduction in ETS was more pronounced after live treatment than after 24 or 48 h of treatment. To sum up, ammonia significantly influences mitochondrial respiration and this effect appears to be almost instantaneous, but recovers with longer time of exposure.

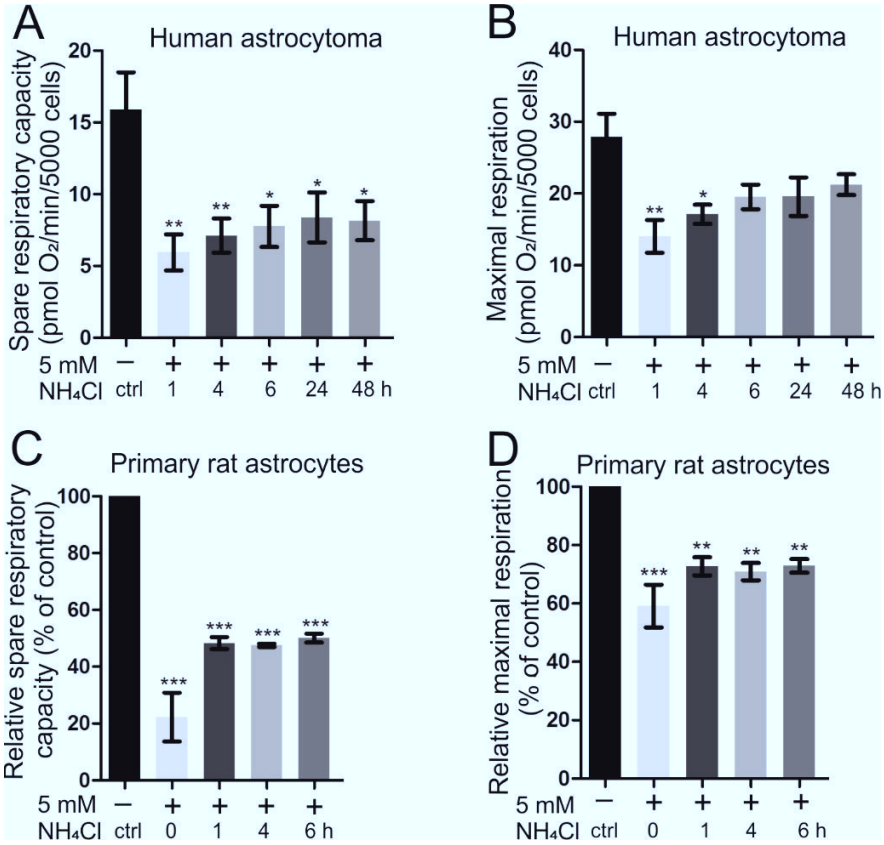

Figure 19: Ammonia rapidly reduces mitochondrial respiration. Oxygen consumption rate (OCR) of human astrocytoma cells and primary rat astrocytes was analyzed on Seahorse XFe96 Extracellular Flux Analyzer with the Mito Stress Test Kit after 5 mM NH_4Cl treatment for indicated duration. (A) Spare respiratory capacity and (B) maximal respiration of human astrocytoma cells after 5 mM NH_4Cl treatment for 1-48 h (n=5-7). (C) Relative spare respiratory capacity and (D) relative maximal respiration of primary rat astrocytes after 5 mM NH_4Cl treatment for 1-6 h and live (n=3-4). Individual biological replicates of C+D normalized to control (100%). Data represented as mean ± SEM. Statistics: One-way ANOVA with Dunnett's post test. *$P < 0.05$, **$P < 0.01$, ***$P < 0.001$.

3.3.3. Detrimental effect of ammonia on mitochondrial respiration is immediate and dose-dependent

Previous results with primary rat astrocytes showed an immediate effect of 5 mM ammonia. However, in patients, ammonia concentrations vary and can also be below 5 mM. It is interesting to see whether lower doses of ammonia will resemble the observed effect on respiration and if these low doses will still be sufficient to yield an immediate response. To follow this, I tested the different NH_4Cl concentrations 1, 2, 5 and 10 mM on human astrocytoma cells treated live (0 h) and measured mitochondrial respiration with the Seahorse Analyzer (Fig. 20). This revealed an immediate effect of ammonia on respiration even at lower concentrations. Concentrations of only 1 mM led to a significant and immediate reduction in

respiration. This effect correlated strongly with dose. In any concentration ranging from 1 to 10 mM the detrimental influence on respiration is immediate and the effect is clearly dose-dependent.

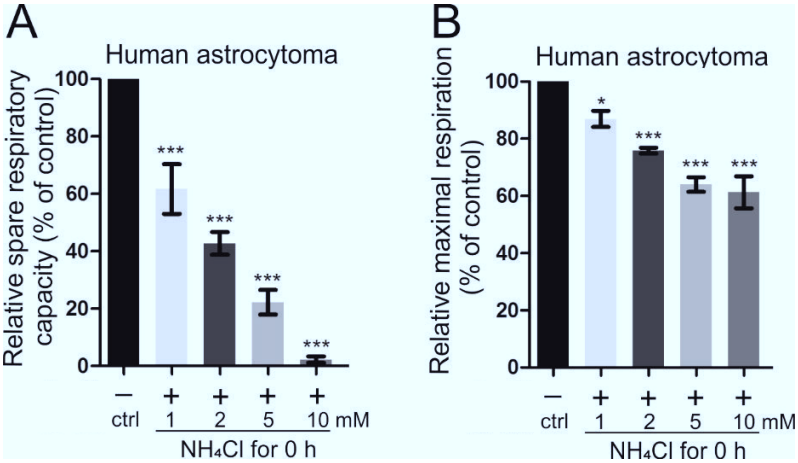

Figure 20: Mitochondrial respiration is immediately impaired by ammonia. Oxygen consumption rate (OCR) of human astrocytoma cells was analyzed on Seahorse XFe96 Extracellular Flux Analyzer with the Mito Stress Test Kit after live treatment with ammonia (0 h). (A) Relative spare respiratory capacity and (B) relative maximal respiration of human astrocytoma cells after live treatment with 1, 2, 5, 10 mM NH_4Cl (n=3). Individual biological replicates normalized to control (100%). Data represented as mean ± SEM. Statistics: One-way ANOVA with Dunnett's post test. **P* < 0.05, ****P* < 0.001.

3.3.4. The decrease in respiration by ammonia is pH-independent

Ammonium in solution has a slightly acidic pH, while ammonia itself is a base causing alkalization of extra- and intracellular conditions. Hence, the question arose if the observed effect on mitochondrial respiration possibly results from a change of pH in medium or cytosol. To shed light on this issue, human astrocytoma cells were treated with 5 mM CH_3NH_3Cl for a duration from 1 to 48 h. Methylammonium chloride (CH_3NH_3Cl) is a pH-mimetic of NH_4Cl, facilitating a similar effect on pH, but without releasing a free ammonium ion. Measuring respiration with the Mito Stress Test Kit on the Seahorse Analyzer showed no significant effect of CH_3NH_3Cl compared to control in the spare respiratory capacity and only after 48 h of treatment when considering maximal respiration (Fig. 21). Hence, it is clear that the observed effect of reduction of mitochondrial respiration is rather mediated by the released free NH_4^+ ion than by possible changes in pH.

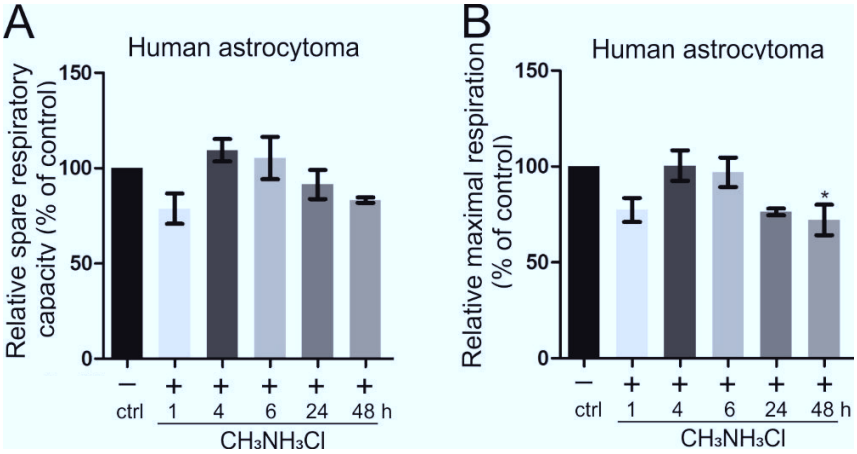

Figure 21: Mitochondrial respiration is impaired in a pH-independent manner. Oxygen consumption rate (OCR) of human astrocytoma cells was analyzed on Seahorse XFe96 Extracellular Flux Analyzer with the Mito Stress Test Kit after treatment with 5 mM methylammonium chloride for indicated duration. (A) Relative spare respiratory capacity and (B) relative maximal respiration of human astrocytoma cells after 5 mM CH_3NH_3Cl (pH-mimetic) treatment for 1-48 h (n=3). Individual biological replicates normalized to control (100%). Data represented as mean ± SEM. One-way ANOVA with Dunnett's post test. *$P < 0.05$.

3.3.5. Ammonia-induced reduction in respiration is quickly reversible

As mitochondrial fragmentation was found to be reversible, I tested whether removal of ammonia for 1 h is sufficient to restore mitochondrial respiration in human astrocytoma cells that have been treated with ammonia for 1 to 48 h. One hour in medium without ammonia led to a full recovery of mitochondrial respiration independent of the previous incubation duration of ammonia (Fig. 22). Interestingly, mitochondrial respiration even showed a tendency to slightly increase after removal of ammonia. This is in consent with my data showing that mitochondrial fragmentation is restored after removal of ammonia from the medium. To conclude, ammonia-induced effects on respiration are quickly reversible after short durations of ammonia removal. The elimination of ammonia even led to an apparent slight increase in respiration, which was however not significant.

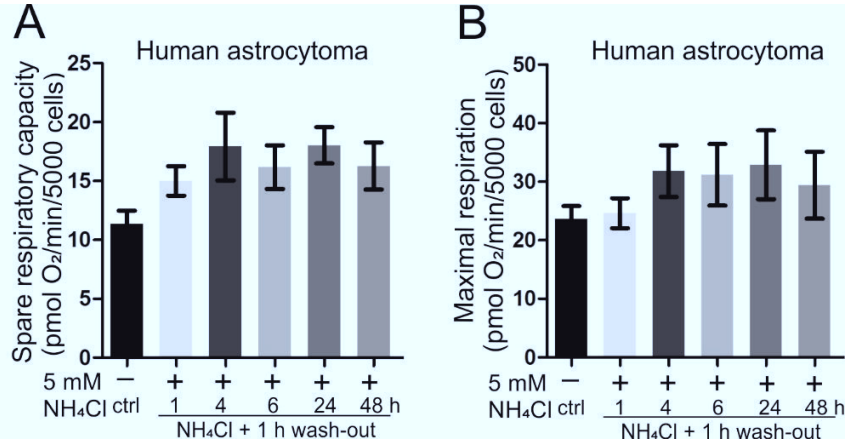

Figure 22: Ammonia-induced decrease in oxygen consumption rate is rapidly reversible. Human astrocytoma cells analyzed with Mito Stress Test Kit on Seahorse XFe96 Extracellular Flux Analyzer. Oxygen consumption rate (OCR) of (A) spare respiratory capacity and (B) maximal respiration after 1 h wash-out of ammonia after treatment with 5 mM NH_4Cl for respective duration 1-48 h. Data represented as mean ± SEM (n=3).

3.3.6. Ammonia rapidly impairs glycolysis

Ammonia negatively influences oxidative phosphorylation. All energetic pathways of the cell are strongly intertwined, which is why in addition to the influence on mitochondrial respiration, I examined the potential influence of ammonia on glycolysis and glycolytic capacity using the Glycolysis Stress Test Kit with the Seahorse Analyzer. Here the extracellular acidification rate (ECAR) is measured under different conditions through the injection of glucose, oligomycin and 2-deoxy-D-glucose, inhibiting glycolysis (Fig. 23 A). This kit is used to estimate glycolysis and glycolytic capacity, which is measured after inhibition of F_1F_O-ATP-synthase by oligomycin and thus represents the capacity of glycolysis to compensate for loss of mitochondrial respiration. This is especially interesting in this context considering the already presented results. For the assay, human astrocytoma cells were treated with 5 mM NH_4Cl for a duration of 1 to 48 h. This led to a significant and rapid reduction of glycolysis and glycolytic capacity when compared to controls (Fig. 23 B, C). This was largely independent of the duration of ammonia treatment and was the case after nearly all treatment durations when looking at glycolysis and glycolytic capacity. In both measured parameters the effect was strongest at early time points, clearly showing the same pattern as observed when measuring with the Mito Stress Kit. As a control, cells were treated with 5 mM CH_3NH_3Cl for 1 and 4 h (Fig. 23 B, C). Treatment with the pH-mimetic compound CH_3NH_3Cl did not have any detrimental effect on glycolysis or glycolytic capacity further corroborating the specific role of ammonia independent from its property to alter the pH. One might have expected an increase of glycolysis at it can theoretically compensate for a loss of energy production in oxidative phosphorylation. On the contrary, glycolysis was also reduced, pointing to a general effect on energy metabolism. Overall, ammonia has a rapid detrimental

effect on glycolysis that cannot be explained by pH changes. Together with the data generated with the Mito Stress Test Kit ammonia appears to strongly change the whole system of energetic pathways in the cell.

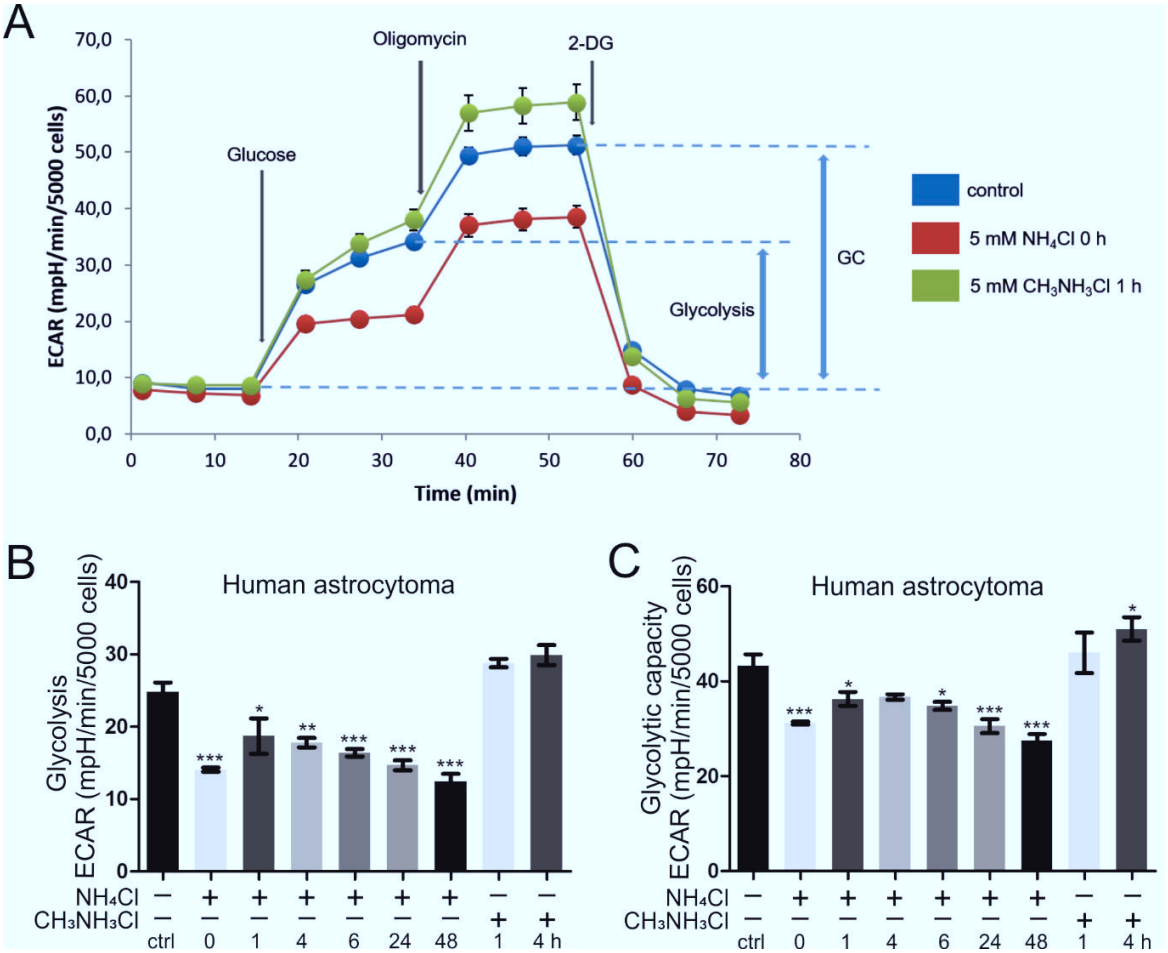

Figure 23: Ammonia rapidly reduces glycolytic function. Extracellular acidification rate (ECAR) was measured in human astrocytoma cells as a proxy for glycolysis using the Glycolysis Stress Test Kit on the Seahorse XFe96 Extracellular Flux Analyzer. (A) Scheme of the Seahorse Glycolysis Stress Test with injections. GC: Glycolytic capacity, 2-DG: 2-deoxy-glucose. (B) Glycolysis and (C) glycolytic capacity of human astrocytoma cells after treatment with 5 mM NH_4Cl for 1-48 h and live (n=3) and treatment with 5 mM pH-mimetic CH_3NH_3Cl for 1 and 4 h (n=2). Data represented as mean ± SEM. Statistics: One-way ANOVA with Dunnett's post test. $*P < 0.05$, $**P < 0.01$, $***P < 0.001$.

3.4. Ammonium chloride influences cell metabolite levels

As described above, ammonia leads to a rapid and drastic change in energy metabolism. To check whether metabolites linked to energy metabolism including amino acids and TCA-cycle intermediates are altered by ammonia treatment, I treated human astrocytoma cells with 5 mM NH_4Cl for durations ranging from 1

to 48 h and subjected them to a targeted metabolomics analysis. Branched chain amino acids (BCAAs) isoleucine, leucine and valine were significantly increased after 24 h. Other essential amino acids methionine, phenylalanine, threonine and tryptophan were increased after 24 h and/or 48 h, respectively. The non-essential amino acids alanine, aspartate, cysteine, proline, serine and tyrosine were increased after 24 h and/or 48 h, while glycine had a significant peak only after 4 h of treatment. The levels of glutamate were not significantly different from controls, however, a clear trend towards an increase was found (Fig. 24 A). Of note, glutamine, asparagine, arginine and histidine cannot be detected with this approach. Lysine was only observed in half of the samples in low concentrations (data not shown). I observed a significant increase in the level of isocitric and/or citric acid after 48 h of ammonia treatment (Fig. 24 B), which are not distinguishable by the GC-MS system used here due to the same mass. Furthermore, a strong increase in glucose levels after 24 and 48 h was observed as well as an increase in the non-proteinogenic amino acid ornithine after 24 h. No changes were seen in all other TCA-cycle intermediates besides (iso)citric acid (Fig. 24 B). Notably, the increase in numerous amino acids after long ammonia treatment durations correlates with the late time points in section 3.3.2., where a slight improvement of mitochondrial respiration was seen (3.3.2., Fig. 19). Treatment with ammonia facilitates a metabolic reprogramming in human astrocytoma cells.

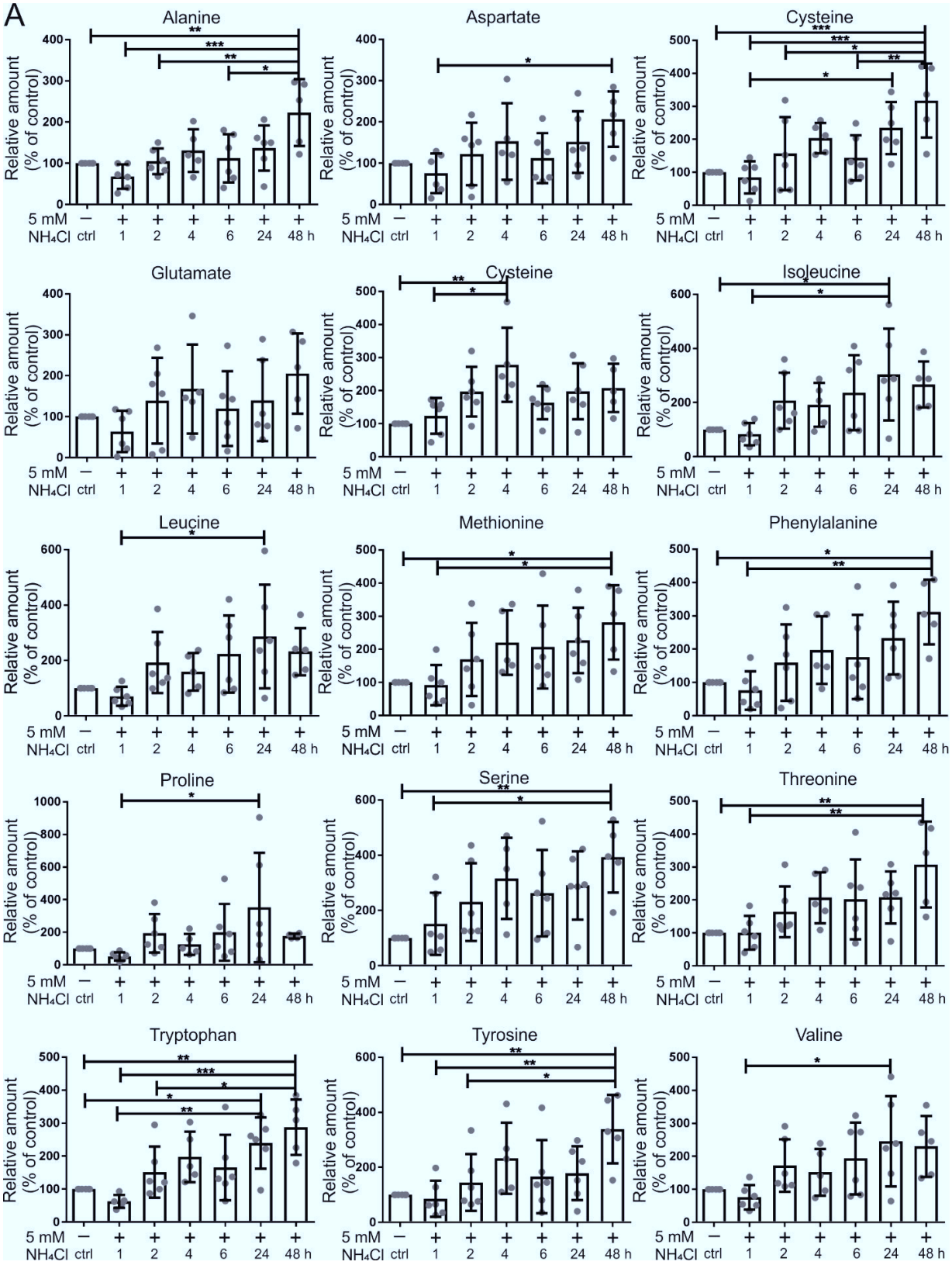
A
Alanine
Aspartate
Cysteine
Glutamate
Cysteine
Isoleucine
Leucine
Methionine
Phenylalanine
Proline
Serine
Threonine
Tryptophan
Tyrosine
Valine
Relative amount (% of control)
5 mM NH4Cl
– ctrl
+ 1
+ 2
+ 4
+ 6
+ 24
+ 48 h

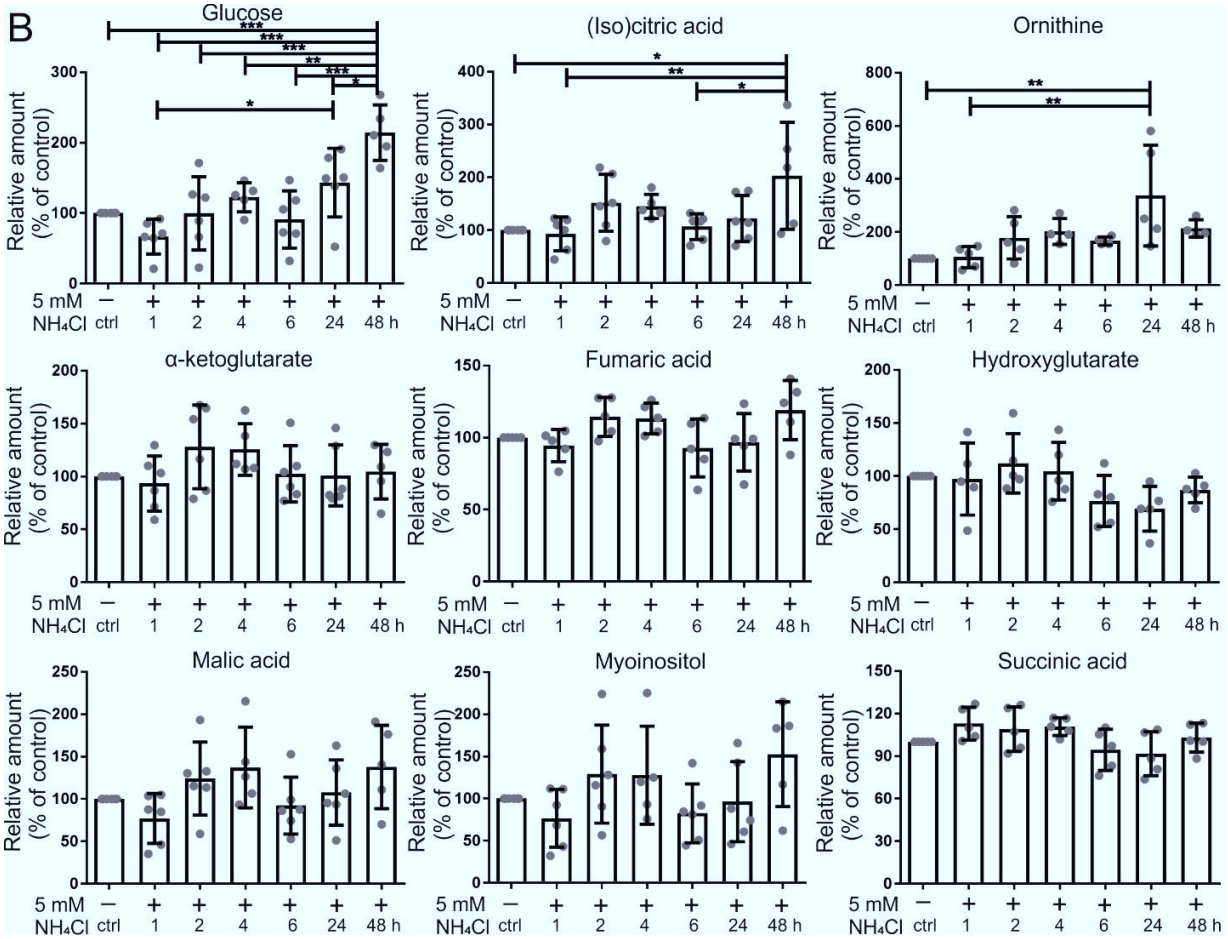

Figure 24: Ammonia alters energy and amino acid metabolism. Mass Spectrometry for steady-state metabolites was done in human astrocytoma cells on GC-QTOF. Treatment with 5 mM NH_4Cl for 1-48 h. (A) Relative abundance of amino acids compared to control (100%) over time. (B) Relative abundance of glucose, ornithine, myoinositol and TCA-cycle intermediates compared to control over time. Data represented as mean ± SD (n=4-6). Individual biological replicates normalized to 100%. Statistics: One-way ANOVA with Tukey's post test. *$P < 0.05$, **$P < 0.01$, ***$P < 0.001$.

3.5. Ammonia-induced changes in energy metabolism are mediated via glutamate dehydrogenase 2

3.5.1. Ammonia is metabolized via glutamate dehydrogenase

The metabolomics approach clearly revealed severe changes of different metabolites after long exposure to ammonia. However, the mechanism behind this and the fate of ammonia in the cell still remains elusive. To test this further, I traced the fate of NH_4^+ in human astrocytoma cells using isotope-labeled $^{15}NH_4Cl$ under the same conditions as before. Treatment with 5 mM $^{15}NH_4Cl$ was done for 1, 2, 4, 6, 24 and 48 h, respectively, compared to non-treated controls. Using LC-MS analysis I revealed that ^{15}N-isotopologues were enriched the most in glutamate and with decreasing abundance in aspartate, proline, and in the

BCAAs valine, leucine and isoleucine, as well as alanine and histidine (Fig. 26). Of note, a strong enrichment occurred already after 1 h, emphasizing a fast incorporation of ammonia-derived nitrogen in these amino acids (Fig. 25, 26 A). The enrichment of ^{15}N-isotopologues was highest after 4 and 24 h and strongest for the three amino acids Glu, Asp, and Pro (Fig. 25 A, B, C and Fig. 26 C, E). Interestingly, glutamate and aspartate enrichments seemed to occur stronger and slightly earlier than enrichment of proline and the BCAAs (Fig. 25). All amino acids labeled by ^{15}N are generated through reactions derived from glutamate in direct synthesis or through transaminase reactions. In turn, nitrogen incorporation into glutamate using ammonia is dependent on the glutamate dehydrogenase (GDH) reaction. This raised the possibility that mitochondrial GDH could be involved in the initial fixation of ammonia in mitochondria.

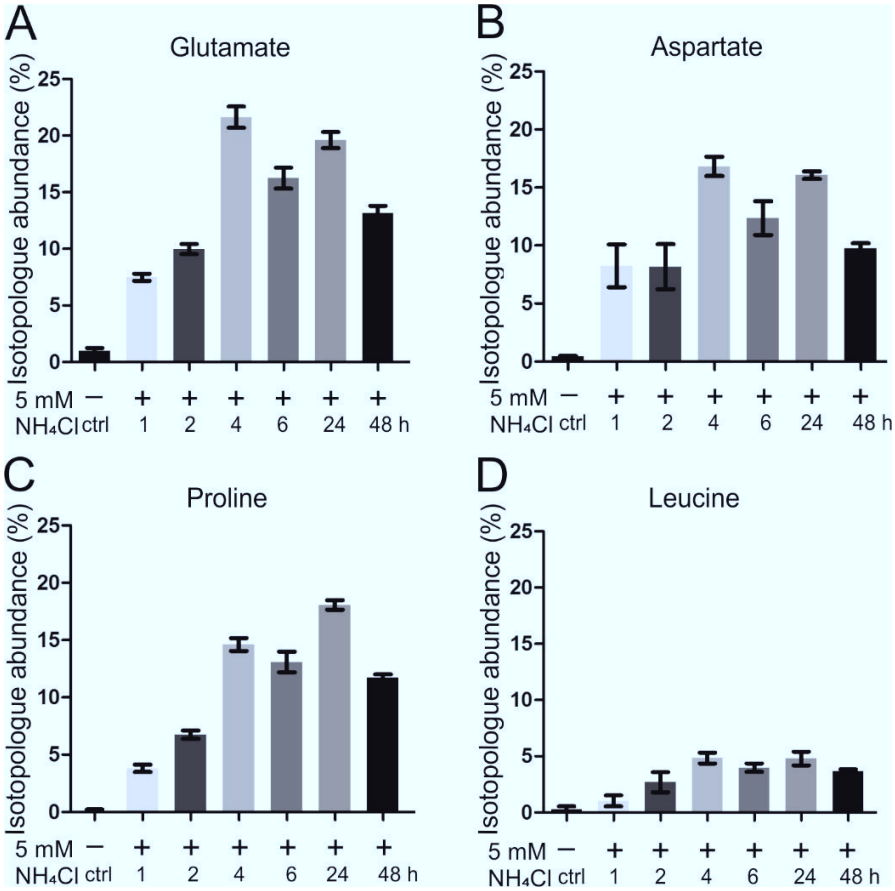

Figure 25: Ammonia is incorporated into amino acids dependent on GDH. Mass Spectrometry for ammonia flux was done in human astrocytoma cells on an LC-MS system. Treatment with $^{15}NH_4Cl$ for 1-48 h. Shown are amino acids mainly found to be enriched in ^{15}N-isotopologue abundance. Isotopologue abundance of ^{15}N in glutamate (A), aspartate (B), proline (C) and leucine (D) over time. Data represented as mean ± SD (n=3).

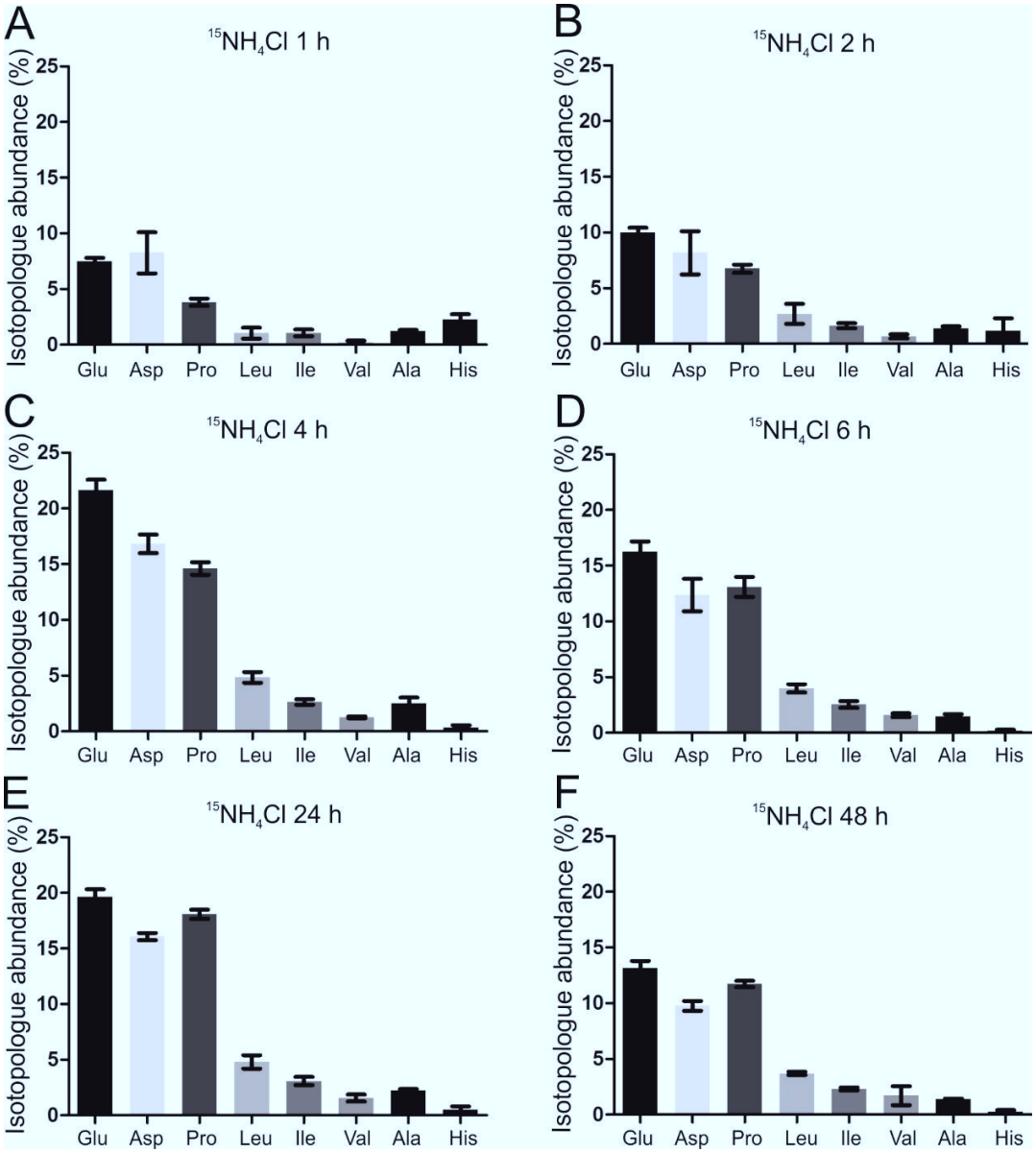

Figure 26: Time course of $^{15}NH_4Cl$ enrichment in amino acids. Mass Spectrometry for ammonia flux was done in human astrocytoma cells on an LC-MS system. Treatment with $^{15}NH_4Cl$ for 1-48 h. All amino acids found to be enriched in ^{15}N-isotopologue abundance shown over time. Isotopologue abundance of ^{15}N after 1 h (A), 2 h (B), 4 h (C), 6 h (D), 24 h (E) and 48 h. Data represented as mean ± SD (n=3).

3.5.2. Knock-down of *GLUD2* rescues the ammonia-induced impairment of mitochondrial respiration

Tracing the fate of ammonia in the cell indicated that ammonia could be primarily metabolized via the mitochondrial glutamate dehydrogenase. To examine the role of GDH2 in hyperammonemia further, GDH2 was downregulated in human astrocytoma cells by targeting the gene encoding for GDH2, *GLUD2*,

using siRNA. The knock-down efficiency was validated using Western blot analysis (Fig. 27 A, B) and qPCR (Fig. 27 C). Knock-down with siGLUD2 for 48 h was effective, compared to the loading control HSP60. Cells depleted for GDH2 were subjected to analysis of OCR using the Mito Stress Test on the Seahorse Analyzer. Depletion of GDH2 efficiently prevented the reduction of mitochondrial respiration upon treatment for 1 h with ammonia, demonstrating an important role of the enzyme in hyperammonemia (Fig. 27 D).

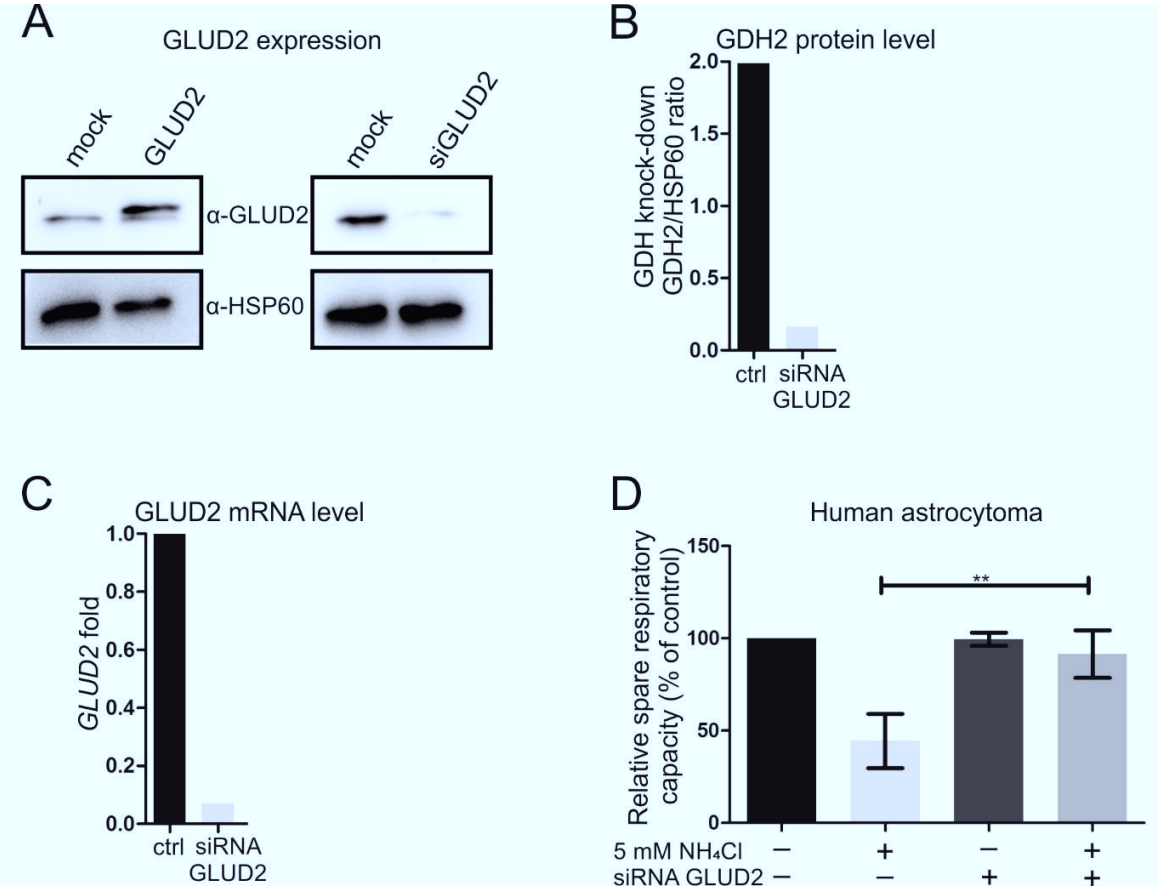

Figure 27: Knock-down of *GLUD2* rescues ammonia-mediated decrease in mitochondrial respiration.
(A) Representative Western blot analysis for human astrocytoma cell lysates from pcDNA3.1-GLUD2 overexpression (48 h) and knock-down (48 h) vs. mock samples, only treated with transfection reagent. α-HSP60 decoration as loading control was done subsequently. (B) Human astrocytoma *GLUD2* knock-down validation. Densitometry of protein level determined by Western blot (A), HSP60 used as loading control. Ratio of GDH2 to HSP60 is shown for knock-down compared to control. (C) mRNA level determined by qPCR, HPRT1 used as housekeeping gene. *GLUD2* fold in knock-down is shown compared to control, normalized to 1. For Western blot and qPCR representative examples are shown. (D) Oxygen consumption rate (OCR) of relative spare respiratory capacity in human astrocytoma cells was analyzed on Seahorse XFe96 Extracellular Flux Analyzer with the Mito Stress Test Kit. *GLUD2* knock-down via siRNA transfection for 48 h ± 5 mM NH_4Cl treatment for 1 h. Individual biological replicates normalized to control (100%) (n=3). Statistics: One-tailed student's t-test comparing 2 groups. Data represented as mean ± SEM. $^{**}P < 0.01$.

3.5.3. *GLUD2* overexpression slightly exacerbates the detrimental effect of ammonia on mitochondrial respiration

To further test the role of GDH2 during hyperammonemia, GDH2 was overexpressed in human astrocytoma cells and they were subjected to OCR measurements employing the Mito Stress Kit. Successful overexpression was validated by Western blot analysis (Fig. 27 A). Treatment of GDH2-overexpressing cells with 5 mM NH_4Cl for 1 h exacerbates the decrease of mitochondrial respiration observed before, with and without additional transfection with siGLUD2 (siRNA not targeting *GLUD2* plasmid sequence) (Fig. 28). In accordance with the GDH2 knock-down results presented before, the transfection with siGLUD2 alone prevented ammonia-induced impairment of respiration (Fig. 28 B), confirming the knock-down results described in section 3.5.2. Taken together, this data strongly supports the hypothesis that GDH2 is a critical factor for the rapid impairment of mitochondrial respiration caused by hyperammonemia and the involvement of this enzyme has not been considered in this context before.

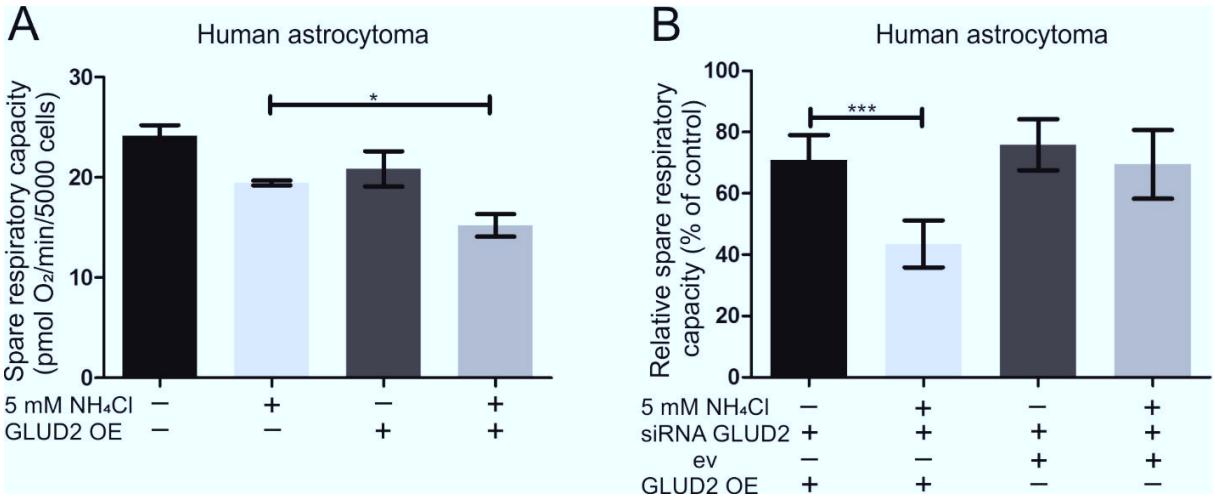

Figure 28: *GLUD2* overexpression exacerbates detrimental effect of NH_4Cl on mitochondrial respiration. (A) Spare respiratory capacity of human astrocytoma cells. *GLUD2* overexpression for 48 h. Treatment with 5 mM NH_4Cl for 1 h (n=5). (B) Relative spare respiratory capacity of human astrocytoma cells. Treatment with 5 mM NH_4Cl for 1 h. Knock-down of *GLUD2* for 48 h when indicated, overexpression of *GLUD2* plasmid or empty vector (ev) for 48 h when indicated. Individual biological replicates normalized to control (100 %, not shown) (n=5). Statistics: One-tailed student's t-test comparing 2 groups. Data represented as mean ± SEM. $*P < 0.05$, $***P < 0.001$.

3.5.4. Overexpression of GDH regulator SIRT4 rescues ammonia-induced impairment of mitochondrial respiration

To investigate the suggested concept of GDH2 contribution in ammonia-induced decrease of respiration another approach was employed targeting a known regulator of GDH. GDH is known to be inhibited by

ADP-ribosylation catalyzed by the mitochondrial sirtuin SIRT4 (Haigis et al., 2006). Therefore, I used HeLa-SIRT4-eGFP cells, a stable cell line overexpressing SIRT4 and the corresponding control cells HeLa-eGFP to test whether inhibition of GDH2 by SIRT4 can also restore mitochondrial respiration in the presence of high ammonia levels. OCR of both cell types was measured using the Mito Stress Kit in the Seahorse XFe96 Analyzer with or without treatment with 5 mM NH_4Cl for 1 h. The spare respiratory capacity of untreated HeLa-SIRT4-eGFP and HeLa-eGFP were not affected whereas after ammonia treatment respiration dropped significantly in HeLa-eGFP cells but not in cells overexpressing SIRT4 (Fig. 29). Regulation of GDH2 by SIRT4 can prevent the detrimental effect of ammonia on respiration, phenocopying the knock-down experiments in section 3.5.2 (Fig. 27 D). Overall, several lines of evidence assign an essential role to the mitochondrial glutamate dehydrogenase, GDH2, for the rapid impairment of mitochondrial respiration under hyperammonemia. These results give rise to a completely new mechanism in the pathogenesis of HE.

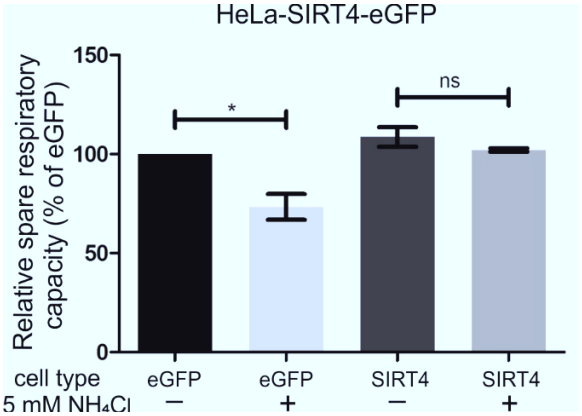

Figure 29: SIRT4 overexpression rescues ammonia-induced decrease in respiration. Relative spare respiratory capacity in % measured with Seahorse XFe96 Extracellular Flux Analyzer using Mito Stress Test Kit. HeLa-eGFP (eGFP) and HeLa-SIRT4-eGFP (SIRT4) cells treated with 5 mM NH_4Cl for 1 h or left untreated as controls. Values of individual biological replicates normalized to HeLa-eGFP cells (100 %) (n=3). Statistics: One-tailed student's t-test comparing 2 groups. Data represented as mean ± SEM. *$P < 0.05$, ns: not significant.

3.5.5. Glutamine and glutamate supplementation rescues ammonia-derived reduction of mitochondrial respiration

If the GDH2 reaction, an important pathway of anaplerosis, plays indeed an important role in the fixation of ammonia thereby disturbing bioenergetic pathways, an anaplerotic supplementation of this and other anaplerotic reactions might rescue the ammonia-induced effect. In order to test this, I supplemented ammonia treated cells with different amino acids. Pretreatments with 10 mM aspartate, α-ketoglutarate,

glutamate, glutamine and pyruvate, respectively, were done directly before treatment with 5 mM NH_4Cl for 1 h. As controls cells were treated with NH_4Cl or respective compound only at same concentration and with same treatment durations as described before. Pretreatment with glutamine led to a full rescue of ammonia-mediated decrease in mitochondrial respiration (Fig. 30 D). In addition, pretreatment with glutamate showed a strong trend to rescue the effect, too (Fig. 30 C). Treatment with pyruvate alone decreased respiration to the same extent as ammonia and hence, treatment with pyruvate and NH_4Cl decreases respiration even more than single-compound treatment (Fig. 30 E). Interestingly, treatment with the compounds aspartate and α-ketoglutarate alone strongly decreased respiration, more than ammonia treatment. Nevertheless, in cells treated with the respective compound and NH_4Cl together there was no additive effect as in pyruvate (Fig. 30 A, B). Rather, ammonia seemed to slightly alleviate the detrimental effect of aspartate and α-ketoglutarate, respectively. Overall, anaplerotic supplementation of certain amino acids can rescue the effect of ammonia.

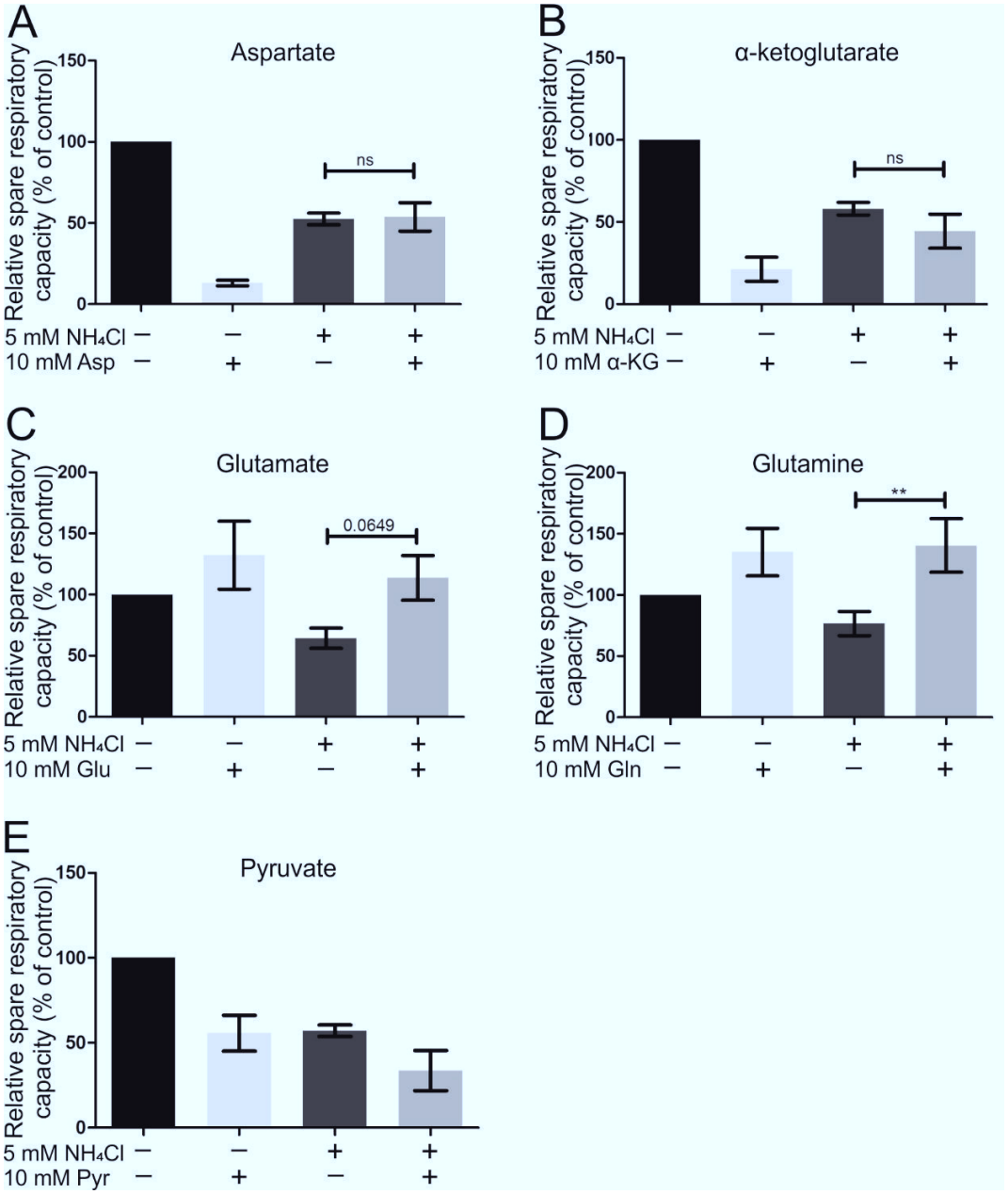

Figure 30: Supplementation of glutamate and glutamine can rescue mitochondrial respiration. Human astrocytoma cells were subject to Mito Stress Kit measurement on Seahorse XFe96 Extracellular Flux Analyzer. Supplementation was tested for (A) aspartate (n=3), (B) α-ketoglutarate (n=7), (C) glutamate (n=4-5), (D) glutamine (n=5) and (E) pyruvate (n=6). Treatment with 10 mM respective compound, 1 h 5 mM NH_4Cl only or simultaneous treatment with 10 mM compound + 1 h 5 mM NH_4Cl. Relative spare respiratory capacity is shown. Individual biological replicates normalized to control (100%). Data represented as mean ± SEM. Statistics: One-tailed student's t-test comparing 2 groups. $^{**}P < 0.01$, ns: not significant, 0.0649: exact *P*-value.

3.6. Galactose medium alleviates ammonia-induced decrease in mitochondrial respiration

In our group it has been shown before that autophagy induction can alleviate the detrimental effect of ammonia (PhD thesis, Kaihui Lu). Galactose medium can induce autophagy (Roa-Mansergas et al., 2018) and this carbohydrate source is often used instead of glucose in media to investigate respiration, as it drives cells towards oxidative phosphorylation (Robinson et al., 1992). To test for an autophagy role, human astrocytoma cells were treated with 5 mM NH_4Cl for a time course ranging from 1-48 h and respiration was measured with the Mito Stress Kit on Seahorse Analyzer as described before, but cells were grown and measured in medium without glucose. Instead, medium and assay medium were supplemented with 1 g/l galactose. Strikingly, the data revealed no significant changes in mitochondrial respiration after ammonia treatment, irrespective of treatment duration (Fig. 31). This is in contrast to data shown in Fig. 19, were cells were grown and measured in 1 g/l glucose medium. Galactose is metabolized via a different pathway than glucose, thus, this apparently has an influence on how ammonia affects mitochondrial respiration, possible via the induction of autophagy through glucose deprivation (Data from Bachelor thesis by Rebecca E. Poss).

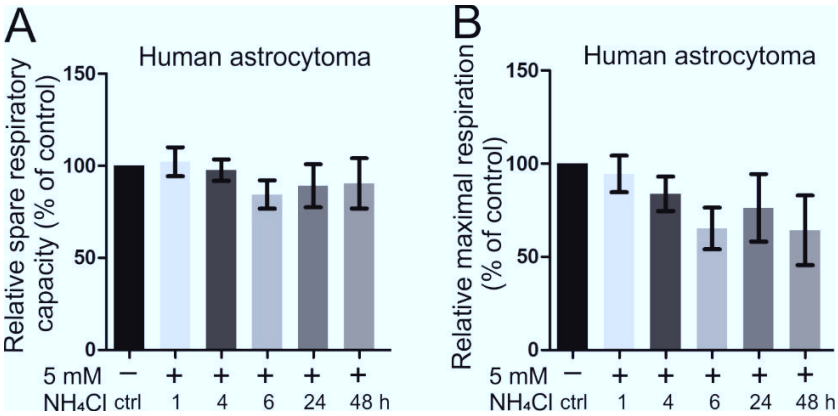

Figure 31: Ammonia has no effect on respiration in galactose medium. Oxygen consumption rate (OCR) of human astrocytoma cells was analyzed on Seahorse XFe96 Extracellular Flux Analyzer with the Mito Stress Test Kit after 5 mM NH_4Cl treatment for indicated duration. Relative spare respiratory capacity (A) and relative maximal respiration (B) shown after 5 mM NH_4Cl treatment for 1-48 h (n=3-4). Individual biological replicates normalized to control (100%). Data represented as mean ± SEM. Significance was tested with one-way ANOVA with Dunnett's post test and yielded no significant results (Data from Bachelor thesis by R.E. Poss).

3.7. Lowering pH in the lysosome can partially rescue ammonia-induced reduction of mitochondrial respiration

To follow up the interesting results obtained with galactose medium, another way of autophagy induction was tested to rescue mitochondrial respiration. Human astrocytoma cells were treated with 25 µg/ml photoactivatable nanoparticles (pa-NPs), which can reacidify the lysosome upon photo-activation (Trudeau et al., 2016), and incubated for 4 h in order to allow pa-NPs to enter the cells. Then, cells were treated with 5 mM NH_4Cl and pa-NPs were activated by UV light for 5 min at 365 nm. Control cells were not exposed to UV light. Ammonia treatment was performed for 24 h with subsequent measurement of mitochondrial respiration on Seahorse Analyzer (Fig. 32). The depicted factor represents the rescue of respiration in comparison to cells treated with ammonia ± pa-NPs. In detail, to calculate this, first $+NH_4Cl$ values were divided by $–NH_4Cl$ values, separately for ± pa-NPs. Then, with these results $+NH_4Cl$ +NP was divided by $+NH_4Cl$ –NPs, which revealed the respective factor of rescue. Without the activation by UV light, the difference between cells with and without pa-NPs was negligible. The slight rescue by factor 1.09 and 1.03 in spare respiratory capacity and maximal respiration (Fig. 32 A, C), respectively, was probably due to light scattering and thereby activation of a small amount of NPs. After photo-activation, pa-NPs mediated a rescue of mitochondrial respiration in spare respiratory capacity and maximal respiration, respectively, when comparing to ammonia-treated cells without pa-NP pretreatment (Fig. 32 B, D). The pa-NPs facilitate an acidification of the lysosome upon photo-activation and can hence promote autophagy. Acidification of the lysosome seems to facilitate a rescue of the ammonia-induced decrease in mitochondrial respiration and could suggest a role of autophagy. This requires further investigation and could reveal a possible target for treatment options.

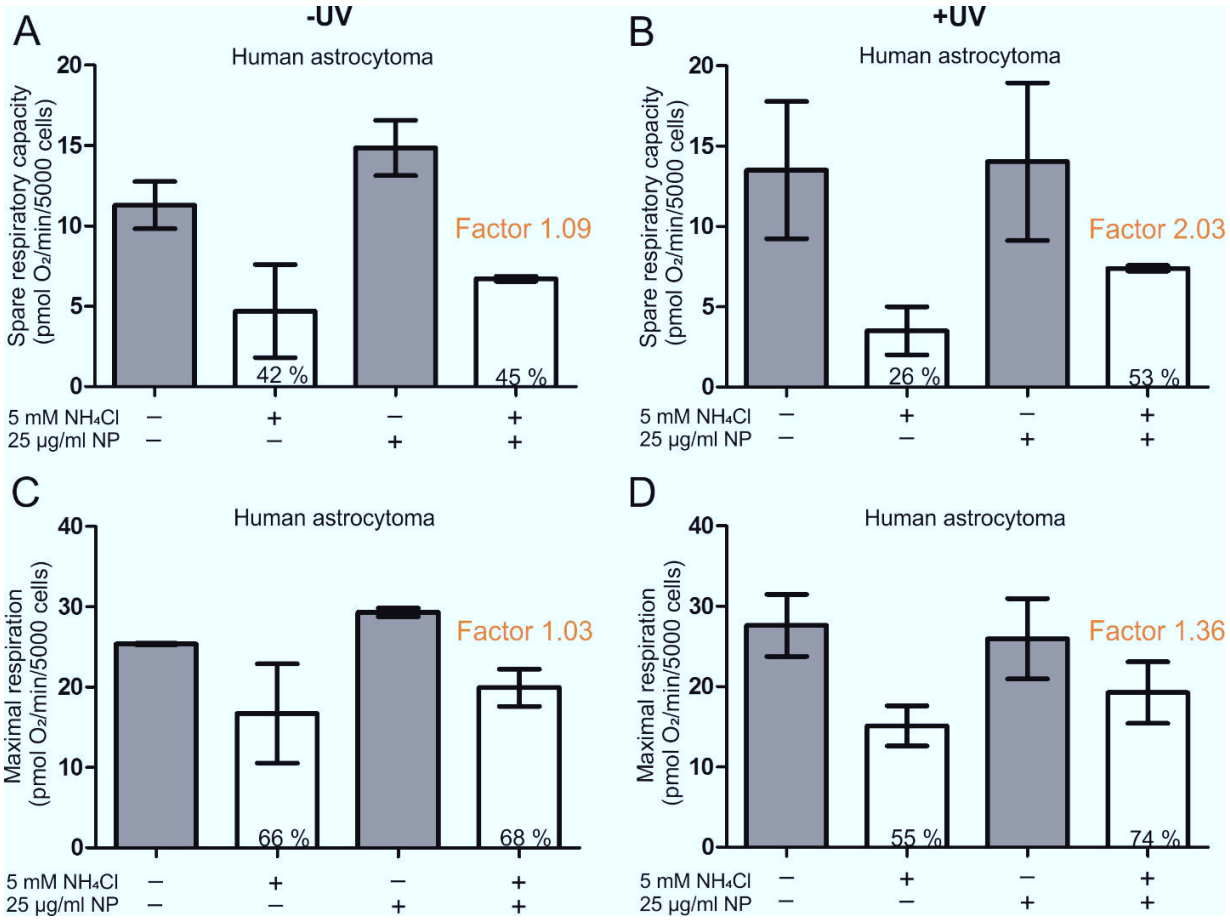

Figure 32: Acidification of lysosome reduces ammonia-mediated decrease of mitochondrial respiration. Human astrocytoma cells were treated with nanoparticles (NPs) for 4 h, subsequently treated with 5 mM NH_4Cl for 24 h and NPs were activated with UV light simultaneously. Measurement on Seahorse XFe96 Analyzer after 24 h treatment. Spare respiratory capacity (A) and maximal respiration (C) of samples treated with NPs, 5 mM NH_4Cl or NPs + NH_4Cl as well as untreated controls. NPs were not activated with UV light. (B) and (D) show spare respiratory capacity and maximal respiration of cells treated as described before but with activated NPs by exposure to 5 min UV light (365 nm). Factor: Rescue in oxygen consumption in NH_4Cl treated samples with addition of NPs, compared to NH_4Cl exposure without NPs; details are explained in the section above. %: Percentage of respective control. Data presented as mean ± SD (n=2).

4. Discussion

Hepatic encephalopathy is a common complication occurring upon severe liver dysfunction. Even so it is largely accepted that hyperammonemia-induced impairment of astrocyte function plays a major role in mediating neurological disturbances (Görg et al., 2018; Häussinger and Görg, 2010; Norenberg, 1987), the underlying molecular mechanisms are still not well understood. One particular aspect that is quite controversially discussed is the role of altered brain energy metabolism caused by hyperammonemia. For example, alterations of the metabolome of the CSF and plasma in HE patients have been discussed (Weiss 2016). Further, differences in respiratory chain enzyme activities were found in rat HE models (Boer et al., 2009; Dhanda et al., 2017). Additionally, different results on altered levels/activities of TCA-cycle metabolites and enzymes have been reported (reviewed in Rama Rao and Norenberg, 2012). Overall, it is clear that a role of alterations in brain energy metabolism and in the TCA-cycle is suspected. So far, to my knowledge a majority of studies investigating acute as well as chronic *in vitro* and *in vivo* HE models address toxic effects of hyperammonemia after one or more days investigating long term effects (Görg et al., 2015; Hazell and Norenberg, 1998; Oenarto et al., 2016; Qvartskhava et al., 2015). However, little is known about the immediate effect of ammonia on brain metabolism, so I focused to investigate rather early effects of hyperammonemia. In this study, I provide several lines of evidence that high ammonia levels lead to a rapid change in morphology and facilitate major metabolic reprogramming of astrocytes. Metabolic dysfunctions in oxidative phosphorylation and glycolysis result from GDH-mediated depletion of α-ketoglutarate, which can be rescued by manipulating GDH activity. The observed changes and impairments represent yet unidentified early events in the pathogenesis of HE. Furthermore, I shed light on a possible involvement of autophagy in the pathogenesis of HE and open doors to the development of novel treatment options.

4.1. Ammonia intensively changes mitochondrial morphology, depending on ROS but not changing the expression of fusion and fission factors

Mitochondrial fragmentation was quantified by confocal microscopy assays after treatment of cells with 5 mM NH_4Cl for different durations. The concentration used was found to not reduce cell viability up to 72 h of ammonia treatment (Fig. 12). Determining mitochondrial morphology via fluorescence microscopy revealed that ammonia introduces rapid mitochondrial fragmentation in both examined cell types, namely human astrocytoma cells and primary rat astrocytes (Fig. 13). In this data, fragmentation in primary cells was more rapidly and more severely observed than in human astrocytoma cells, which could be attributed

to metabolic differences known to exist in tumor cells (Hsu and Sabatini, 2008). Still, besides the differences in reaction time, both cell types demonstrate the same reaction to ammonia, which interestingly reaches a plateau after 24 h. Of note, mitochondrial fragmentation was reversible after removal of ammonia (Fig. 16). Alterations of mitochondrial morphology are well known to occur upon mitochondrial dysfunction. For example, Duvezin-Caubet and colleagues showed that proteolytic processing of OPA1 is very important for the induction of fragmentation, especially when mitochondrial energy levels are compromised (Duvezin-Caubet et al., 2006). Furthermore, fission and fusion defects are important features in mitochondrial diseases, such as optic atrophy 1 (Delettre et al., 2000, 2002) and Charcot-Marie-Tooth subtype 2A (Züchner et al., 2004).

There is evidence on the influence of ROS in HE pathogenesis. It was shown that hyperammonemia causes an increase in RNOS via the activation of the NADPH oxidase and nitric oxide synthase, leading to protein tyrosine nitration, RNA oxidation and gene expression changes downstream (Görg et al., 2008, 2013; Häussinger and Görg, 2010). As ROS is one of the known contributors to HE it is interesting to observe that scavenging ROS with NAC reduces mitochondrial fragmentation after 24 h of ammonia treatment in human astrocytoma and primary rat astrocytes (Fig. 14, 15). Intriguingly, this rescue effect is less evident after 48 h, which most likely is due to the complete consumption of NAC as it was only added at the beginning of the rather long treatment period. Interestingly, fission and fusion factors were shown to be changed upon different stressors leading to fragmentation, for example after exposure to oxidative stress (Iqbal and Hood, 2014; Wu et al., 2011). Changes in mRNA levels were not detectable in this study (data not shown). It is notable to mention that in our group a dose-dependent increase of the fusion protein OPA1 was found, which however could also be due to an increase in mitochondrial biogenesis (PhD thesis, Kaihui Lu). An underlying mechanistic change or primary or secondary influences of ammonia on translation or transcription of fission of fusion factors do not seem to be existent. Therefore, I presume fragmentation to rather be a result of energy deficiency, which has been shown to induce fragmentation before (reviewed in Westermann, 2012) or that increased fragmentation after ammonia exposure is merely a reaction of the cell to the exogenous stressor (*e.g.* as shown for ROS in Frank et al., 2012) in order to avoid a possible distribution of damages throughout the mitochondrial network.

4.2. Energy metabolism is rapidly impaired by ammonia in a pH-independent manner

To determine changes in function of mitochondria, cells were subject to measure mitochondrial respiration in the Oroboros Oxygraph and Seahorse XFe96 Extracellular Flux Analyzer. First tests in the Oroboros with HeLa WT and human astrocytoma cells already revealed a tendency for a detrimental effect

of ammonia on respiration, especially after short treatment periods (Fig. 17). This was even more evident after measurement in the Seahorse Analyzer examining a large time scale of ammonia treatments. Hyperammonemia resulted in a strong impairment of mitochondrial respiration in primary rat astrocytes and human astrocytoma (Fig. 19), even more intense after short time points than after long treatment durations, resembling results observed in the Oroboros Oxygraph. Of note, in both systems the basal respiration remained intact, all changes described refer to challenged respiration induced by uncouplers CCCP or FCCP, respectively. This means ATP is still produced and all basic energy requirements can still be met. However, as soon as the system is challenged, in physiological means *e.g.* in situations of stress, disease or simply phases of high energy demands, ammonia drastically reduces the capacity in respiration to deal with the situation. The inhibitory effect of ammonia on respiration was fast (Fig. 19, 20), in detail within minutes, and was concentration dependent (Fig. 20). To my knowledge such an early event in hyperammonemia has not been shown to date. Importantly, the effect was not mediated by possible changes in cellular pH by NH_4Cl, as a pH-mimetic compound did not impair respiration (Fig. 21) excluding the immediate effect on mitochondrial function to be a secondary pH-mediated effect. In this study, when ammonia was removed from medium for only one hour, the detrimental effect on respiration not only vanished, but respiration rather reached OCR levels above control levels, in particular after longer pretreatments with ammonia (Fig. 22). This could be due to accumulated amino acids (Fig. 24) or other metabolites (Weiss et al., 2016) rapidly engaging in anaplerotic reactions and thus, driving the TCA-cycle as soon as ammonia is removed. Furthermore, detrimental effects of ammonia are quickly reversible which was also seen in mitochondrial morphology (Fig. 16, 22). This is of interest, because HE has long been considered to be a reversible condition after liver transplantation, albeit a persistence in cognitive impairment in patients with preceding episodes of overt HE have been reported as well (Bajaj et al., 2010). Naturally, results from cell culture experiments often cannot be transferred to patients one-to-one, but my experiments provide the molecular basis for approaches regarding energy metabolism in HE. Moreover, glycolysis was markedly hampered during hyperammonemia (Fig. 23), which is in concordance with the observed increase in glucose over time investigated in my metabolomics approach (Fig. 24 B). To sum up, it is obvious that ammonia strongly interferes with energy metabolism and that this effect is rapid and quickly reversible to a full extent.

4.3. Metabolic reprogramming of the cell is triggered by ammonia

Metabolomic analyses revealed severe changes in astrocytoma cells treated with ammonia. Ammonia treatment resulted in an increase of several amino acids including those that are directly or indirectly able

to engage in anaplerotic reactions feeding the TCA-cycle (Fig. 24). Furthermore, increase is highest after 24 and/or 48 h of ammonia exposure, which is consistent with the data on mitochondrial respiration revealing a less prominent effect of ammonia on OCR at these time points (Fig. 19). Possibly, a higher availability of amino acids can compensate for the defect in respiration. The increase in amino acids could result from an increase in autophagy or proteasomal degradation or result from the fact that they cannot be used for anaplerosis and thus accumulate. Interestingly, from all TCA-cycle intermediates measured, only isocitric/citric acid (Fig. 24 B) (indistinguishable by GC-QTOF) showed an increase; the reason can only be subject for speculations. Glucose levels were strongly increased consistent with the observation that glycolysis is inhibited rapidly in hyperammonemia (Fig. 24 B).

4.4. Glutamate dehydrogenase 2 plays a striking role in the pathogenesis of hyperammonemia

To further trace the fate of ammonia in cells, treatment of astrocytoma cells with $^{15}NH_4Cl$ was performed and samples measured on LC-QTOF. Isotope-labeling of ammonia and metabolic tracing showed that ammonia is rapidly fixed in glutamate and metabolites swiftly derived from glutamate, such as aspartate, proline and the branched-chain amino acids (Fig. 25), which are either directly synthesized via glutamate dehydrogenase (glutamate), synthesized from glutamate directly (*e.g.* proline) or via transaminase reactions (*e.g.* aspartate) (Fig. 33).

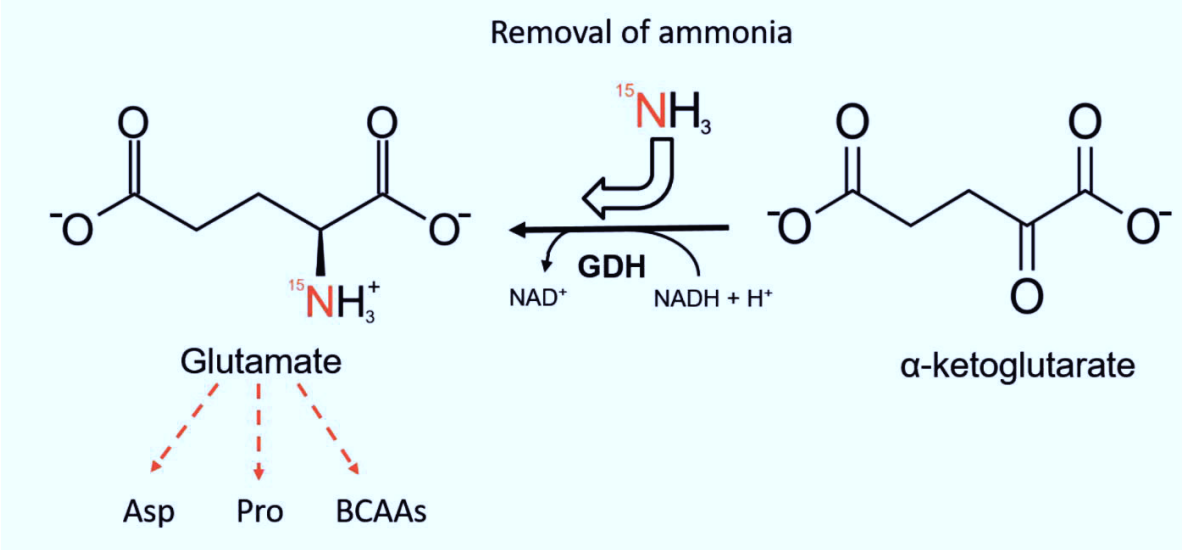

Figure 33: Fate of nitrogen after $^{15}NH_4Cl$ labeling. Pathway of ^{15}N-ammonia recycling and utilization via glutamate dehydrogenase (GDH) and secondary reactions. Red arrows indicate the path of nitrogen.

This prompted me to investigate the role of glutamate dehydrogenase, which catalyzes the reductive amination of α-ketoglutarate and ammonia to glutamate. Indeed, ammonia-induced inhibition of mitochondrial respiration is strongly dependent on the mitochondrial GDH2 suggesting that removal of ammonia may occur via GDH2. Knock-down of *GLUD2*, the gene encoding for GDH2, rescued the ammonia-induced effect on respiration in human astrocytoma cells (Fig. 27). This is supported by the observation that GDH2 inhibition by SIRT4 overexpression can phenocopy the GDH2 knock-down effect (Fig. 29). Moreover, GDH2 overexpression resulted in a sensitization of astrocytes to ammonia (Fig. 28). Lastly, glutamate as well as glutamine addition was beneficial (Fig. 30). Under hyperammonemia the GDH2 reaction is reversed, away from anaplerosis, because the concentration of ammonia in the mitochondria is a lot higher than the ones of glutamate and α-ketoglutarate. Hence, when supplementing with even higher (10 mM) amounts of glutamate (or glutamine), the reaction equilibrium is shifted back to the usual anaplerotic direction. These results are further emphasizing a crucial role of the GDH2-catalyzed anaplerotic reaction.

Taken together, I present several consistent lines of evidence that a critical entry point of excessive ammonia is the reductive amination of α-ketoglutarate by GDH2 causing impairment of the TCA-cycle and thus consequently of respiration as well as glycolysis (Fig. 35 B). GDH2 is known to play an important part specifically in astrocytes, yet its role under hyperammonemia is not well understood. It was reported that *hGLUD2* expression in astrocytes increases the capacity for uptake and oxidative metabolism of glutamate, particularly during increased workload and aglycemia, implying GDH2 as an important reaction allowing to replenish the TCA-cycle from glutamate (Nissen et al., 2017). This is in line with my data showing that increasing glutamate levels can indeed ameliorate the effect of hyperammonemia on respiration (Fig. 30). A recent study showed that metabolic differences between transgenic *hGLUD2* mice and control mice during postnatal brain development center on metabolic pathways surrounding the TCA-cycle (Li et al., 2016). These results put another line of support to the importance of the GDH2-dependent modulation of energy metabolism in the brain.

In contrast to the prevailing view, my data show that under hyperammonemia α-ketoglutarate is primarily converted to glutamate and not *vice versa* (Fig. 35 A, B). To my knowledge, this direction of the GDH reaction was not considered to be relevant for the pathogenesis of HE so far. This does not dispute the role of glutamate dehydrogenase as an important enzyme for anaplerosis, but GDH was not considered to be able to remove ammonia in the brain when concentrations are high enough to drive the reaction into the opposite direction. Still, a hint for an ammonia-detoxifying role of GDH was already found in the rat liver, where an injection of ammonia led to a decrease in α-ketoglutarate and a change in the concentration ratio of [glutamate]/[α-ketoglutarate]+[NH_4^+] (Williamson et al., 1967). This was also

proposed based on a mathematical model employed to investigate the mechanism of ammonia detoxification in the liver (Ghallab et al., 2016). Consistent with this, intravenous injection of GDH and α-ketoglutarate with cofactors into mice led to a reduction of ammonia blood levels to normal levels within 15 minutes (Ghallab et al., 2016). Additionally, a rapid decrease in α-ketoglutarate concentration in the rat liver was reported after injection of ammonium chloride solution (Williamson et al., 1967). To my knowledge, the role of GDH-dependent ammonia detoxification in other tissues than the liver was not addressed so far. Thus, the data support the idea that GDH2 in human astrocytes on one hand helps to remove the ammonia load, but on the other hand impairs the TCA-cycle. It acts as a double-edged sword as GDH2-mediated removal of ammonia is not only beneficial, as commonly expected, but rather detrimental to astrocytes. As a result of impairing the TCA-cycle it is explainable why glycolysis as well as OXPHOS is impaired rapidly as a consequence. It might have been expected that glycolysis would increase in order to compensate for OXPHOS reduction. The contrary is the case (Fig. 23), which could result from a decrease in TCA-cycle flux, leading to reduction of channeled acetyl-CoA to the TCA-cycle in turn resulting in an inhibition of pyruvate dehydrogenase and thus, glycolysis as a whole (Fig. 34). I see a clear concentration dependency of ammonia-induced effects on respiration (Fig. 20). This is in accordance to most patient data showing a correlation between blood ammonia levels and severity of disease (Stahl, 1963). Nevertheless, there are exceptions were ammonia levels are not directly correlated to the patient's state of health, but reasons for this are still unknown (Ong et al., 2003; Sherlock, 1958; Stahl, 1963). It is not clear, why the metabolomics approach does not show a significant elevation of glutamate after ammonia exposure (Fig. 24 A). Possible explanations for this discrepancy could be the strong entanglement of GDH2 and glutamate in the mitochondrial metabolism. Figure 34 shows the many reactions around glutamate, which could simply mask the effect in a steady-state measurement. Another possible reason could be the quick conversion from glutamate to glutamine, an amino acid that was not measurable by the GC-MS system used. Data from patients also show increased values of glutamine in the brain and CSF (Hourani et al., 1971; McConnell et al., 1995), so it is well possible that a rise in glutamate is therefore not seen in a steady-state approach. However, still a clear trend of glutamate increase can be observed. Furthermore, I cannot observe a decrease in α-ketoglutarate in steady-state metabolomics (Fig. 24 B). Possibly, this is because before metabolomics measurement mitochondrial respiration was not challenged by an uncoupler and thus the changes here are not as strong. However, an increase has been observed by others (Williamson et al., 1967) and in steady-state measurements fast and strongly intertwined reactions or its intermediates can easily be masked as it is the case for α-ketoglutarate (see Fig. 34).

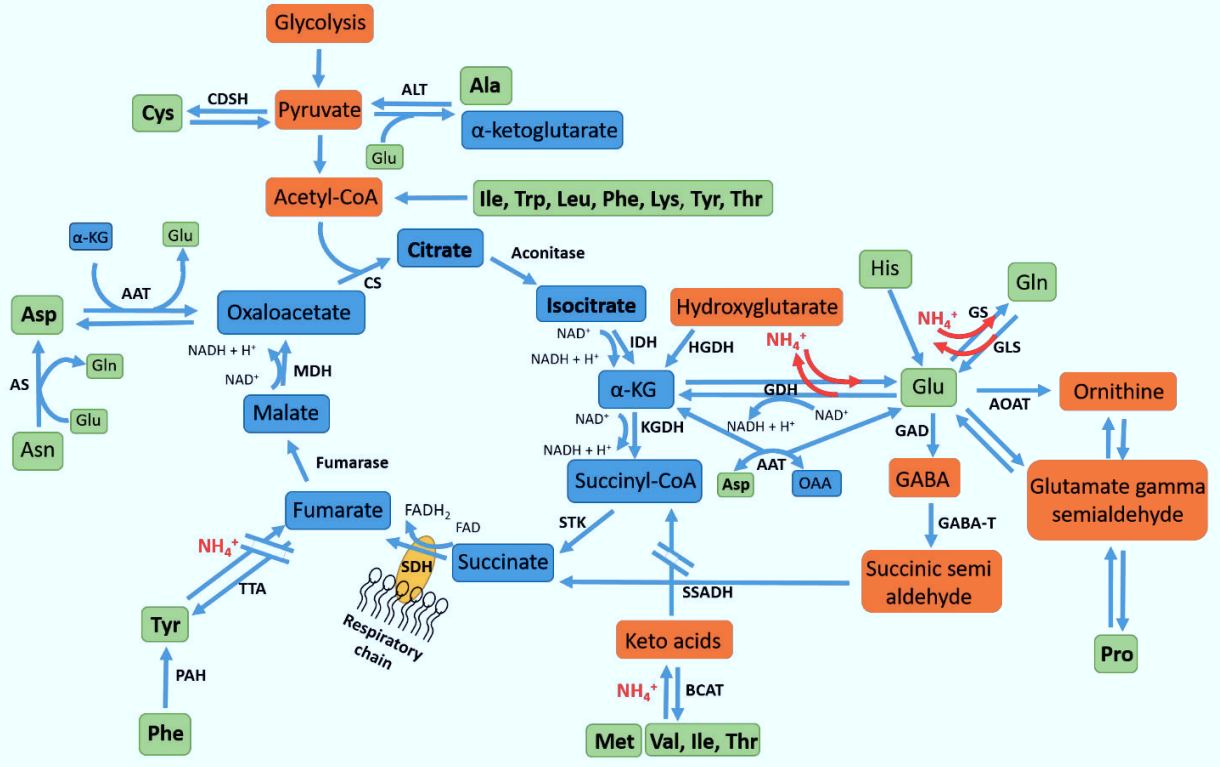

Figure 34: Anaplerosis and role of ammonia in cellular metabolism. TCA-cycle and anaplerotic reactions including role of ammonia. Amino acids and TCA-cycle intermediates increased in steady-state metabolites are depicted in bold. α-KG: α-ketoglutarate, AAT: aspartate aminotransferase, ALT: alanine aminotransferase, AOAT: acetyl ornithine aminotransferase, CDSH: Cysteine desulfhydrase, CS: citrate synthase, GABA-T: GABA-transaminase, GAD: glutamate decarboxylase, GDH: glutamate dehydrogenase, GLS: glutaminase, GS: glutamine synthetase, HGDH: hydroxyglutarate dehydrogenase, IDH: isocitrate dehydrogenase, KGDH: α-ketoglutarate dehydrogenase, MDH: malate dehydrogenase, OAA: oxaloacetate, PAH: phenylalanine hydroxylase, SDH: succinate dehydrogenase, SSADH: succinate semialdehyde dehydrogenase, STK: succinate thiokinase, TTA: tyrosine transaminase.

It is interesting to note that humans and great apes, in contrast to other mammals, have two genes encoding for GDH, namely GDH1 and GDH2, encoded by *GLUD1* and *GLUD2*, respectively. GDH1 is found in all mammals in the cytosol and mitochondria and is widely expressed in all tissues. On the other hand, *GLUD2* encodes an exclusively mitochondrial form of GDH that is expressed solely in testis, epithelial kidney cells and astrocytes of great apes and humans. It is proposed that *GLUD2* appeared in evolution after retroposition of the *GLUD1* gene, probably in an ape ancestor less than 23 million years ago (Burki and Kaessmann, 2004). The mature forms of human GDH1 (hGDH1) and hGDH2 are highly homologous with a sequence similarity of about 97% (Mastorodemos et al., 2009). Under physiological conditions, the GDH reaction is mainly catalyzing the oxidative deamination to form α-ketoglutarate (Adeva et al., 2012). GDH is regulated by SIRT4, a mitochondrial enzyme that uses NAD^+ to ADP-ribosylate GDH and by that to inhibit its activity (Haigis et al., 2006) (Fig. 35 A).

Another argument allowing to conclude that ammonia is utilized in the GDH reaction towards glutamate was obtained from ^{15}N-labeled NH_4Cl, which is accumulated mainly in glutamate, aspartate and proline as well as in leucine, isoleucine, valine, alanine and histidine to a lower extent (Fig. 25, 26). Glu, Pro, Asp and the BCAAs are directly associated with GDH reactions or acquire the nitrogen through secondary reactions, such as transaminases (Fig. 33). It is interesting to note that also breast cancer cells were reported to fix ammonia via the GDH reaction (Spinelli et al., 2017). The study by Spinelli *et al.* reported that in breast cancer cell lines ammonia is primarily assimilated through reductive amination catalyzed by GDH and the high accumulation of labeled nitrogen they find in Glu, Pro, Asp and Ala, among others, is strongly reminiscent to my data for astrocytes.

Other studies support the critical role of the TCA-cycle in HE. Weiss and colleagues published data examining metabolomics to highlight dysfunctions of metabolic pathways in CSF and plasma samples of HE patients. They revealed the accumulation of acetylated compounds, which also points towards a defect in the TCA-cycle. Additionally, the metabolites that were increased are involved in ammonia, amino acid and energy metabolism, for example glutamate, glutamine, methionine, phenylalanine and others; many of which I also found elevated in the astrocytoma samples (Weiss et al., 2016). Other patient data show an association between arterial hyperammonemia and increase of glutamine concentration in the brain (Tofteng et al., 2006), which could result from GDH activity towards glutamate and subsequently glutamine. It was further shown that under normal conditions GDH is important to sustain the catalytic activity of the TCA-cycle in mouse astrocytes by mediating the net formation of TCA-intermediates and that reduced GDH expression induces the usage of alternative substrates such as BCAAs (Nissen et al., 2015).

On the contrary, I show that when ammonia levels are high with increased time of treatment the concentration of amino acids such as BCAAs increase (Fig. 24). The question is why the effect of ammonia on mitochondrial respiration is most prevalent at short time points but becomes less pronounced with time. I suggest this to be a compensatory mechanism that involves the induction of anaplerotic reactions other than the one catalyzed by the GDH. Such a mechanism could be enhanced proteolysis by autophagy or by proteasomal degradation of proteins. Indeed, autophagy was found to be induced at lower ammonia concentrations (up to 1 mM) in primary rat astrocytes (PhD thesis, Kaihui Lu), in the *substantia nigra* of mice with liver damage and subsequent hyperammonemia (Bai et al., 2018) as well as in *Ulk1/2* DKO mouse embryonic fibroblasts (MEF) treated with 2 mM NH_4Cl for 24 h (Cheong et al., 2011). Additionally, my data on mitochondrial respiration in cells grown in galactose medium (Fig. 31) and rescue of respiration by lysosome-reacidifying nanoparticles (Fig. 32) further support a role of autophagy here. This data is discussed in the next chapter.

Hohnholt and colleagues could also show the importance of GDH for mitochondrial respiration. In Cns-*Glud1*$^{-/-}$ mice (GDH1 knock-out in synaptosomes) the basal respiration in brain mitochondria in presence of glutamate and malate was significantly reduced. In GDH1 knock-out neurons they show that without stimulation of respiration (*e.g*. by FCCP) there is no effect of GDH1 knock-out on respiration, while upon stimulation by FCCP the cells do not respond with an increased respiration (Hohnholt et al., 2017). This shows that under conditions of basal respiration the anaplerotic GDH reaction is dispensable, which is not the case when respiration is challenged. This is in line with my results showing that hyperammonemia does not grossly affect basal mitochondrial respiration but strongly when respiratory activity is induced *e.g.* by dissipation of the membrane potential; however, these experiments by Hohnholt and colleagues were only performed in neurons, which have a different metabolism than astrocytes. Still, this is an interesting aspect as it implies that cells can be more severely impaired under hyperammonemia when mitochondrial energy conversion is increased, which could be the case under increased neuronal activity.

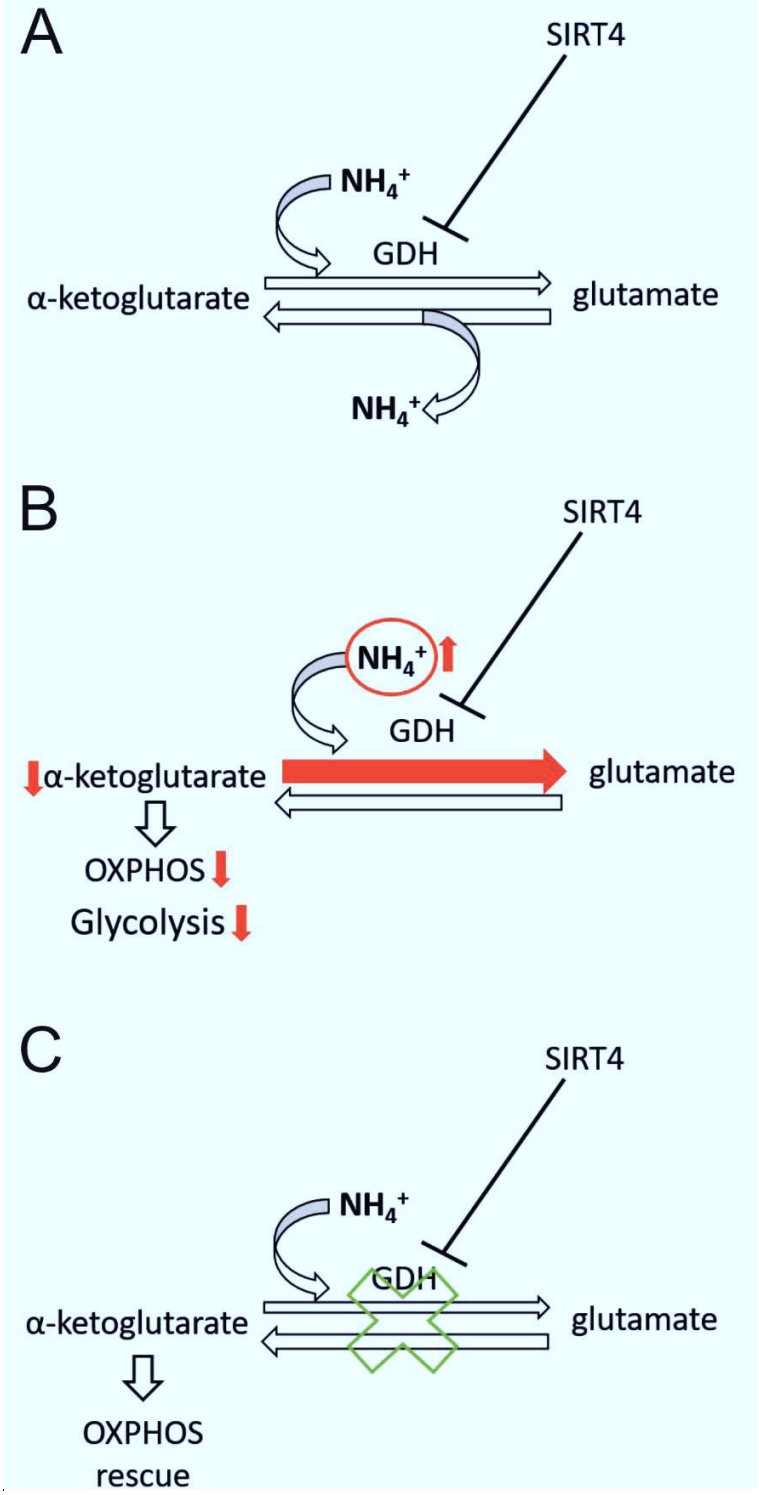

Figure 35: Role of glutamate dehydrogenase (GDH) in hyperammonemia. (A) The anaplerotic reaction replenishing the TCA-cycle via GDH is physiologically favoring the synthesis of α-ketoglutarate. (B) In hyperammonemia more glutamate is synthesized from α-ketoglutarate and NH_4^+, leading to a depletion of α-ketoglutarate and the TCA-cycle and in turn to a reduction in OXPHOS and glycolysis. (C) If GDH activity is inhibited either by SIRT4 regulation or via RNA interference anaplerosis and thus OXPHOS is restored.

As described above, supplementation with glutamate or glutamine before ammonia treatment could rescue ammonia-induced decrease in respiration (Fig. 30 C, D). Interestingly, a pretreatment with α-ketoglutarate or aspartate did not facilitate a rescue (Fig. 30 A, B). An explanation could be that aspartate is used for the synthesis of oxaloacetate via the aspartate aminotransferase, another anaplerotic reaction. This reaction uses α-ketoglutarate and aspartate to form glutamate and oxaloacetate (Fig. 34). Hence, the abundance of α-ketoglutarate could be even further decreased. The effect of supplementation with α-ketoglutarate directly is more difficult to interpret. First, it is questionable if the substance is even imported into the mitochondria or if it is rather already metabolized in the cytoplasm, for example in the alanine aminotransferase using α-ketoglutarate and alanine to form pyruvate and glutamate. Another possible explanation is the involvement of the malate-aspartate-shuttle (MAS). Aspartate and α-ketoglutarate inhibit the shuttle (Cederbaum et al., 1973; LaNoue and Williamson, 1971; McGivan et al., 1969), so an increase in both substances could reduce the availability of NADH on complex I of the respiratory chain. However, it is still controversially discussed in which tissues the MAS is present. According to textbook knowledge, the MAS in mammals is only found in mitochondria of the heart, liver and kidneys. In other tissues, especially brain and muscles, the NADH transport from cytosol to mitochondria is thought to be mediated via the glycerol-3-phosphate-shuttle (Leveille et al., 1980; reviewed in McKenna et al., 2006; Waagepetersen et al., 2001). Hence, it should not be involved in astrocyte metabolism. However, proteins aralar1 and citrin of the aspartate-glutamate-carrier, which is part of the MAS, have been found in neurons and glial cells of the rat brain (Ramos et al., 2003) and other groups also found evidence for the existence of this shuttle in different brain cells of different organisms (reviewed in McKenna et al., 2006).

4.5. Autophagy plays a role in ammonia-mediated decrease of mitochondrial respiration

As already mentioned above, Bai *et al.* and Cheong *et al.* found evidence for an induction of autophagy in hyperammonemia in mice brains and MEFs, respectively (Bai et al., 2018; Cheong et al., 2011). In this study I also provide data suggesting a role of autophagy in the pathogenesis of HE. A fascinating result was obtained when repeating the Mito Stress Test on the Seahorse Analyzer with human astrocytoma cells grown and measured in medium without glucose, but supplemented with galactose instead. Astonishingly, there was no effect on mitochondrial respiration in these cells, regardless of previous ammonia treatment durations (Fig. 31). Of note, cells were grown in galactose medium for a few days, hence, the chance of adjustment or compensation by the cells was given. Galactose can be used for glycolysis, as it is also converted to glucose-1-phosphate, but the utilization occurs at a much slower rate compared to glucose

(Novelli and Reichardt, 2000; Robinson et al., 1992). For this reason, galactose medium is often used as a medium to induce respiration, as it forces cells to increase OXPHOS to compensate for slower ATP production via glycolysis. From this data I hypothesize that glucose starvation is sufficient to induce autophagy. Increased autophagy provides more amino acids, which can be used for anaplerosis and are hence capable to replenish the TCA-cycle comparable to the experiments showing a rescue of mitochondrial respiration with the supplementation of glutamine and glutamate (Fig. 30 C, D) by shifting the GDH reaction equilibrium back towards anaplerosis. As cells were grown in galactose medium for a few days before ammonia exposure, excess amino acids were already available at ammonia treatment and thus, the effect of ammonia on respiration was not initiated (Fig. 36).

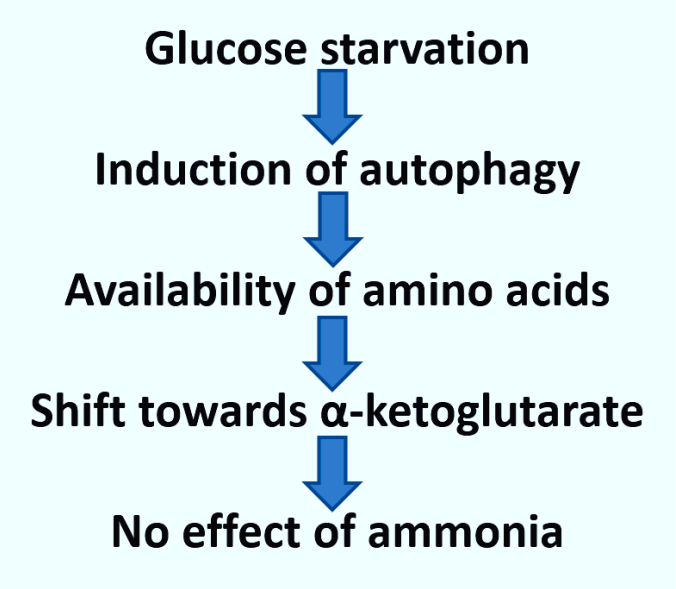

Figure 36: Effect of galactose media on ammonia-induced toxicity. Cells grown in galactose medium are less susceptible to ammonia. Glucose starvation could facilitate an induction of autophagy and thereby the availability of amino acids. This could in turn shift the equilibrium of the GDH reaction back to α-ketoglutarate replenishing the TCA-cycle and thus, strongly reduce the effect of high ammonia on respiration.

Markedly, there are controversial discussions if glucose starvation is even capable to induce autophagy. In human mesenchymal stem cells it was found that these cells survived glucose deficiency by the engagement of autophagy (Roa-Mansergas et al., 2018), which is in concordance with my data. However, other researchers tested the role of autophagy in glucose deprivation already in 2013 and came to a different conclusion. They employed four different cell lines, namely HEK293, HeLa, Rh4 and Bax/Bak deficient MEFs, and did not observe an increase in autophagic flux upon glucose starvation in any of them (Ramírez-Peinado et al., 2013). Nevertheless, the experimental conditions were very different as they worked with different cell lines and solely compared glucose medium to medium without any saccharides,

2-DG medium or HBSS. This is not comparable to my data where galactose as a carbon source is always present and thus the cells in my experiment still were capable of producing energy through glycolysis. Possibly, in my experimental settings autophagy could be induced as cells still had sufficient amounts of energy, as autophagy is an energy demanding mechanism. On the other hand, could the need for adjustment of cells to galactose medium generally have led to a shift towards a stronger TCA-cycle, in the sense of an increase in available carbon mass. This would yield cells less susceptible to ammonia.

Another interesting finding further supports a role of autophagy in hyperammonemia. The pretreatment of human astrocytoma cells with pa-NPs, which enter and reacidify the lysosome before ammonia treatment shows a trend to initiate partial rescue of ammonia-induced decrease in respiration (Fig. 32). Upon photo-activation by UV light the pa-NPs promote autophagy (Trudeau et al., 2016) and can thus possibly facilitate a similar rescue effect on respiration as observed in cells grown in galactose medium. The idea that it is important to induce a sufficient amount of autophagy before treatment with ammonia in order to rescue the decrease in respiration as it is the case in the galactose experiments described above, is further supported by the fact that pretreatment with pa-NPs only mediated a partial rescue after 24 h of ammonia and thus pa-NP exposure, but not after only 6 h (data not shown). Overall, my data suggests that the induction of autophagy has a beneficial effect on ammonia-induced decrease in respiration, but this still needs further investigation. As described above, an autophagy induction has been found by others in brain tissues of mice (Bai et al., 2018) and in MEF cells (Cheong et al., 2011) after ammonia exposure. Additionally, in the liver, ammonia induced hepatic autophagy in various animal models through the inhibition of mTORC1 and this was found to contribute majorly to ammonia detoxification, also by supporting urea synthesis (Soria et al., 2018). Modulation of autophagy could therefore be an interesting target for further research with regards to potential treatment options in the future.

4.6. Conclusion

Based on this study one can clearly state that (i) hyperammonemia aggravates several aspects of the whole cellular energy metabolism and (ii) that this is mainly mechanistically mediated via the mitochondrial enzyme glutamate dehydrogenase 2. From this, I suggest a new mechanism in the pathogenesis of hepatic encephalopathy, involving the major pathways of energy metabolism with a special emphasis on the role of glutamate dehydrogenase 2 and its regulation by SIRT4 (Fig. 35). Future experiments on the regulation and manipulation of GDH2 could present a new way how to tackle HE treatment in the future. An interesting next approach would be the generation of a humanized mouse model with a *GLUD2* and/or a *GLUD1* overexpressing mouse. This would serve to study the role of GDH as well as possible rescue and

treatment mechanisms systematically. Furthermore, more work on SIRT4 could lead to a deeper understanding of the GDH regulation mechanism. Targeting sirtuins is already studied intensively regarding cancer research. However, this only holds true for SIRT1-3 and 5. For these sirtuins activators and inhibitors are known and studied extensively as potential cancer treatment options (reviewed in Hu et al., 2014). For SIRT4 no such modulators are known so far, but it would present a very promising future therapeutic target in novel treatments of hepatic encephalopathy.

My data also suggests a possible beneficial role of autophagy in the pathogenesis of HE. More research is needed to fully comprehend this relationship and to elucidate whether factors involved in autophagy modulation, such as mTORC1, can reduce the ammonia-induced effect on fragmentation and energy metabolism. Promising results were obtained utilizing photoactivatable acidic nanoparticles; however, more research is needed here in cell culture and possibly animal models to understand the whole mechanism of the rescue to further develop this idea of intervention. While I only have some indications that glucose starvation indeed induces autophagy and thereby rescues the respiration defect, further studies are needed to confirm this by directly observing autophagy. Deciphering the relationship of autophagy and the cellular energy metabolism would shed more light on the mechanism that can alleviate the detrimental effects of ammonia.

With this study, I present two possible new targets, the GDH2 reaction and autophagy, that might open revolutionary treatment strategies for hepatic encephalopathy to improve patient life quality, disease progression and patient outcome in general. My results even challenge some former therapeutic instructions. For example, for decades patients were advised to reduce dietary protein intake in order to avoid ammonia generation in the gastrointestinal tract through bacterial digestion (reviewed in Cordoba, 2014). Fortunately, this practice has been revoked as weakening patients through protein restriction is not beneficial for recovery. The data presented here suggests that reducing the amount of amino acids could even increase the effects of ammonia-induced toxicity. This emphasizes that treatment should always be critically appraised in the light of new research results and that a lot still has to be investigated. A straight forward approach based on this investigation would be the supplementation of amino acids, *e.g.* glutamate, which could help to reduce symptoms. Supplementation of BCAAs is already used as symptomatic treatment, but the mechanism on how they act is not completely clear (Gluud et al., 2013). Naturally, mice and human intervention studies based on these results are needed beforehand.

Further studies following up the results presented here, especially on the potential role of SIRT4 and GDH2 regulation and supplementation of amino acids, are needed. It has to be resolved mechanistically in detail, if inhibiting the GDH2 reaction, either directly or through SIRT4 regulation, or changing the direction of the GDH reaction through anaplerotic supplementation with amino acids can fully reverse all phenotypical

aspects of HE. These findings could on the long run (i) increase the quality of life of patients, (ii) prolong survival until liver transplantation is possible and (iii) prevent irreversible brain damages that might persist even after successful transplantation.

Another energetic pathway that has not yet been looked at in detail is fatty acid oxidation. If this pathway is also changed in hyperammonemia and if a manipulation thereof or a supplementation with fatty acids would also provide a rescue approach still has to be investigated. If this is the case it would open doors for supplementation of nutrition with different fatty acids, possible also in combination with beneficial amino acids. Additionally, it remains elusive if a manipulation of mitochondrial dynamics in a way that prevents ammonia-induced fragmentation might be of benefit for ammonia-treated cells.

While substantial additional research has to be done to fully understand all of the aspects of ammonia-induced toxicity during hepatic encephalopathy, this work provides a crucial mechanistic insight into its pathogenesis and contributes to the improvement of current HE therapies.

5. Summary

Hepatic encephalopathy (HE) is a common neurological complication in patients with severe liver disease or portosystemic shunt. An estimated 50-70% of cirrhosis patients develop HE. Besides decades of research the pathological mechanisms behind HE remain largely unknown and symptomatic treatment options are mainly based on empirical observations. Symptoms can be mild to severe, ranging from personality changes, impaired intellect, disturbed sleeping and depressed level of consciousness to hepatic coma and death. HE with liver cirrhosis has a very poor prognostic and, without liver transplantation, which remains the only curative approach, the one-year survival rate is only 42% after the first episode of HE. There are many hypotheses on the pathogenesis of HE, but it is widely accepted that ammonia is the primarily responsible neurotoxin. Ammonia is produced mainly in the gastrointestinal tract and accumulates in the blood stream when not removed by an insufficient liver. It can pass the blood-brain-barrier, enter the astrocytes, which are known to be the primarily affected brain cells, and cause neurological dysfunctions. Additionally, some studies attribute a role to an increase in ROS through ammonia exposure, as well as to autophagy as a potential target of ammonia.

There is some evidence of a mitochondrial contribution to HE pathogenesis, *e.g.* changes in mitochondrial dynamics and a decrease in enzyme activity in the respiratory chain complexes. However, the exact mechanisms, especially regarding rapid effects of ammonia and influences on energy metabolism, remain unclear. To gain a thorough mechanistic insight on the role of mitochondrial energy metabolism in the early stages of HE, I employed an HE model based on human astrocytoma cells and rat-derived primary astrocytes to explore morphological and bioenergetic changes. In the investigated models hyperammonemia induced mitochondrial fragmentation within hours and compromised mitochondrial respiration and glycolysis within minutes. The effect was rapid, independent of possible pH changes mediated by NH_4Cl and strongly dose-dependent, which is in line with most patient data showing an increase in disease severity proportional to blood or cerebrospinal fluid ammonia levels. Mitochondrial fragmentation as well as decrease in respiration were quickly reversible upon ammonia removal. Further, a directed metabolomics approach showed an accumulation of glucose and nearly all investigated amino acids. Isotope labeling of NH_4Cl confirmed the incorporation of ammonia-derived nitrogen mainly into glutamate, aspartate, proline and the branched-chain amino acids; amino acids primarily or secondarily derived from the glutamate dehydrogenase (GDH). GDH2, a purely mitochondrial GDH isozyme that has evolved in great apes and humans, typically catalyzes the reaction from glutamate to α-ketoglutarate to feed the TCA-cycle. However, targeting GDH2 with RNA interference and negative regulation by SIRT4 as

well as anaplerotic supplementation of glutamate and glutamine rescued the ammonia-induced impact on respiration. Overall, I propose a new mechanism in HE pathogenesis where the ammonia-detoxifying GDH reaction in hyperammonemia reduces α-ketoglutarate levels, thereby driving a truncation of the TCA-cycle and impairing mitochondrial respiration. This suggest that hyperammonemia reverses the direction of the GDH2 reaction. Furthermore, my results together with other results obtained by the group suggest a role of autophagy in HE pathogenesis. Glucose starvation, possibly inducing autophagy, and driving autophagy by nanoparticle pretreatment alleviated the ammonia-induced effect on respiration. Hence, manipulation of autophagy, GDH2 activity or the cell energy metabolism as a whole are promising new targets for the development of novel HE treatment strategies.

6. Zusammenfassung

Hepatische Enzephalopathie (HE) ist eine häufige neurologische Komplikation von Patienten mit einer schweren Leberdysfunktion oder einer portosystemischen Gefäßverbindung (Lebershunt). Geschätzte 50-70 % der Zirrhosepatienten entwickeln HE. Trotz jahrzehntelanger Forschung ist der pathologische Mechanismus von HE noch immer weitestgehend unverstanden und die symptomatischen Behandlungsoptionen basieren größtenteils auf empirischen Beobachtungen. Symptome von HE rangieren von leicht bis schwer und zeichnen sich durch Veränderungen der Persönlichkeit, beeinträchtigten Intellekt, Schlafstörungen und einen verminderten Bewusstseinszustand aus, bis hin zu hepatischem Koma und Tod. HE ausgelöst durch Leberzirrhose hat eine sehr schlechte Prognose mit einer 1-Jahr-Überlebensrate von nur 42 % nach dem ersten Auftreten von HE, ohne Lebertransplantation, welches noch immer die einzige Heilungschance bietet.

Es gibt viele Hypothesen, die die Pathogenese von HE zu erklären versuchen, doch die am meisten akzeptierte benennt Ammoniak als das hauptverantwortliche Neurotoxin. Ammoniak wird hauptsächlich im Gastrointestinaltrakt produziert und reichert sich im Blut an, wenn es nicht durch die geschädigte Leber abgebaut werden kann. Der Stoff kann die Blut-Hirn-Schranke überqueren, wo er sich in den Astrozyten anreichern und neurologische Störungen auslösen kann. Astrozyten sind diejenigen Gehirnzellen welche im Wesentlichen von Ammoniak beeinträchtigt werden. Zudem werden die Erhöhung von ROS sowie Autophagie als potenzielle Angriffspunkte von Hyperammonämie diskutiert.

Es gibt Hinweise auf eine Beteiligung der Mitochondrien an der HE-Pathogenese, gezeigt wurden beispielsweise Veränderungen in der mitochondrialen Dynamik und eine Verringerung von Enzymaktivitäten in der Atmungskette. Dennoch sind die genauen Mechanismen, insbesondere in Bezug auf rapide Ammoniakeffekte sowie einen möglichen Einfluss auf den Energiemetabolismus, noch weitestgehend unverstanden. Um mechanistische Erkenntnisse über die Rolle des mitochondrialen Energiemetabolismus in der frühen Pathogenese von HE zu erlangen arbeitete ich mit zellbasierten HE-Modellen, zum einen mit humanen Astrozytoma Zellen, zum anderen mit primären Astrozyten der Ratte. Diese dienten der Untersuchung von morphologischen und bioenergetischen Veränderungen auf Grund von Hyperammonämie. In den untersuchten Modellen hat eine erhöhte Ammoniakexposition innerhalb weniger Stunden mitochondriale Fragmentierung sowie innerhalb von Minuten eine starke Verminderung von mitochondrialer Atmung und Glykolyse ausgelöst. Dieser Effekt war schnell, unabhängig von möglichen NH_4Cl-bedingten pH-Änderungen und stark dosisabhängig, was Erkenntnisse aus Patientendaten wiederspiegelt, wonach die Schwere der Erkrankung meist proportional zur Höhe der

Ammoniakwerte in Blut und Rückenmarksflüssigkeit ist. Die mitochondriale Fragmentierung sowie die Verminderung der Atmung waren schnell reversibel, sobald die Ammoniakexposition beendet wurde. Des Weiteren zeigte ein zielgerichteter Metabolomikversuch die Anreicherung von Glukose und fast allen untersuchten Aminosäuren in den Zellen. Isotopenmarkierung von NH_4Cl untermauerte die Aufnahme von Stickstoff aus Ammoniak hauptsächlich in Glutamat, Aspartat, Prolin und den verzweigtkettigen Aminosäuren; alles Aminosäuren welche primär oder sekundär über Glutamat Dehydrogenase (GDH) synthetisiert werden. GDH2, ein rein mitochondriales GDH Isozym, welches in Menschenaffen und Menschen evolviert ist, katalysiert normalerweise die Reaktion von Glutamat zu α-Ketoglutarat zur Anaplerose des TCA-Zyklus. Der knock-down von GDH2 via RNA-Interferenz sowie die negative Regulierung dessen Aktivität durch SIRT4 und die anaplerotische Supplementierung von Glutamat und Glutamin hob den negativen Effekt von Ammoniak auf die mitochondriale Atmung auf.

Als Ergebnis dieser Arbeit schlage ich einen neuen Mechanismus der HE-Pathogenese vor, in welchem die Ammoniak-detoxifizierende GDH Reaktion zu einer Verringerung von α-Ketoglutarat führt. Dies wiederum löst eine Störung des TCA-Zyklus aus und führt so zur Reduzierung der mitochondrialen Atmung. Dies zeigt, dass Hyperammonämie zu einer Umkehrung der GDH2 Reaktion führt. Ferner deuten meine Daten, zusammen mit anderen Arbeiten der Gruppe, auf eine Rolle der Autophagie hin. Glukose-Limitierung, welche möglicherweise Autophagie induziert, sowie Vorbehandlung mit Autophagie treibenden Nanopartikeln vor der Zugabe von Ammoniak kann den negativen Effekt auf die Atmung verhindern. Somit sind Veränderungen an Stellschrauben der Autophagie, der GDH2-Aktivität sowie am zellulären Energiemetabolismus im Ganzen vielversprechende neue Ziele für die Entwicklung von neuartigen Behandlungsmöglichkeiten der HE.

7. References

Books:

Müller-Esterl, W., Biochemie – Eine Einführung für Mediziner und Naturwissenschaftler. 1. Auflage 2004, Elsevier GmbH München, Spektrum Akademischer Verlag.

Berg, J.M., Tymoczko, J.L., Gatto jr., G.J., Stryer, L., Stryer Biochemie. 8. Auflage 2018, Springer-Verlag GmbH Deutschland.

Websites:

https://www.uniprot.org/uniprot/P49448 (16. May 2019, 11:47 am CET)

https://www.uniprot.org/uniprot/P00367 (16. May 2019, 11:50 am CET)

Theses:

Bachelor thesis: Poss, R.E. Rolle von Glucoselimitierung und Autophagie in einem in vitro Modell für hepatische Enzephalopathie. Submitted in Düsseldorf August 2018.

Doctoral thesis: Lu, K. Involvement of autophagy and mitophagy in the pathogenesis of hepatic encephalopathy. Submitted in Düsseldorf April 2018.

Publications:

Acharya, C., et al. (2017). "Overt hepatic encephalopathy impairs learning on the EncephalApp stroop which is reversible after liver transplantation." Liver Transpl **23**(11): 1396-1403.

Adeva, M. M., et al. (2012). "Ammonium metabolism in humans." Metabolism **61**(11): 1495-1511.

Ahboucha, S. and R. F. Butterworth (2004). "Pathophysiology of hepatic encephalopathy: a new look at GABA from the molecular standpoint." Metab Brain Dis **19**(3-4): 331-343.

Akram, M. (2013). "Mini-review on glycolysis and cancer." J Cancer Educ **28**(3): 454-457.

Al Sibae, M. R. and B. M. McGuire (2009). "Current trends in the treatment of hepatic encephalopathy." Ther Clin Risk Manag **5**(3): 617-626.

Alexander, C., et al. (2000). "OPA1, encoding a dynamin-related GTPase, is mutated in autosomal dominant optic atrophy linked to chromosome 3q28." Nat Genet **26**(2): 211-215.

Bai, Y., et al. (2018). "Hepatic encephalopathy changes mitochondrial dynamics and autophagy in the substantia nigra." Metab Brain Dis **33**(5): 1669-1678.

Bajaj, J. S., et al. (2010). "Persistence of cognitive impairment after resolution of overt hepatic encephalopathy." Gastroenterology **138**(7): 2332-2340.

Barbaro, G., et al. (1998). "Flumazenil for hepatic encephalopathy grade III and IVa in patients with cirrhosis: an Italian multicenter double-blind, placebo-controlled, cross-over study." Hepatology **28**(2): 374-378.

Boer, L. A., et al. (2009). "Inhibition of mitochondrial respiratory chain in the brain of rats after hepatic failure induced by carbon tetrachloride is reversed by antioxidants." Brain Res Bull **80**(1-2): 75-78.

Boore, J. L. (1999). "Animal mitochondrial genomes." Nucleic Acids Res **27**(8): 1767-1780.

Burki, F. and H. Kaessmann (2004). "Birth and adaptive evolution of a hominoid gene that supports high neurotransmitter flux." Nat Genet **36**(10): 1061-1063.

Bustamante, J., et al. (1999). "Prognostic significance of hepatic encephalopathy in patients with cirrhosis." J Hepatol **30**(5): 890-895.

Butterworth, R. F. (2016). "Neurosteroids in hepatic encephalopathy: Novel insights and new therapeutic opportunities." J Steroid Biochem Mol Biol **160**: 94-97.

Capocaccia, L., et al. (1979). "Influence of phenylethanolamine on octopamine plasma determination in hepatic encephalopathy." Clin Chim Acta **93**(3): 371-376.

Cash, W. J., et al. (2010). "Current concepts in the assessment and treatment of hepatic encephalopathy." QJM **103**(1): 9-16.

Cederbaum, A. I., et al. (1973). "Characterization of shuttle mechanisms for the transport of reducing equivalents into mitochondria." Arch Biochem Biophys **158**(2): 763-781.

Chan, D. C. (2006). "Mitochondria: dynamic organelles in disease, aging, and development." Cell **125**(7): 1241-1252.

Chen, H., et al. (2005). "Disruption of fusion results in mitochondrial heterogeneity and dysfunction." J Biol Chem **280**(28): 26185-26192.

Cheong, H., et al. (2011). "Ammonia-induced autophagy is independent of ULK1/ULK2 kinases." Proc Natl Acad Sci U S A **108**(27): 11121-11126.

Contreras, L., et al. (2010). "Mitochondria: the calcium connection." Biochim Biophys Acta **1797**(6-7): 607-618.

Cordoba, J. (2014). "Hepatic Encephalopathy: From the Pathogenesis to the New Treatments." ISRN Hepatol **2014**: 236268.

Cordoba, J., et al. (1998). "Chronic hyponatremia exacerbates ammonia-induced brain edema in rats after portacaval anastomosis." J Hepatol **29**(4): 589-594.

Dallman, P. R. (1986). "Biochemical basis for the manifestations of iron deficiency." Annu Rev Nutr **6**: 13-40.

Delettre, C., et al. (2000). "Nuclear gene OPA1, encoding a mitochondrial dynamin-related protein, is mutated in dominant optic atrophy." Nat Genet **26**(2): 207-210.

Delettre, C., et al. (2002). "OPA1 (Kjer type) dominant optic atrophy: a novel mitochondrial disease." Mol Genet Metab **75**(2): 97-107.

Dhanda, S., et al. (2018). "Mitochondrial dysfunctions contribute to energy deficits in rodent model of hepatic encephalopathy." Metab Brain Dis **33**(1): 209-223.

Dimauro, S. and G. Davidzon (2005). "Mitochondrial DNA and disease." Ann Med **37**(3): 222-232.

DiMauro, S. and E. A. Schon (2003). "Mitochondrial respiratory-chain diseases." N Engl J Med **348**(26): 2656-2668.

Duvezin-Caubet, S., et al. (2006). "Proteolytic processing of OPA1 links mitochondrial dysfunction to alterations in mitochondrial morphology." J Biol Chem **281**(49): 37972-37979.

Elmore, S. (2007). "Apoptosis: a review of programmed cell death." Toxicol Pathol **35**(4): 495-516.

Elmore, S. P., et al. (2001). "The mitochondrial permeability transition initiates autophagy in rat hepatocytes." FASEB J **15**(12): 2286-2287.

Ferenci, P. (2017). "Hepatic encephalopathy." Gastroenterol Rep (Oxf) **5**(2): 138-147.

Ferenci, P., et al. (2002). "Hepatic encephalopathy--definition, nomenclature, diagnosis, and quantification: final report of the working party at the 11th World Congresses of Gastroenterology, Vienna, 1998." Hepatology **35**(3): 716-721.

Ferenci, P. and F. Wewalka (1978). "Plasma amino acids in hepatic encephalopathy." J Neural Transm Suppl(14): 87-94.

Fiehn, O. and T. Kind (2007). "Metabolite profiling in blood plasma." Methods Mol Biol **358**: 3-17.

Figge, M. T., et al. (2013). "Quality control of mitochondria during aging: is there a good and a bad side of mitochondrial dynamics?" Bioessays **35**(4): 314-322.

Ford, M. G., et al. (2011). "The crystal structure of dynamin." Nature **477**(7366): 561-566.

Frackowiak, R. S., et al. (1981). "Regional cerebral oxygen supply and utilization in dementia. A clinical and physiological study with oxygen-15 and positron tomography." Brain **104**(Pt 4): 753-778.

Frank, M., et al. (2012). "Mitophagy is triggered by mild oxidative stress in a mitochondrial fission dependent manner." Biochimica Et Biophysica Acta-Molecular Cell Research **1823**(12): 2297-2310.

Frey, P. A. and G. H. Reed (2012). "The ubiquity of iron." ACS Chem Biol **7**(9): 1477-1481.

Friedman, J. R., et al. (2011). "ER tubules mark sites of mitochondrial division." Science **334**(6054): 358-362.

Friedman, J. R. and J. Nunnari (2014). "Mitochondrial form and function." Nature **505**(7483): 335-343.

Frohlich, C., et al. (2013). "Structural insights into oligomerization and mitochondrial remodelling of dynamin 1-like protein." EMBO J **32**(9): 1280-1292.

Garcea, R., et al. (1980). "Phospholipid composition of inner and outer mitochondrial membranes isolated from Yoshida hepatoma AH-130." Cancer Lett **11**(2): 133-139.

Gerbitz, K. D., et al. (1995). "Mitochondrial diabetes mellitus: a review." Biochim Biophys Acta **1271**(1): 253-260.

Ghallab, A., et al. (2016). "Model-guided identification of a therapeutic strategy to reduce hyperammonemia in liver diseases." J Hepatol **64**(4): 860-871.

Gibson, G. E., et al. (1988). "Reduced activities of thiamine-dependent enzymes in the brains and peripheral tissues of patients with Alzheimer's disease." Arch Neurol **45**(8): 836-840.

Gluud, L. L., et al. (2013). "Oral branched-chain amino acids have a beneficial effect on manifestations of hepatic encephalopathy in a systematic review with meta-analyses of randomized controlled trials." J Nutr **143**(8): 1263-1268.

Gorg, B., et al. (2018). "Hepatic Encephalopathy and Astrocyte Senescence." J Clin Exp Hepatol **8**(3): 294-300.

Gorg, B., et al. (2015). "Ammonia-induced senescence in cultured rat astrocytes and in human cerebral cortex in hepatic encephalopathy." Glia **63**(1): 37-50.

Gorg, B., et al. (2008). "Ammonia induces RNA oxidation in cultured astrocytes and brain in vivo." Hepatology **48**(2): 567-579.

Gorg, B., et al. (2013). "Osmotic and oxidative/nitrosative stress in ammonia toxicity and hepatic encephalopathy." Arch Biochem Biophys **536**(2): 158-163.

Gu, L., et al. (2007). "LC-MS/MS assay for protein amino acids and metabolically related compounds for large-scale screening of metabolic phenotypes." Anal Chem **79**(21): 8067-8075.

Haigis, M. C., et al. (2006). "SIRT4 inhibits glutamate dehydrogenase and opposes the effects of calorie restriction in pancreatic beta cells." Cell **126**(5): 941-954.

Hanekamp, T., et al. (2002). "Maintenance of mitochondrial morphology is linked to maintenance of the mitochondrial genome in Saccharomyces cerevisiae." Genetics **162**(3): 1147-1156.

Hashimoto, M., et al. (2003). "Role of protein aggregation in mitochondrial dysfunction and neurodegeneration in Alzheimer's and Parkinson's diseases." Neuromolecular Med **4**(1-2): 21-36.

Haussinger, D. and B. Gorg (2010). "Interaction of oxidative stress, astrocyte swelling and cerebral ammonia toxicity." Curr Opin Clin Nutr Metab Care **13**(1): 87-92.

Haussinger, D., et al. (2000). "Hepatic encephalopathy in chronic liver disease: a clinical manifestation of astrocyte swelling and low-grade cerebral edema?" J Hepatol **32**(6): 1035-1038.

Haussinger, D. and F. Schliess (2008). "Pathogenetic mechanisms of hepatic encephalopathy." Gut **57**(8): 1156-1165.

Hawkins, R. A., et al. (1994). "Neomycin reduces the intestinal production of ammonia from glutamine." Adv Exp Med Biol **368**: 125-134.

Hazell, A. S. and M. D. Norenberg (1998). "Ammonia and manganese increase arginine uptake in cultured astrocytes." Neurochem Res **23**(6): 869-873.

Helle, S. C. J., et al. (2017). "Mechanical force induces mitochondrial fission." Elife **6**.

Hermann, G. J., et al. (1998). "Mitochondrial fusion in yeast requires the transmembrane GTPase Fzo1p." J Cell Biol **143**(2): 359-373.

Hertz, L. and G. Kala (2007). "Energy metabolism in brain cells: effects of elevated ammonia concentrations." Metab Brain Dis **22**(3-4): 199-218.

Hohnholt, M. C., et al. (2018). "Glutamate dehydrogenase is essential to sustain neuronal oxidative energy metabolism during stimulation." J Cereb Blood Flow Metab **38**(10): 1754-1768.

Hoppins, S., et al. (2007). "The machines that divide and fuse mitochondria." Annu Rev Biochem **76**: 751-780.

Hourani, B. T., et al. (1971). "Cerebrospinal fluid glutamine as a measure of hepatic encephalopathy." Arch Intern Med **127**(6): 1033-1036.

Hsu, P. P. and D. M. Sabatini (2008). "Cancer cell metabolism: Warburg and beyond." Cell **134**(5): 703-707.

Hu, J., et al. (2014). "Sirtuin inhibitors as anticancer agents." Future Med Chem **6**(8): 945-966.

Ingerman, E., et al. (2005). "Dnm1 forms spirals that are structurally tailored to fit mitochondria." J Cell Biol **170**(7): 1021-1027.

Iqbal, S. and D. A. Hood (2014). "Oxidative stress-induced mitochondrial fragmentation and movement in skeletal muscle myoblasts." Am J Physiol Cell Physiol **306**(12): C1176-1183.

Jalan, R. and W. M. Lee (2009). "Treatment of hyperammonemia in liver failure: a tale of two enzymes." Gastroenterology **136**(7): 2048-2051.

Johnson, A. B. and N. R. Blum (1970). "Nucleoside phosphatase activities associated with the tangles and plaques of alzheimer's disease: a histochemical study of natural and experimental neurofibrillary tangles." J Neuropathol Exp Neurol **29**(3): 463-478.

Jornayvaz, F. R. and G. I. Shulman (2010). "Regulation of mitochondrial biogenesis." Essays Biochem **47**: 69-84.

Katunuma, N., et al. (1966). "Regulation of the urea cycle and TCA cycle by ammonia." Adv Enzyme Regul **4**: 317-336.

Kukreja, L., et al. (2014). "Increased mtDNA mutations with aging promotes amyloid accumulation and brain atrophy in the APP/Ld transgenic mouse model of Alzheimer's disease." Mol Neurodegener **9**: 16.

Labrousse, A. M., et al. (1999). "C. elegans dynamin-related protein DRP-1 controls severing of the mitochondrial outer membrane." Mol Cell **4**(5): 815-826.

Lane, N. and W. Martin (2010). "The energetics of genome complexity." Nature **467**(7318): 929-934.

Lang, A., et al. (2017). "SIRT4 interacts with OPA1 and regulates mitochondrial quality control and mitophagy." Aging (Albany NY) **9**(10): 2163-2189.

LaNoue, K. F. and J. R. Williamson (1971). "Interrelationships between malate-aspartate shuttle and citric acid cycle in rat heart mitochondria." Metabolism **20**(2): 119-140.

Lee, Y. J., et al. (2004). "Roles of the mammalian mitochondrial fission and fusion mediators Fis1, Drp1, and Opa1 in apoptosis." Mol Biol Cell **15**(11): 5001-5011.

Letts, J. A. and L. A. Sazanov (2017). "Clarifying the supercomplex: the higher-order organization of the mitochondrial electron transport chain." Nat Struct Mol Biol **24**(10): 800-808.

Leveille, P. J., et al. (1980). "Immunocytochemical localization of glycerol-3-phosphate dehydrogenase in rat oligodendrocytes." Brain Res **196**(2): 287-305.

Li, Q., et al. (2016). "Mice carrying a human GLUD2 gene recapitulate aspects of human transcriptome and metabolome development." Proc Natl Acad Sci U S A **113**(19): 5358-5363.

Lowell, B. B. and G. I. Shulman (2005). "Mitochondrial dysfunction and type 2 diabetes." Science **307**(5708): 384-387.

Lozeva, V., et al. (2004). "Increased brain serotonin turnover correlates with the degree of shunting and hyperammonemia in rats following variable portal vein stenosis." J Hepatol **40**(5): 742-748.

Martinez-Hernandez, A., et al. (1977). "Glutamine synthetase: glial localization in brain." Science **195**(4284): 1356-1358.

Mastorodemos, V., et al. (2009). "Human GLUD1 and GLUD2 glutamate dehydrogenase localize to mitochondria and endoplasmic reticulum." Biochem Cell Biol **87**(3): 505-516.

Mavrothalassitis, G., et al. (1988). "Isolation and characterization of cDNA clones encoding human liver glutamate dehydrogenase: evidence for a small gene family." Proc Natl Acad Sci U S A **85**(10): 3494-3498.

McConnell, J. R., et al. (1995). "Proton spectroscopy of brain glutamine in acute liver failure." Hepatology **22**(1): 69-74.

McGivan, J. D., et al. (1969). "The inhibition of 2-oxoglutarate entry into rat liver mitochondria by L-aspartate." FEBS Lett **4**(4): 247-250.

McKenna, M. C., et al. (2006). "Neuronal and astrocytic shuttle mechanisms for cytosolic-mitochondrial transfer of reducing equivalents: current evidence and pharmacological tools." Biochem Pharmacol **71**(4): 399-407.

Meeusen, S., et al. (2004). "Mitochondrial fusion intermediates revealed in vitro." Science **305**(5691): 1747-1752.

Michalak, A., et al. (1996). "Neuroactive amino acids and glutamate (NMDA) receptors in frontal cortex of rats with experimental acute liver failure." Hepatology **24**(4): 908-913.

Modica-Napolitano, J. S. and K. K. Singh (2004). "Mitochondrial dysfunction in cancer." Mitochondrion **4**(5-6): 755-762.

Montes, S., et al. (2001). "Striatal manganese accumulation induces changes in dopamine metabolism in the cirrhotic rat." Brain Res **891**(1-2): 123-129.

Morgan, M. Y., et al. (1978). "Plasma ratio of valine, leucine and isoleucine to phenylalanine and tyrosine in liver disease." Gut **19**(11): 1068-1073.

Mozdy, A. D., et al. (2000). "Dnm1p GTPase-mediated mitochondrial fission is a multi-step process requiring the novel integral membrane component Fis1p." J Cell Biol **151**(2): 367-380.

Nissen, J. D., et al. (2017). "Expression of the human isoform of glutamate dehydrogenase, hGDH2, augments TCA cycle capacity and oxidative metabolism of glutamate during glucose deprivation in astrocytes." Glia **65**(3): 474-488.

Nissen, J. D., et al. (2015). "Dysfunctional TCA-Cycle Metabolism in Glutamate Dehydrogenase Deficient Astrocytes." Glia **63**(12): 2313-2326.

Norenberg, M. D. (1987). "The role of astrocytes in hepatic encephalopathy." Neurochem Pathol **6**(1-2): 13-33.

Norenberg, M. D., et al. (2004). "Oxidative stress in the pathogenesis of hepatic encephalopathy." Metab Brain Dis **19**(3-4): 313-329.

Novelli, G. and J. K. Reichardt (2000). "Molecular basis of disorders of human galactose metabolism: past, present, and future." Mol Genet Metab **71**(1-2): 62-65.

Oenarto, J., et al. (2016). "Ammonia-induced miRNA expression changes in cultured rat astrocytes." Sci Rep **6**: 18493.

Ogun, A. S. and M. Valentine (2019). Biochemistry, Heme Synthesis. StatPearls. Treasure Island (FL).

Ong, J. P., et al. (2003). "Correlation between ammonia levels and the severity of hepatic encephalopathy." Am J Med **114**(3): 188-193.

Orth, M. and A. H. Schapira (2002). "Mitochondrial involvement in Parkinson's disease." Neurochem Int **40**(6): 533-541.

Osellame, L. D., et al. (2012). "Cellular and molecular mechanisms of mitochondrial function." Best Pract Res Clin Endocrinol Metab **26**(6): 711-723.

Otera, H., et al. (2010). "Mff is an essential factor for mitochondrial recruitment of Drp1 during mitochondrial fission in mammalian cells." J Cell Biol **191**(6): 1141-1158.

Ott, P. and F. S. Larsen (2004). "Blood-brain barrier permeability to ammonia in liver failure: a critical reappraisal." Neurochem Int **44**(4): 185-198.

Palomero-Gallagher, N. and K. Zilles (2013). "Neurotransmitter receptor alterations in hepatic encephalopathy: a review." Arch Biochem Biophys **536**(2): 109-121.

Parker, W. D., Jr., et al. (1990). "Cytochrome oxidase deficiency in Alzheimer's disease." Neurology **40**(8): 1302-1303.

Parone, P. A., et al. (2008). "Preventing mitochondrial fission impairs mitochondrial function and leads to loss of mitochondrial DNA." PLOS ONE **3**(9): e3257.

Patidar, K. R. and J. S. Bajaj (2015). "Covert and Overt Hepatic Encephalopathy: Diagnosis and Management." Clin Gastroenterol Hepatol **13**(12): 2048-2061.

Pfanner, N., et al. (2014). "Uniform nomenclature for the mitochondrial contact site and cristae organizing system." J Cell Biol **204**(7): 1083-1086.

Pietschmann, T., et al. (1999). "Foamy virus capsids require the cognate envelope protein for particle export." J Virol **73**(4): 2613-2621.

Plaitakis, A., et al. (2000). "Nerve tissue-specific (GLUD2) and housekeeping (GLUD1) human glutamate dehydrogenases are regulated by distinct allosteric mechanisms: implications for biologic function." J Neurochem **75**(5): 1862-1869.

Priault, M., et al. (2005). "Impairing the bioenergetic status and the biogenesis of mitochondria triggers mitophagy in yeast." Cell Death Differ **12**(12): 1613-1621.

Puigserver, P., et al. (1998). "A cold-inducible coactivator of nuclear receptors linked to adaptive thermogenesis." Cell **92**(6): 829-839.

Qvartskhava, N., et al. (2015). "Hyperammonemia in gene-targeted mice lacking functional hepatic glutamine synthetase." Proc Natl Acad Sci U S A **112**(17): 5521-5526.

Rama Rao, K. V. and M. D. Norenberg (2012). "Brain energy metabolism and mitochondrial dysfunction in acute and chronic hepatic encephalopathy." Neurochem Int **60**(7): 697-706.

Ramirez-Peinado, S., et al. (2013). "Glucose-starved cells do not engage in prosurvival autophagy." J Biol Chem **288**(42): 30387-30398.

Ramos, M., et al. (2003). "Developmental changes in the Ca2+-regulated mitochondrial aspartate-glutamate carrier aralar1 in brain and prominent expression in the spinal cord." Brain Res Dev Brain Res **143**(1): 33-46.

Rensvold, J. W., et al. (2016). "Iron Deprivation Induces Transcriptional Regulation of Mitochondrial Biogenesis." J Biol Chem **291**(40): 20827-20837.

Roa-Mansergas, X., et al. (2018). "CPT1C promotes human mesenchymal stem cells survival under glucose deprivation through the modulation of autophagy." Sci Rep **8**(1): 6997.

Robinson, B. H., et al. (1992). "Nonviability of cells with oxidative defects in galactose medium: a screening test for affected patient fibroblasts." Biochem Med Metab Biol **48**(2): 122-126.

Roellecke, K., et al. (2016). "Optimized human CYP4B1 in combination with the alkylator prodrug 4-ipomeanol serves as a novel suicide gene system for adoptive T-cell therapies." Gene Ther **23**(7): 615-626.

Rose, C., et al. (1999). "Manganese deposition in basal ganglia structures results from both portal-systemic shunting and liver dysfunction." Gastroenterology **117**(3): 640-644.

Rosso, L., et al. (2008). "Mitochondrial targeting adaptation of the hominoid-specific glutamate dehydrogenase driven by positive Darwinian selection." PLoS Genet **4**(8): e1000150.

Sagan, L. (1967). "On the origin of mitosing cells." J Theor Biol **14**(3): 255-274.

Saneto, R. P. (2017). "Genetics of Mitochondrial Disease." Adv Genet **98**: 63-116.

Scarpelli, M., et al. (2017). "Mitochondrial diseases: advances and issues." Appl Clin Genet **10**: 21-26.

Schafer, A. and A. S. Reichert (2009). "Emerging roles of mitochondrial membrane dynamics in health and disease." Biol Chem **390**(8): 707-715.

Schindelin, J., et al. (2012). "Fiji: an open-source platform for biological-image analysis." Nat Methods **9**(7): 676-682.

Seo, A. Y., et al. (2010). "New insights into the role of mitochondria in aging: mitochondrial dynamics and more." J Cell Sci **123**(Pt 15): 2533-2542.

Shashidharan, P., et al. (1997). "Nerve tissue-specific human glutamate dehydrogenase that is thermolabile and highly regulated by ADP." J Neurochem **68**(5): 1804-1811.

Shashidharan, P., et al. (1994). "Novel human glutamate dehydrogenase expressed in neural and testicular tissues and encoded by an X-linked intronless gene." J Biol Chem **269**(24): 16971-16976.

Sherlock, S. (1958). "Pathogenesis and management of hepatic coma." Am J Med **24**(5): 805-813.

Singh, K. K. (2004). "Mitochondrial dysfunction is a common phenotype in aging and cancer." Strategies for Engineered Negligible Senescence: Why Genuine Control of Aging May Be Foreseeable **1019**: 260-264.

Smith, E. L. (1979). "Evolution of Glutamate-Dehydrogenases and a Hypothesis for the Insertion or Deletion of Multiple Residues in the Interior of Polypeptide-Chains." Proceedings of the American Philosophical Society **123**(1): 73-84.

Sorbi, S., et al. (1983). "Decreased pyruvate dehydrogenase complex activity in Huntington and Alzheimer brain." Ann Neurol **13**(1): 72-78.

Soria, L. R., et al. (2018). "Enhancement of hepatic autophagy increases ureagenesis and protects against hyperammonemia." Proc Natl Acad Sci U S A **115**(2): 391-396.

Spinelli, J. B., et al. (2017). "Metabolic recycling of ammonia via glutamate dehydrogenase supports breast cancer biomass." Science **358**(6365): 941-946.

Stahl, J. (1963). "Studies of the blood ammonia in liver disease. Its diagnostic, prognostic, and therapeutic significance." Ann Intern Med **58**: 1-24.

Stobart, J. L. and C. M. Anderson (2013). "Multifunctional role of astrocytes as gatekeepers of neuronal energy supply." Front Cell Neurosci **7**: 38.

Strauss, E., et al. (1992). "Double-blind randomized clinical trial comparing neomycin and placebo in the treatment of exogenous hepatic encephalopathy." Hepatogastroenterology **39**(6): 542-545.

Suarez, I., et al. (2002). "Glutamine synthetase in brain: effect of ammonia." Neurochem Int **41**(2-3): 123-142.

Swain, M., et al. (1992). "Ammonia and related amino acids in the pathogenesis of brain edema in acute ischemic liver failure in rats." Hepatology **15**(3): 449-453.

Swerdlow, R. H. (2018). "Mitochondria and Mitochondrial Cascades in Alzheimer's Disease." J Alzheimers Dis **62**(3): 1403-1416.

Tofteng, F., et al. (2006). "Persistent arterial hyperammonemia increases the concentration of glutamine and alanine in the brain and correlates with intracranial pressure in patients with fulminant hepatic failure." J Cereb Blood Flow Metab **26**(1): 21-27.

Trudeau, K. M., et al. (2016). "Lysosome acidification by photoactivated nanoparticles restores autophagy under lipotoxicity." J Cell Biol **214**(1): 25-34.

Twig, G., et al. (2008). "Fission and selective fusion govern mitochondrial segregation and elimination by autophagy." EMBO J **27**(2): 433-446.

Twig, G., et al. (2006). "Tagging and tracking individual networks within a complex mitochondrial web with photoactivatable GFP." Am J Physiol Cell Physiol **291**(1): C176-184.

Waagepetersen, H. S., et al. (2001). "Elucidation of the quantitative significance of pyruvate carboxylation in cultured cerebellar neurons and astrocytes." J Neurosci Res **66**(5): 763-770.

Watanabe, A., et al. (1984). "Glutamic acid and glutamine levels in serum and cerebrospinal fluid in hepatic encephalopathy." Biochem Med **32**(2): 225-231.

Weber, T. A., et al. (2013). "APOOL is a cardiolipin-binding constituent of the Mitofilin/MINOS protein complex determining cristae morphology in mammalian mitochondria." PLOS ONE **8**(5): e63683.

Weiss, N., et al. (2016). "Cerebrospinal fluid metabolomics highlights dysregulation of energy metabolism in overt hepatic encephalopathy." J Hepatol **65**(6): 1120-1130.

Westermann, B. (2012). "Bioenergetic role of mitochondrial fusion and fission." Biochim Biophys Acta **1817**(10): 1833-1838.

Wiek, C., et al. (2015). "Identification of amino acid determinants in CYP4B1 for optimal catalytic processing of 4-ipomeanol." Biochem J **465**(1): 103-114.

Williamson, D. H., et al. (1967). "The redox state of free nicotinamide-adenine dinucleotide in the cytoplasm and mitochondria of rat liver." Biochem J **103**(2): 514-527.

Wu, S., et al. (2011). "Mitochondrial oxidative stress causes mitochondrial fragmentation via differential modulation of mitochondrial fission-fusion proteins." FEBS J **278**(6): 941-954.

Yamamoto, H., et al. (1987). "Glutamine synthetase of the human brain: purification and characterization." J Neurochem **49**(2): 603-609.

Yoneda, M., et al. (1994). "Complementation of mutant and wild-type human mitochondrial DNAs coexisting since the mutation event and lack of complementation of DNAs introduced separately into a cell within distinct organelles." Mol Cell Biol **14**(4): 2699-2712.

Yurdaydin, C., et al. (1995). "Gut bacteria provide precursors of benzodiazepine receptor ligands in a rat model of hepatic encephalopathy." Brain Res **679**(1): 42-48.

Zaganas, I., et al. (2012). "Expression of human GLUD2 glutamate dehydrogenase in human tissues: functional implications." Neurochem Int **61**(4): 455-462.

Zhang, X. Y., et al. (2004). "Transduction of bone-marrow-derived mesenchymal stem cells by using lentivirus vectors pseudotyped with modified RD114 envelope glycoproteins." J Virol **78**(3): 1219-1229.

Zimmermann, M. and A. S. Reichert (2018). "How to get rid of mitochondria: crosstalk and regulation of multiple mitophagy pathways." Biological Chemistry **399**(1): 29-45.

Zimorski, V., et al. (2014). "Endosymbiotic theory for organelle origins." Curr Opin Microbiol **22**: 38-48.

Zuchner, S., et al. (2004). "Mutations in the mitochondrial GTPase mitofusin 2 cause Charcot-Marie-Tooth neuropathy type 2A." Nat Genet **36**(5): 449-451.

Zwingmann, C., et al. (2003). "Selective increase of brain lactate synthesis in experimental acute liver failure: results of a [H-C] nuclear magnetic resonance study." Hepatology **37**(2): 420-428.

8. Publication

Drews, L., Zimmermann, M., Poss, R.E., Brilhaus, D., Bergmann, L., Wiek, C., Piekorz, R.P., Weber, A.P.M., Mettler-Altmann, T., Reichert, A.S. (2019). Ammonia inhibits energy metabolism in astrocytes in a rapid and GDH2-dependent manner. Published on pre-print server bioRxiv: https://doi.org/10.1101/683763

Contribution of Leonie Drews to the manuscript:

Writing of entire first draft of manuscript; completion with advice and help of M. Zimmermann and A.S. Reichert. Preparation of all figures. Ideas for experiments together with M. Zimmermann and A.S. Reichert. Planning of all experiments. Conduction of all experiments except for LC-MS and GC-MS (by D. Brilhaus and T. Mettler-Altmann from CEPLAS facility), data analysis and statistics. HeLa-SIRT4 cell lines by R.P. Piekorz.

Parts of the following paragraphs/figures of this thesis were adapted from the manuscript:

- 2.4.1. Cell lines
- 2.5.11. Transfection of plasmids and siRNA
- 2.7.1. Metabolomics
- 2.11. Statistics
- 3.2.1. Ammonium chloride induces mitochondrial fragmentation
- 3.4. Ammonium chloride influences cell metabolite levels
- 3.5.1. Ammonia is metabolized via glutamate dehydrogenase
- 3.5.2. Knock-down of *GLUD2* rescues ammonia-induced impairment of mitochondrial respiration
- 3.5.3. *GLUD2* overexpression slightly exacerbates detrimental effect of ammonia on mitochondrial respiration
- 3.5.4. Overexpression of GDH regulator SIRT4 rescues ammonia-induced impairment of mitochondrial respiration
- Figures 11, 16, 18, 19, 20, 21, 22, 23, 24 B, 25, 27, 28, 29, 30 C + D, 34
- Discussion: Small paragraphs/sentences distributed throughout the whole discussion are based on the manuscript and were adapted from it. The prevailing part of the discussion is written newly for this thesis.

The following figures of this thesis were taken completely from the manuscript:

- Figure 13, 24 A, 26, 33, 35 B

9. Acknowledgements

Many people deserve gratitude for their participation and help in this project. Very first, of course, my thanks go to Prof. Dr. Andreas Reichert, who has given me the chance to do my thesis in his lab. He was always supportive without giving too much pressure. I felt welcome in the lab from the very beginning. Thank you for the help and support, the great ideas and scientific discussions, for all the time you spend, for conferences and courses and for letting me celebrate Weiberfastnacht every year!

Second, I want to thank my mentor and co-supervisor Prof. Dr. Nikolaj Klöcker for his support and advice at our annual meetings.

Thank you to Dr. Marcel Zimmermann for continuous help and support throughout the years. Especially in the beginning of my work you took time and patience to introduce me to the lab and all the methods. You always had an "open ear" to any problems and questions I had, about science, cars or whatever else. Thanks for many discussions and great ideas and even more laughs… .

Thanks go to Dr. Ruchika Anand and Dr. Arun Kondadi, who were always supportive with scientific questions and contributed well to all the fun we had in the lab, in the office, especially behind closed office doors ;-), or when we all went out for dinner and drinks.

Big thanks to Jennifer Urbach, my PhD student colleague and friend. The lab would only have been half the fun without you! Thanks for the blasts we had with dry ice, Anton, Jacque and Mildred, thanks for Ramen, Ramen, Ramen, the "special exhibition" and a lot more! And finally, thanks for the math (and all the fish).

Thank you to the technicians Andrea Borchardt, Tanja Portugall and Gisela Pansegrau for help and support and many good times. Thanks to Laura Winkels for all the help with tons of paperwork and bureaucracy throughout the years. Without you nothing would work here! Also, thank you for the good (private) talks and laughs we shared!

Thanks to Dr. Nahal Brocke-Ahmadinejad for all her support regarding computer problems.

Thank you to Rebecca Poss, my great student and Hiwi, who contributed many hours of lab work to this study.

Thanks to Dr. Rajesh Kumar, Mathias Golombek, Mona Hendlinger, Oliver Nortmann and all former lab members for the great atmosphere we have and always had. I am thankful for every single one in the group for the solidarity, the fun and the laughs that accompanied me through the last years in the lab, I know that this is not a matter of course.

More thanks go to Prof. Dr. Wilhelm Stahl and Prof. Dr. Peter Brenneisen and everybody from their groups now and in former times for good discussions and fun, especially at the Vlodrop retreat!

Thanks to Dr. Tabea Mettler-Altmann and Dr. Dominik Brilhaus and their technicians at the CEPLAS for supporting me with the metabolomics data acquisition and analysis. Thanks to Dr. Roland Piekorz and Laura Bergmann for providing the HeLa-SIRT4-eGFP overexpression cell line. Also thanks to Prof. Dr. Dieter Häussinger and Dr. Boris Görg and his staff, who kindly provided us with primary rat astrocytes.

Als letztes möchte ich meiner ganzen Familie, ganz besonders meinen Eltern danken. Eine Kindheit voller Neugier, alten Mikroskopen im Keller und der Möglichkeit jede Menge Getier zu halten und zu beobachten hat den Weg für mich geebnet. Danke für eure Unterstützung, auch wenn meinen Experimenten auch mal die ein oder andere Kaktee zum Opfer fiel. Außerdem danke ich meinem Mann und meinen engsten Freunden, einfach dafür, dass es euch gibt und für alles was ihr je für mich getan habt. Für Unterstützung, Hilfe und Freundschaft in allen Lebenslagen. Ohne euch wäre ich jetzt nicht hier! Jedem von euch gehört mein Dank und ihr habt alle einen Teil zu dieser Arbeit beigetragen. Danke, ich habe euch sehr lieb!

Eidesstattliche Erklärung

Ich versichere an Eides Statt, dass die vorliegende Dissertation von mir selbständig und ohne unzulässige fremde Hilfe unter Beachtung der Grundsätze zur Sicherung guter wissenschaftlicher Praxis an der Heinrich-Heine-Universität Düsseldorf erstellt worden ist. Die aus fremden Quellen übernommenen Gedanken sind als solche kenntlich gemacht. Die Dissertation wurde in der vorgelegten oder in ähnlicher Form noch bei keiner anderen Institution eingereicht. Ich habe bisher keine erfolglosen Promotionsversuche unternommen.

Düsseldorf, den 24.07.2019 Leonie Drews